

Max-Planck-Institut für Biochemie
Abteilung Membran- und Neurophysik

Cell-substrate distance measurement in correlation with distribution of adhesion molecules by fluorescence microscopy

Yoriko Iwanaga

Vollständiger Abdruck der von der Fakultät für Physik der Technischen
Universität München zur Erlangung des akademischen Grades eines

Doktors der Naturwissenschaften

genehmigten Dissertation.

Vorsitzender: Univ.-Prof. Dr. J.L. van Hemmen

Prüfer der Dissertation: 1. Hon.-Prof. Dr. P. Fromherz
2. Univ.-Prof. Dr. E. Sackmann

Die Dissertation wurde am 12.07.2000 bei der Technischen Universität München eingereicht und
durch die Fakultät für Physik am 29.08.2000 angenommen.

Acknowledgements

The work presented here was completed in the Abteilung für Membran- und Neurophysik at the Max-Planck-Institut für Biochemie, Martinsried under the supervision of Prof. Dr. Peter Fromherz.

I would like to thank Prof. Dr. Peter Fromherz for the opportunity to work in his department and for his guidance in completing this thesis. I am grateful to have worked in this excellent research condition with wonderful colleagues. The collaboration with other groups have also given me numerous scientifically and personally valuable experiences.

Mein Dank geht an alle Mitglieder der Abteilung Membran- und Neurophysik für ihre Hilfsbereitschaft, ihre Unterstützung und das angenehme Arbeitsklima. Mein ganz besonderer Dank gebührt Dr. Dieter Braun, der mir immer mit zahlreichem fachkundigen und hilfreichem Rat betreuend zur Seite stand. Bei Dr. Jürgen Kupper möchte ich mich dafür bedanken, dass er mir Techniken der Molekularbiologie beigebracht hat.

Bei Prof. Reinhard Fässler und Dr. Cord Brakebusch möchte ich mich für die Hilfe und die Unterstützung bei Umgang mit der Zellkultur und bei der komplizierten Konstruktion des GFP- β 1 Integrin Fusions Proteins bedanken. Allen Mitarbeitern von Prof. Fässler an der Universität Lund danke ich für fruchtbare Diskussionen und für ihre Hilfsbereitschaft während meines zweimonatigen Aufenthaltes.

Für die harmonische Zusammenarbeit während der Arbeiten mit der TIRAF Mikroskopie und IRM möchte ich Peter Geggier, Prof. Günther Fuhr und seiner Abteilung an der Humboldt Universität zu Berlin herzlich danken.

Außerdem möchte ich Karl-Friedrich Giebel and Dr. Martin Bastmeyer für die Zusammenarbeit auf dem Gebiet der SPR Mikroskopie danken.

I am grateful to my uncle Prof. Sadaaki Iwanaga for the idea and his support to initially come to Max-Planck-Institute. I would also like to thank both of my grand fathers for their support and incentives. Above all, I am grateful to my parents and my sister for their continuous support and inspirations.

Summary

Geometry of cell to solid substrate interface was studied by optical techniques and through localization of the cell adhesion sites by molecular biological techniques.

Measurement of cell-substrate distance with fluorescence interference contrast (FLIC) microscopy performed on various extracellular matrix (ECM) protein-coated silicon chip has yielded in a large range between 15-100 nm, depending on the size as well as on the conformation of the ligand. The cellular morphology and the efficiency of adhesion were specific to each ECM protein.

Focal contacts in fibroblasts localized by vinculin tagged with green fluorescent protein (GFP) observed by FLIC microscopy did not exhibit the expected sharp close cell-substrate adhesion. The classical stripes of vinculin clustering in response to fibronectin induced ruffling of the membrane parallel to but not exactly at the focal contacts. The cells in neuronal culture with smooth membrane recruited vinculin mainly at cell periphery.

Sites of ligand-receptor interaction was visualized by tagging $\beta 1$ integrin subunit with GFP and correlated simultaneously with FLIC microscopy. The presence of grainy distribution of $\beta 1$ integrin in fibroblasts adhered to fibronectin corresponded to the region where the membrane was held at dominating cell-substrate separation. The point contact-like dots of the fusion protein did not induce any membrane deformation in cells of neuronal culture.

Focal contacts in fibroblasts were observed concurrently by total internal reflection aqueous fluorescence (TIRAF) microscopy and interference reflection microscopy (IRM) to compare the cell-substrate distance analysis by each technique. Dark patches interpreted as sites of close contact in these images precisely matched the vinculin distribution localized by tagging with the fluorescence protein. Calculation of the cell-substrate distance at focal contacts by both techniques reveal sensitivity to local variations in optical parameters, which explains the discrepancies at these sites from the estimations by FLIC microscopy.

Table of contents

| | |
|--|-----------|
| 1. INTRODUCTION | 11 |
| 1.1 Cell-chip junction | 11 |
| 1.2 Approach | 12 |
| 1.2.1 Distance measurements | 12 |
| 1.2.2 FLIC microscopy and GFP-tagging | 13 |
| 1.3 Biology of extracellular matrix | 14 |
| 1.3.1 Fibronectin and its recombinant modules | 15 |
| 1.3.2 Laminin and its fragments | 15 |
| 1.3.3 Collagen type IV and its fragment CB3 | 17 |
| 1.3.4 Vitronectin | 17 |
| 1.4 Biology of cell adhesion | 18 |
| 1.4.1 Focal adhesion | 18 |
| 1.4.2 Integrins | 19 |
| 2. MATERIALS AND METHODS | 23 |
| 2.1 Generation of fusion constructs | 23 |
| 2.1.1 Basic steps | 23 |
| 2.1.2 EGFP/ECFP-vinculin | 24 |
| 2.1.3 EGFP/ECFP-integrin β 1 | 25 |
| 2.2 Cell culture | 28 |
| 2.2.1 Fibroblasts | 28 |
| 2.2.2 Primary neuronal cell culture | 28 |
| 2.2.3 Substrates | 29 |
| 2.2.4 Transient transfection | 29 |
| 2.3 FLIC microscopy | 30 |
| 2.3.1 Theory | 31 |
| 2.4 Total internal reflection aqueous fluorescence microscopy | 37 |
| 2.4.1 Theory | 38 |
| 2.5 Interference reflection microscopy | 42 |
| 2.5.1 Theory | 42 |

| | |
|--|-----------|
| 2.6 TIRAF-IRM-fluorescence microscopy | 43 |
| 3. CELL-SUBSTRATE SEPARATION | 45 |
| 3.1 Fibronectin | 45 |
| 3.2 Laminin | 48 |
| 3.3 Collagen Type IV | 54 |
| 3.4 Vitronectin | 56 |
| 3.5 Polylysine | 56 |
| 3.6 Discussion | 56 |
| 4. DISTANCE MAPS AND VINCULIN | 61 |
| 4.1 Fibroblasts | 61 |
| 4.1.1 Fibronectin | 61 |
| 4.1.2 Laminin | 66 |
| 4.2 Neuronal culture | 67 |
| 4.2.1 Fibronectin and laminin | 67 |
| 4.3 Discussion | 72 |
| 5. DISTANCE MAPS AND INTEGRIN β1 | 75 |
| 5.1 Fibroblasts | 75 |
| 5.1.1 Fibronectin | 75 |
| 5.1.2 Laminin | 78 |
| 5.2 Neuronal culture | 81 |
| 5.2.1 Fibronectin and laminin | 81 |
| 5.3 Discussion | 87 |
| 5.3.1 Cell-substrate distance at vinculin and integrin β 1 | 87 |
| 6. GFP-SUBSTRATE DISTANCE | 91 |
| 6.0.2 GFP-vinculin to substrate | 92 |
| 6.0.3 GFP- β 1 integrin to substrate | 93 |
| 7. COMPARISON OF DISTANCE MEASUREMENTS | 95 |
| 7.1 Dependence on cell parameters | 95 |

| | |
|--|------------|
| 7.1.1 TIRAF microscopy | 96 |
| 7.1.2 IRM..... | 97 |
| 7.1.3 FLIC microscopy | 100 |
| 7.2 Analysis of experimental data | 101 |
| 7.2.1 TIRAF microscopy | 101 |
| 7.2.2 TIRAF microscopy and IRM..... | 104 |
| 7.3 Discussion | 105 |
| | |
| 8. CONCLUSIONS | 111 |
| 8.1 Finally..... | 111 |
| 8.2 Perspectives | 112 |
| | |
| 9. APPENDIX | 115 |
| A. Abbreviations..... | 115 |
| | |
| Literature..... | 117 |

Chapter 1

Introduction

In an attempt to reduce membrane-substrate separation of a cell cultured on silicon surface consisting of transistors, cell adhesion was studied with an optical method, fluorescence interference contrast (FLIC) microscopy and a molecular biological method, green fluorescent protein (GFP)-tagging.

Optimal coating of the silicon chip was searched by plating cells on silicon chips coated with various extracellular matrix (ECM) proteins. The membrane-substrate distance was estimated and cell morphology was observed by FLIC microscopy.

Possibility of molecular manipulation of cell adhesion was explored by closely studying adhesion sites, focal contacts. These sites of cytoskeleton-ECM interactions were localized by fusing GFP to vinculin, a microfilament-associated protein known to be present in highly enriched focal contacts [4]. The ventral membrane-substrate gap at these sites were determined by FLIC microscopy.

The molecular binding site of cell membrane with ECM protein was directly localized by tagging a subunit of a transmembrane receptor, $\beta 1$ integrin, with GFP. The distribution of $\beta 1$ integrin expression was correlated with the membrane-substrate topography with FLIC microscopy.

The complex structure, focal contacts were further studied by comparing other optical methods, total internal reflection aqueous fluorescence (TIRAF) microscopy and interference reflection/reflection interference contrast microscopy (IRM/RICM). The correlation experiment with GFP-tagging of vinculin was repeated with these techniques under common conditions. Fundamental optical theories underlying all three methods in applying to cell systems were evaluated.

1.1 Cell-chip junction

In designing optimal material surfaces for implantation and tissue engineering, an ability to predict and control the interactions of cells with non-biological materials have been crucial. The cells cultured on artificial material must maintain their differentiated properties and functions in the new environment for any biological purpose. By constructing a simplified, artificial network of neuronal cells, behavioral studies of complex brain system may be conducted. In such experimental setup, individual cellular physiology could be monitored using transistors on which

the cells are cultured. Observation of cellular processes retaining that of *in vivo* requires that the experimental setup be also similar to the natural environment for the cells. At the same time, technical prerequisites for such physiological measurements as performed with transistors consist of independent conditions. In particular, culturing cells on semiconductors comprising microprocessed structures of transistors brings forward the need of additional defined parameters essential for signal detections and stimulations. The cell-substrate separation must be reduced as much as possible and smooth spreading of the cells on the substrate is crucial in performing electrophysiology. These cellular behavior should be enhanced biologically for both purposes, to bring us any information about how in fact the nature functions and also to mimic the biological system that could replace the original system for medical purposes. Here, knowledge of the morphology the cells and tissues assume according to their environment becomes necessary. Only then, development of general principles essential to engineer chemically useful implantable devices and tissue engineered construction design of biocompatible implants and tissue devices become possible.

1.2 Approach

Recent investigations done in biochemistry and molecular biology have been providing and allowing extensive comprehension over how the cells attach to solid surface. Adhesion molecules that localize the cellular signal to a specific region of the cell surface and extracellular molecules are known to determine various cellular behaviors, including guidance of migrating cells which depends on the presence of local cues in the environment. There is exploding amount of information on the adhesion molecules that are found to influence morphology and migration of the cells through cytoskeletal organization and interaction with extracellular cues. The optical and genetic techniques employed in this study are introduced in this section.

1.2.1 Distance measurements

As mentioned at the beginning, the distance that cells retain from the solid substrate as they adhere and undergo cell processes is an important parameter in performing electrophysiology with transistors. Until now, there exist several optical techniques that enable visualization of the ventral cell surface-substrate interface. Attaining a high resolution in determining the geometry of cell adhesion in the most biological system has been subject of many optical studies. Interference reflection/reflection interference contrast microscopy (IRM/RICM) is an interferometry method that has been applied to cell-substratum separation measurement, since the pioneering cell biological application by Curtis [21][93]. This method has been used extensively to examine the closeness of contact between cell membrane and the solid surface, establishing well accepted cell parameters. Another optical technique, total internal reflection fluorescence microscopy (TIRFM) or total internal reflection aqueous fluorescence microscopy (TIRAF) have been demonstrated by theoretical treatment of microscopy to be significantly more sensitive to the small fluctuations

at the thin membrane-substratum contact layer [84]. However, it is known to be still difficult to evaluate the absolute distance between cell and substrate with these either techniques. For instance, the pattern of low reflection seen by IRM could be interpreted either as close apposition to the substrate or as an optically dense region on the cytoplasmic side. TIRFM involves difficulties in calibration due to effect by stray light and adjustment problems. Development of a novel method of fluorescence interference contrast (FLIC) microscopy has allowed to estimate the absolute cell-separation in *in vitro* environment. In this method, cells are cultured on a silicon chip with defined terraces of silicon dioxide [53][11][12]. The plasma membrane is labeled with a fluorescent dye. Since silicon behaves as a mirror, the fluorescence intensity of the membrane depends on the distance from the surface due to the interference of the incident and reflected illumination and of the emitted and reflected fluorescence light. Appropriate calibration allows the use of the intensity to determine the distance with a precision of 1 nm. FLIC microscopy combines the advantages of TIRFM/TIRAF and IRM; the specific labeling of the membrane and the precision of an interference method. At the same time, the complexity of optical properties of the cell that hinders accurate evaluation of IRM is irrelevant in this method due to the dominating effect of the reflecting silicon surface. The optical adjustments critical for multi-angle TIRFM are not required due to the type of integrated intensity calibration on microstructured silicon chips.

1.2.2 FLIC microscopy and GFP-tagging

There have been many studies of cell adhesion conducted by immunostaining of focal adhesion complexes combined with optical techniques. Most information concerning the geometry of cell membrane exactly at these sites is provided by the observations on fixed cells. Possible artifact due to the fixation procedure which may affect the analysis cannot be excluded. Thus in order to visualize the process of cell adhesion *in vitro*, the sites of cytoskeletal organization was localized biochemically by labeling one of its components, vinculin, with green fluorescent protein (GFP) or its variant, cyan fluorescent protein (CFP). Fluorescence micrographs of these fusion proteins were followed by observation of the cell-substrate interface at the same position with FLIC microscopy within a negligible time delay. Pattern of sites of the direct molecular interaction between integrin and the ECM proteins was visualized in the same manner, but by labeling $\beta 1$ integrin subunit with GFP and by comparing with FLIC micrograph of the same cell. Through these correlation studies, the effect of vinculin and integrin clustering on static membrane morphology was analyzed. Two methods, IRM and TIRAF were evaluated by performing the measurements under the same conditions. The same cell system expressing GFP-vinculin was employed as common parameter for the analysis of the three techniques.

Green Fluorescent Protein (GFP)

Briefly, the autofluorescent reporter molecule from the jellyfish *Aequorea victoria* is a widely used tool for visualizing various molecular events in living cells [56]. It contains a fluorescent

cyclic tripeptide whose fluorescence is preserved in chimeric fusions, thus allows DNA manipulation with molecules of interest only with a concern left not to perturb its expression and functions. Its relatively benign fluorophore, owing probably to the fact that it is so tightly buried within the enveloping barrel structure, reduces such risk. Since its discovery, there has been many variations also commercially available that are optimized for fluorescence microscopy. Enhanced green fluorescence protein (EGFP) used in the experiments here contains F64L and S65T mutations, and has excitation maxima at 488 nm and emission maxima at 507 nm. Another reporter used here, enhanced cyan fluorescence protein (ECFP) contains K26R, F64L, S65T, Y66W, N146I, M153T, V163A, N164H, N212K mutations. Its excitation maxima is shifted to 433 (453) nm and emission maxima at 475 (501) nm with lower extinction coefficient as EGFP. In chapters following materials and methods, simple abbreviations, GFP/CFP are used to refer to EGFP/ECFP.

1.3 Biology of extracellular matrix

Extracellular matrix (ECM) is a complex network of secreted extracellular macromolecules through which the cells in tissues are in contact. Their constituent molecules including collagens and glycoproteins, such as fibronectin, laminin and vitronectin are known to modulate cell adhesion, spreading, growth, morphology, differentiation and life span. Most of these macromolecules are secreted locally by cells in the matrix. Basement membrane bordering between the endothelial cells and the connective tissues is found to be in close proximity with cell membranes. Through specific interactions with cell membrane receptors, they are adapted to each of its own physiological functions. Many of the adhesion molecules contain a sequence of three amino acids, arginine, glycine and aspartate (RGD), which is found to be a major recognition site of integrins. The binding of integrin and the RGD sequence is found to be rather transient, where tight adhesion is achieved through many of these weak attachments collectively forming a stronger one [47].

Basement membrane

A more distinct sheath of the ECM known as basement membrane covers the basal surfaces of virtually all epithelia. It also surrounds the surfaces of muscle fibers and ensheathes nerves. This essential layer between tissues forms stable sheets through specific self-assembly mechanisms. Several of its constituent ligands interact with cellular receptors such as integrins. These interactions influence cells in many ways by controlling cell shape, gene expression, cell migration, cell proliferation and programmed cell death. It also provides tissue compartmentalization by acting as barriers to cell penetration and filtration. The major architectural features of basement membranes are characterized by two independent networks. Reticular lamina produced by fibroblasts of the underlying connective tissue is formed from collagen IV, a highly cross-linked non-fibrillar molecule, thus considered to maintain mechanical stability. The network is shown also to contain fibrillar collagens. Basal lamina located immediately adjacent to the cells on the other hand con-

tains a variety of adhesive ECM glycoproteins, such as some laminin isoforms. It consists mainly of a non-covalent nature and are thus probably more dynamic.

1.3.1 Fibronectin and its recombinant modules

Fibronectin is the most extensively studied noncollagenous ECM protein. The molecule is found to mainly promote cellular adhesion to solid substrates and to attach cells to the ECM by binding to integrin and other constituents of ECM. In vivo, assembly of the soluble dimeric fibronectin into insoluble fibrils is important in formation of the ECM. Fibronectin is also involved in embryonic differentiation, cell morphology, cell migration, and thrombosis. Fibronectin constitutes a dimer of similar subunits, each 250 kDa, which are joined by a pair of disulfide bonds near their carboxyl-termini and are folded into a series of globular domains separated by regions of flexible polypeptide chain. In electron micrographs, the dimer appears as an approximately 120 nm long flexible strand [74]. Fibronectins are found in three forms; a soluble dimeric form that circulates in the blood and other body fluids, oligomers of fibronectin found transiently attached to the cell surface and highly insoluble fibronectin fibrils formed in the ECM [1]. Here, the second form of the molecule is concerned by allowing it to adsorb to the cell culturing substrate surface.

Fibronectin molecule comprises an array of about 30 polypeptide modules of three different kinds (figure 1.1, top left) and consists of domains with various functions such as a binding domain for collagen and heparin. These specific roles played by the different domains have been analyzed by cleaving the molecule into its separate domains with proteolytic enzymes or by synthesizing protein fragments either chemically or by recombinant DNA techniques. This has allowed to localize the cell-binding activity to the tripeptide sequence, RGD, which is a motif common in many of extracellular adhesive proteins. It is found that the integrins bind to domains 7-10 in fibronectin. This central cell-binding domain spans two repeats of type III labeled as 9 and 10, and integrin binding requires a RGD tripeptide in type III-10 and a PHSRN 'synergy' site in type III-9.

Immunostaining of fibronectin shows that the fibroblast cells produce its own fibronectin. Cell adhesion to fibronectin through integrin that generates complex signalling events necessary for various cell behavior is a well investigated process. Upon cell attachment, integrin heterodimers, $\alpha 5\beta 1$ and $\alpha v\beta 3$, are found to bind both to the RGD sequence and to the amino-terminus of fibronectin [45].

1.3.2 Laminin and its fragments

Laminin is a prominent component of basement membranes [82], the thin extracellular matrices that surround epithelial tissues at the interface to connective tissues, which appear at the early stage in embryogenesis. It is also found to occur in some non-basement membrane localizations.

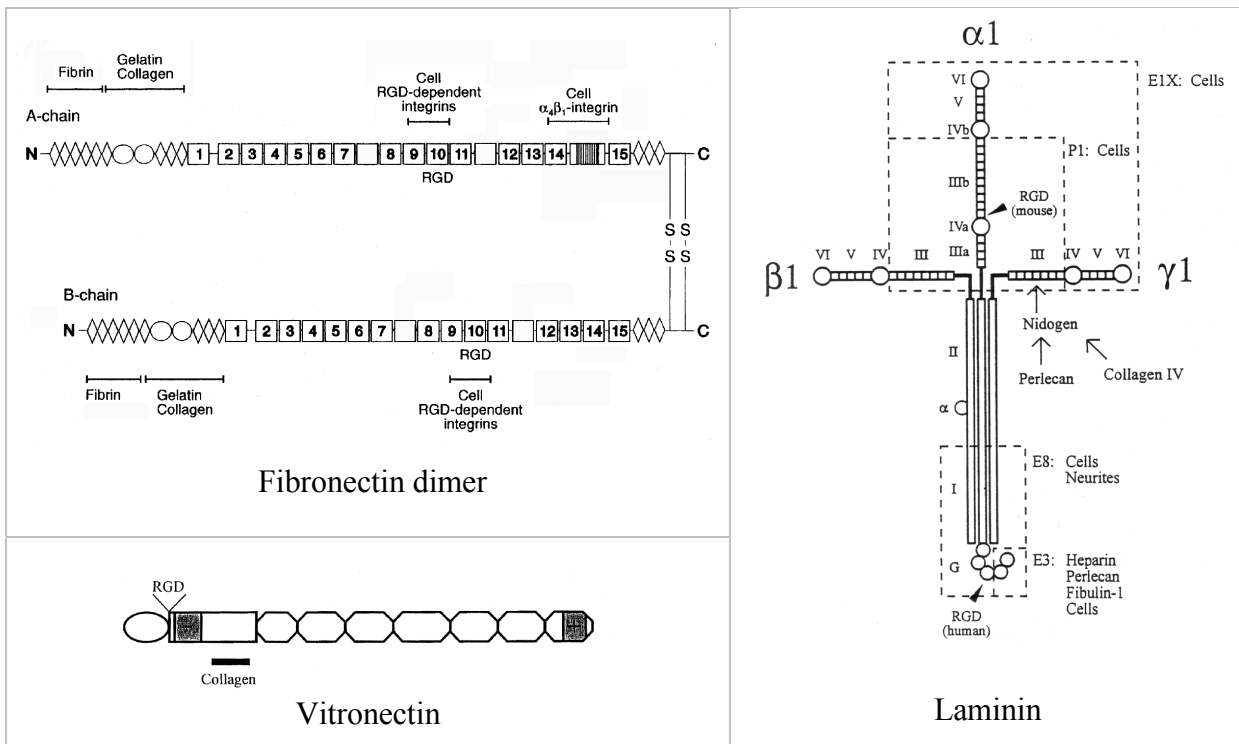


Figure 1.1: Domain organization of: fibronectin dimer (top left), vitronectin (bottom left) and laminin-1 (right).

This adhesive multidomain glycoprotein is found to promote cell adhesion, spreading, migration and guidance of nerve cell axons [59]. For instance, laminin is produced in the central nervous system after injury, where it is found to be involved in regeneration. Until now, various laminin isoforms with specific functions are already known. Laminin-1 used in this present study is isolated from murine Engelbreth-Holm Swarm tumour consists of three chains, $\alpha 1$ of 400 kDa, $\beta 1$ and $\gamma 1$ with 200 kDa each, which are held together through many inter- and intra-chain disulfide bonds. As depicted in figure 1.1, (right) the molecule appears as an asymmetric cross-shaped structure of approximately 110 nm in length. Characterization of laminin fragments derived through proteolytic digestion have deduced wide range of active regions with distinct biological activities [58]. At the long arm of the molecule a strong neuronal outgrowth promoting domain recognized by $\alpha 1\beta 1$ and $\alpha 6\beta 3$ integrin is located. Near the center of the cruciform molecule is found to be recognized by $\alpha 1\beta 1$ integrin in neuronal cells.

E8 fragment

E8 is a laminin fragment derived from the end of the long arm consisting of the globular domain plus a 32 nm long rod. This fragment is composed of about 1250 amino acid residues originating from all three chains of laminin [23]. This carboxy-terminus of laminin molecule is found to

have the most wide-spread effects on cells. It contains a neurite-outgrowth and cell locomotion-promoting sites, as well as heparin binding globule. Mainly integrin $\alpha 6\beta 1$, but also $\alpha 7\beta 1$ are shown to bind to this domain.

LN $\alpha 1$ VI/V

LN $\alpha 1$ VI/V is a proteolytic fragment derived from amino-terminal domains VI and V of $\alpha 1$ chain in laminin-1 with approximately 20 nm in length. Domain VI comprises mixtures of α -helix, β -sheet and random coil and are likely to form globules as also visible in electron micrographs. This domain is found to be essential for laminin polymerization [25]. Rod-like domain V on the other hand is rich in cysteines and glycines which create many turns and contain many homologous repeats. These two domains also contain heparin-binding and $\alpha 1\beta 1$ integrin-binding sites.

1.3.3 Collagen type IV and its fragment CB3

The collagens are a family of fibrous proteins and are the major structural component in the basement membranes. They are most abundant proteins mainly secreted by connective tissue cells [1]. Type IV collagen molecule, exclusively found in the basement membrane, consists of a 400 nm long flexible rod and a 30 nm long stiff triple helix with frequent interruption by non-triple helical segments of 20 or more amino acid residues, and forms sheet-like networks. It differs from the fibrillar collagen molecules common in other members of the collagen family. As well as being the primary structural component of most matrices, collagen is sometimes also adhesive. The triple helical domain contains recognition sites of the $\alpha 1\beta 1$ and $\alpha 2\beta 1$ integrins in an area that is stabilized by intermolecular disulfide bonds [24].

One of cyanogen-bromide-treated peptides, CB3, is a 20 nm long fragment isolated from collagen type IV which contains the RGD sequence and intramolecular disulfide bonds [75]. CB3 has affinity for $\alpha 1\beta 1$ and $\alpha 2\beta 1$ integrins, thus its presence is known to disrupt collagen IV assembly [30].

1.3.4 Vitronectin

Vitronectin is a multifunctional glycoprotein present mainly in blood plasma and ECM as a folded monomer [77][78]. It has a similar molecular structure as fibronectin containing an RGD sequence and is involved in the cell attachment, spreading and migration. Additionally, it is involved in regulation of the proteolytic degradation of matrix and of clot formation, and also involved in the immune response, thereby provides a unique regulatory link between cell adhesion and physiological proteolysis [77]. It is a molecule of size 75 kDa and is found to bind to $\alpha v\beta 3$, $\alpha v\beta 5$, $\alpha v\beta 1$, $\alpha IIb\beta 3$, $\alpha v\beta 6$ and $\alpha v\beta 8$ integrins. This molecule identified as serum protein was shown to provide for cell attachment in serum-free cell culture media, and to possess affinity to glass substrate [46]. Subsequent investigations have allowed its purification and determination of its amino acid sequence, and based on its properties, the name "vitronectin" was proposed [42].

1.4 Biology of cell adhesion

Cell attachment to ECM protein plays a major role in triggering bidirectional signaling that determine cellular activities such as cell locomotion, differentiation, proliferation and polarization. For instance, replication of normal adherent cells such as fibroblasts and endothelial cells requires anchorage to a solid substratum coated with ECM protein. In order to better understand the adhesion process of cells, knowledge of cell structure, biochemistry and physiology, as well as knowledge of surfaces on which cells are attached to become necessary. In association with cell adhesion, three parameters are proposed [74]; the minimum force required for detachment, the area of contact between two adhering surfaces and the typical distance between two adhering surfaces. Molecular biochemistry has been an intensely studied aspect of the interaction between cells and their underlying extracellular matrices. This interaction is found to take place in a specialized region of the plasma membrane called focal contacts.

1.4.1 Focal adhesion

Focal contacts are mostly described as regions where cell-substratum and cytoskeleton-membrane interactions take place [15]. They are known to serve as sites for coordination between cell adhesion and cell motility [17]. This structure typically found in tissue culture is comprised of integrins as the major adhesion receptors and associated cytoplasmic plaque proteins including actin, talin, vinculin, α -actinin, tensin, paxillin and a number of protein kinases [49]. Assembly of the highly organized aggregate of these molecules is regulated both by ECM ligand binding events and by intracellular signaling events [39]. Actin is the most abundant protein involved in the construction of the cytoplasmic face of the focal adhesion. Focal contacts are thus major sites of actin filament attachment at the cell membrane surface that feature dynamic structures, existing for a limited period of time, as tightly controlled by a finely balanced equilibrium of their components.

Upon contacting of plasma membrane to the ECM proteins at the periphery of leading lamella, reorganization or activation of integrin is induced influenced by conformational changes in ECM motifs. As a default at the other end, cytoplasmic domains of the β -subunits of integrins have intrinsic signals for focal adhesion localization, but the incorporation of the integrins into focal adhesions is prevented by the α -subunits of the heterodimers. This inhibition is relieved by the ligand binding as a consequence of cell adhesion, and allows the β -subunit cytoplasmic tail signals to recruit the integrin dimer into the focal adhesion. Previous studies have shown for instance, that the ligand binding controls the localization of $\beta 1$ - and $\beta 3$ -containing integrins [49]. In an appropriate conformation, integrin dimers further recruit cytoskeletal proteins. For effective focal adhesion assembly, a combination of receptor occupancy and occupancy by ligand are required. The induced clustering of the receptor triggers a synergistic response that includes the reorganization of the cytoskeleton and associated cytoplasmic plaque proteins, and the activation

of local signaling pathways. Possible molecular composition and signalling involved through integrins postulated based on recent investigations are depicted in figure 1.2 adapted from [34]. In the earliest stage of this multitude of cascades in fibroblasts, talin is an early structural component collected into F-actin-rich foci, preceding the accumulation of vinculin. Consequently, α -actinin enforces these structures by linking either vinculin/talin or F-actin to the β -subunit of the integrin complex. The earliest structures are observed as a spot-like concentration of actin at the plasma membrane. With the help of the cross-linkers, α -actinin, the terminal portions of actin filaments are seen tightly bundled near the plasma membrane. Syntheses of the essential components such as vinculin and α -actinin are stimulated by cellular contact with the ECM.

Vinculin, 115 kDa in size, are able to form self-aggregates and are found to be highly concentrated in focal contacts [33][16]. This way the cytoskeleton become organized to give the cell a defined structure and further allow diverse signals critical for cell survival to be transmitted from extracellular environment into the cytoplasmic side, by activation of molecules that reside in focal adhesions. In highly motile cells, easily distinguishable focal adhesions are often absent, most likely because of their transient nature and lack of distinctive distribution.

There are several specialized structures in cells attached to ECM, where high level of actin filaments are found as described in [61]. Filopodia are simplest protrusive structure, comprised of thin cylinders that can extend tens of microns from the main cell body. They contain a tight bundle of long actin filaments oriented in the direction of protrusion. Lamellipodia on the other hand are thin protrusive sheets that dominate the leading edges of cultured fibroblasts and other motile cells. Electron micrographs have shown that the characteristic ruffling appearance of fibroblast leading edges is due to lamellipodia that lift up off the substrate and move backward. The web of actin filaments that shapes lamellipodia is organized as an orthogonal cross-weave between two sets of filaments oriented at approximately 45^\pm to the direction of protrusion. In many cell types, lamellipodia are punctuated at intervals by rib-like microspikes that resemble short filopodia. In the cell body, actin filaments are found in lamella, the region with intermediate thickness between the nucleus and protrusive structures. Electron microscopy of lamellae of motile animal cells have shown cortical actin (subplasmalemma) as a loose meshwork of apparently short, randomly organized filaments. Neuronal growth cones are observed to have long homopolar actin filament bundles with barbed ends primarily in the direction of protrusion.

1.4.2 Integrins

As implicated in the previous section, integrins are major transmembrane receptor by which cells attach to extracellular matrices, and some integrins also mediate important cell-cell adhesion events. Expressed as heterodimers, the molecule is found in most mammalian cells. The receptors have diverse biological functions ranging from stabilization of anchorage-dependent cells to the basement membrane to promotion of cell movement. The integrin-mediated attachment to a

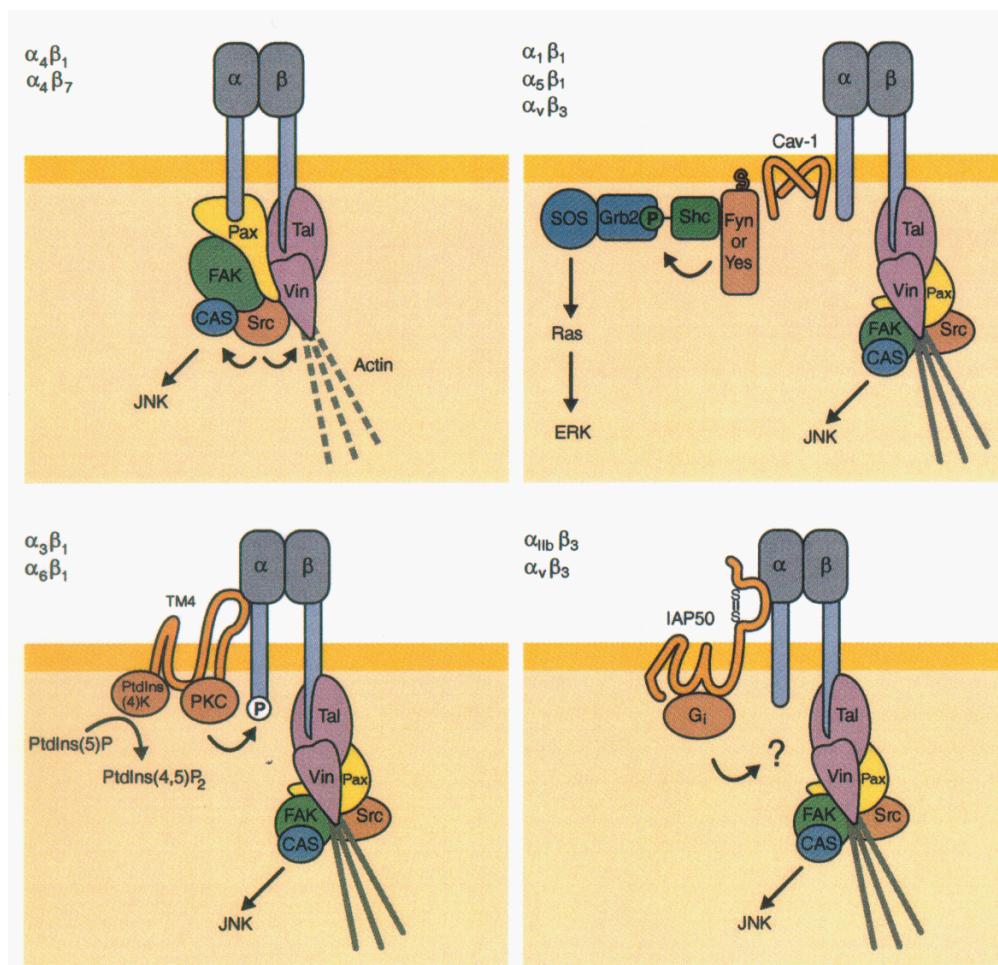


Figure 1.2: The major signalling pathways activated by integrins through their cytoskeletal subunits. Specificity of integrin-ECM and integrin-cytoskeletal interactions is found to be defined by the cytoskeletal subunits involved. (Giancotti, (2000))

substrate serves as a checkpoint of cell cycle progression. Its distribution and activity can be regulated in a dynamic manner bidirectionally across the plasma membrane, by a combination of conformational changes and clustering.

Structure

The heterodimer consists of α - and β -subunits, each with its own variants. Both subunits are transmembrane glycoproteins with single hydrophobic transmembrane segment. The molecule appears with a head extending into the cytoplasmic side between 80-120 Å out of 95-130 kDa, on the extracellular domain of α - and β -subunits extending 20 Å and 180-200 Å respectively, comprised of 130-210 kDa. A structural model introduced in [65] predicts the receptor with globular head and two stalks that extend from the lipid bilayer approximately 2 nm at cytoplasmic side and 20-23 nm at extracellular side, respectively. β -subunit has tightly folded amino-terminal domain of 40-50 kDa contributing to the ligand-binding domain. Divalent cations are essential for receptor function and α -subunit which features divalent cation binding sites is responsible for the affinity and also for ligand-binding. The α -subunits (120-180 kDa) and β -subunits (90-110 kDa) interact through non-covalent association with each other to form small cytoplasmic domains (less than 50 amino acids). $\beta 4$ integrin is an exception with more than 1000 amino acids at its cytoplasmic domain. Studies conducted with integrin fragments have shown that the extracellular domains (>75 kDa for β -subunits, and >100 kDa for α -subunits) associate to form the $\alpha\beta$ heterodimers. This is supported by the fact that truncated forms lacking transmembrane and cytoplasmic domains can be expressed and do form functional $\alpha\beta$ dimers [48].

Function and molecular interactions

Integrin heterodimers provide tight anchoring of cells to the extracellular environment. However, each molecule is known to bind with both ECM ligands and cytoskeletal elements with low affinity, at $K_d \approx 10^{-6}$ M for both integrin-fibronectin and integrin-talin interactions [74]. These weak interactions are through a large number of binding sites, which form the strong cell-substrate adhesion as a whole. Biochemical investigations have revealed several subunits with their specific functions and affinities [48]. Majority of the integrins' ligands are either cell-surface members of immunoglobulin superfamily or ECM molecules. They are also known to bind to RGD (Arg-Gly-Asp) sequence present in fibronectin, vitronectin and other molecules featuring EGF-like domains. Previous studies have indicated that some integrins such as $\alpha 5\beta 1$ and $\alpha v\beta 3$'s recognize Lys-Gln-Ala-Gly-Asp-Val (KQAGDV) in fibrinogen, and other integrins recognize further different sequences. Extracellular interactions that lead to occupation of integrin receptors by their ligands induce conformational change in integrin that would further transmit signals intracellularly. In fibroblasts, a cascade of reactions including tyrosine phosphorylation, cytoplasmic alkalization occur upon integrin $\beta 1$ binding to fibronectin. These events correlates with the parallel stimulation of cell spreading, growth and proliferation. There, presence of multiple integrin binding domains in ECM proteins could cluster the receptors to generate combined signals. Cell

spreading of fibroblasts, an essential process in this study, is initiated by a contact of fibroblasts with surfaces coated with fibronectin or other ECM proteins. It induces signaling events including release of arachidonic acid by phospholipase A2, production of diacylglycerol with subsequent activation of PKC, activation of the GTP-binding protein Rho with subsequent activation of a phosphatidylinositol phosphate 5-kinase and activation of protein tyrosine kinases. Here, it is found that the β cytoplasmic domain is sufficient to induce recruitment of other integrins. Receptor occupancy by RGD peptide leads to unmasking of this functionally critical $\beta 1$ cytoplasmic domain, further allowing interaction with and recruitment of cytoskeletal components.

At the cytoplasmic side, most integrins thus interact somehow with the actin-based cytoskeleton where both subunits are required. This association of integrins with cytoskeletal actin filaments has been shown to be via an indirect linkage involving talin, vinculin, α -actinin and other cytoskeletal-associated molecules. The cytoplasmic events involving the integrin heterodimers are complex and each component is still to be untangled. For instance, there is also an evidence suggesting that α -actinin could bind directly to $\beta 1$ and $\beta 3$ integrins, by interacting with the β -subunits alone [17]. Also, different cytoplasmic domains trigger different functions such that two integrins which bind the same ligand can provide distinct cellular signals. A comparative studies have shown that for example, both $\alpha v\beta 3$ and $\alpha v\beta 5$ interact with vitronectin, but only the former co-localizes with vinculin and the ends of actin filaments [87]. A special case, $\alpha 6\beta 4$ (with large $\beta 4$ cytoplasmic domain) is found "concentrated at hemidesmosomes in epithelial cells, where it most likely interacts somehow with intermediate filaments, which are characteristically associated with hemidesmosomes" [48].

The fact that individual integrins are able to often bind more than one ligand implies their functional redundancy; same integrin heterodimer can recognize several ECM proteins and a particular ECM ligand may be recognized by more than one integrin as well. Binding specificity of individual integrin heterodimers is dependent on the expression system. This specific affinity for different ligands comes from the inside-out signaling of the cell in which they are expressed [47]. Conformational changes induced intracellularly by such signaling switches integrin heterodimer between activated and deactivated states, thereby determine specificity and affinity. This signaling cascade via integrins at its down stream is found also to contribute in matrix assembly.

Chapter 2

Materials and Methods

First, the genetical techniques used and the steps taken in order to construct the fusion proteins, EGFP/ECFP-vinculin and EGFP/ECFP- β 1 integrin (depicted in figure 2.1), are described in this section. Cell adhesion was studied by introducing these fusion constructs into a mouse cell line and a primary cell culture prepared from rat hippocampus. Culturing of the mouse cell line and the primary cell culture along with the procedure to introduce the foreign DNAs to the cells are also described. Finally, the theoretical background of the three optical methods and the experimental setup are summarized.

2.1 Generation of fusion constructs

2.1.1 Basic steps

For the construction of all EGFP/ECFP-vinculin and - β 1 integrin, the following procedures were repeatedly carried out:

A bacterial system, *E.coli* DH5[®] (Gibco) was used for all plasmid preparations. *E.coli* were transformed with prokaryotic/eukaryotic expression vector with a gene of interest and also a cDNA for specific antibody resistance. Bacteria containing the plasmid of interest was then selectively grown on agar plates with the antibody. Bacterial colonies that survived on the agar plates (i.e. the ones that contain the recombinant plasmids) were picked to be grown in LB medium containing the antibody for further amplification. After harvesting the bacterial cells, the DNA was purified

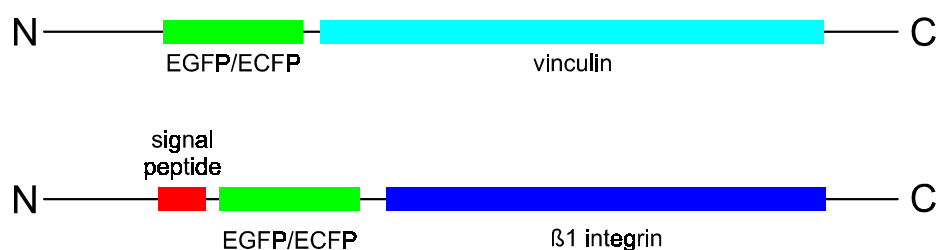


Figure 2.1: The fusion chimeras used to localize sites of cell adhesion; EGFP/ECFP-vinculin (top) and EGFP/ECFP- β 1 integrin (bottom).

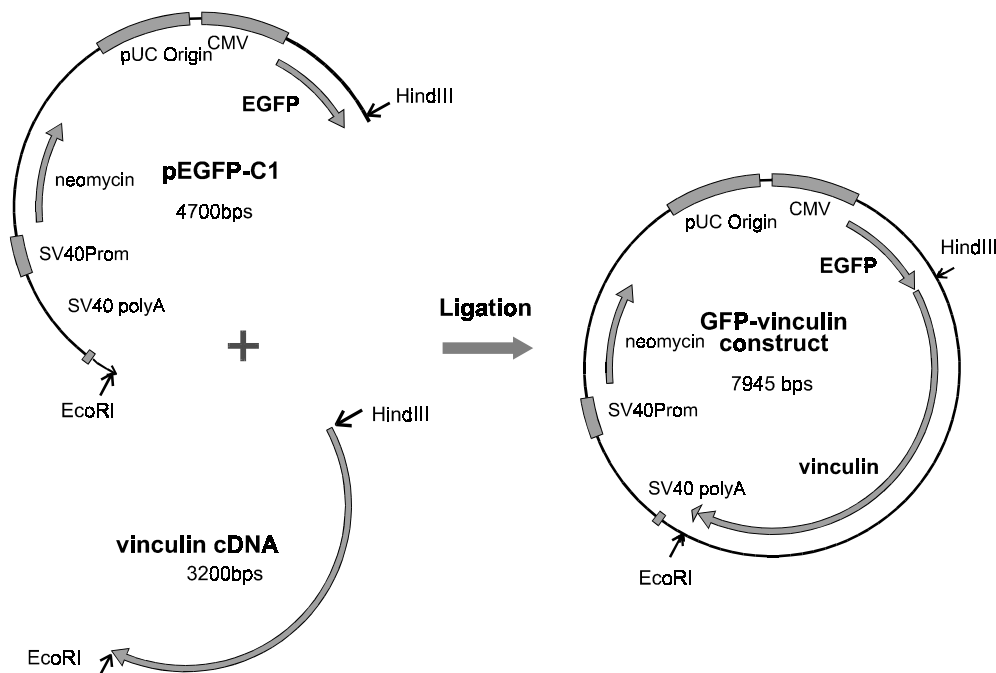


Figure 2.2: Cloning steps of EGFP-vinculin construct. The cDNA of vinculin from PCR amplification was ligated into pEGFP-C1 in frame with EGFP cDNA at multiple cloning site between HindIII and EcoRI.

by a Quick prep for use in further cloning processes, or with QIAGEN Plasmid-Kits (Qiagen, Hilden) for further use in transfection of mammalian cells.

DNA fragments obtained by PCR amplification were isolated by QIAquick PCR Purification or by gel electrophoresis followed by QIAGEN Gel Extraction Kit. Digested DNA fragments were isolated by gel electrophoresis followed by the Gel Extraction Kit. Ligation of DNA fragments were carried out overnight at 10°C . The correct plasmids were selected as follows; first the ligation product was amplified in *E.coli* by transformation and then by plating the bacteria on agar plates with an appropriate antibody. The plasmids were then prepared (with a Quick prep) from several colonies grown on agar plates. The plasmids from each colony was examined by gel electrophoresis after digesting them with restriction enzymes that result in recognizable fragments.

All restriction enzymes, DNA polymerase, T4-DNA-ligase, alkaline phosphatase were obtained from Boehringer Mannheim (Mannheim) and New England Biolabs (Schwalbach). All cDNAs of EGFP and ECFP employed here were from the pEGFP-C1/pECFP-C1 expression vectors from CLONTECH Laboratories GmbH (Heidelberg).

2.1.2 EGFP/ECFP-vinculin

The cDNA of the fluorescent protein was cloned to the amino-terminus of vinculin in the expression vector pEGFP-C1/pECFP-C1.

The cDNA encoding a chicken vinculin [69] in eukaryotic expression vector pJ4 was amplified by PCR (Expand High Fidelity PCR System, Boehringer Mannheim, Germany). Oligodeoxynucleotides 5' | TTGCTAATAAAGCTTCAGGATCTGGTATGCCCGTCTTCC | 3' and 5' | TTAAGAATTCTTATTACTGATACCATGG | 3' were used as primers with the plasmid pJ4 as template. As a result, the fragment contained a unique HindIII site (AAGCTT) followed by a linker before the start codon for vinculin, so that it would be in-frame with EGFP/ECFP cDNA. It also created a unique EcoRI site (GAATTC) after the stop codon of vinculin to enable ligation into the multiple cloning site of the pEGFP-C1/pECFP-C1 vector. The isolated fragment was then excised at these newly created HindIII and EcoRI sites. This fragment was ligated into the multiple cloning site of pEGFP-C1/pECFP-C1 expression vectors between HindIII and EcoRI, behind and in-frame with the EGFP/ECFP cDNA. The inserted vinculin cDNA was sequenced in order to confirm the integrity of the PCR amplified product. The steps taken to attain the final construct of the fluorescent protein tagged to amino-terminus of vinculin is illustrated in figure 2.2.

2.1.3 EGFP/ECFP-integrin β 1

Also the fluorescent protein was cloned to the amino-terminus of β 1 integrin subunit. The cDNA of this subunit consist of start codon followed by a signal peptide sequence of 19 amino acids (57 nucleotides). This hydrophobic signal peptide sequence at the amino-terminus is found to be cut off from the peptide by post-translational process during its translocation to the cell surface [83]. Thus we have cloned the cDNA of EGFP/ECFP directly to the β 1 integrin sequence after this signal peptide in order to avoid digestion that would separate the cDNAs of the fluorescent protein and β 1 integrin. Based on the existing restriction sites in these cDNAs, we have ligated (i) a foreign signal peptide (from mouse brevicin) known to function well in transportation of transmembrane protein to the cell surface to the amino-terminus of (ii) EGFP/ECFP followed by (iii) β 1 integrin cDNA without its endogenous signal peptide sequence.

The cloning procedure follows the steps as illustrated in figures 2.3 and 2.4: first, an oligonucleotide 5' | CTCGAGCTACCATGGAATTCTCCGGAGTCGACGCGGCCGC | 3' was ligated into pBluescript II KS between its XhoI and NotI in order to create necessary restriction sites, NheI, NcoI and BspEI in advance. The cDNA encoding for EGFP was cleaved from pEGFP-C1 at NcoI and BspEI restriction sites and ligated into the pBluescript in the created polylinker. The cDNA encoding for β 1A integrin subunit in p β 1A(N) was PCR amplified using 5' | GCGGGATCCTCCGGAGGCCAAACAGATAAAAATAGATGT | 3' and 5' | GCGGAATTCGCGGCCGCGGATTCATTTTCCCTCATACTTC | 3' as primers in order to create a new unique BspEI site after its endogenous signal peptide sequence at amino-terminus behind its start codon, and a unique NotI site after its stop codon. The PCR product of β 1A integrin cDNA without the endogenous signal peptide sequence was cleaved with BspEI and NotI, and consequently cloned in-frame with the start codon of EGFP cDNA, downstream of

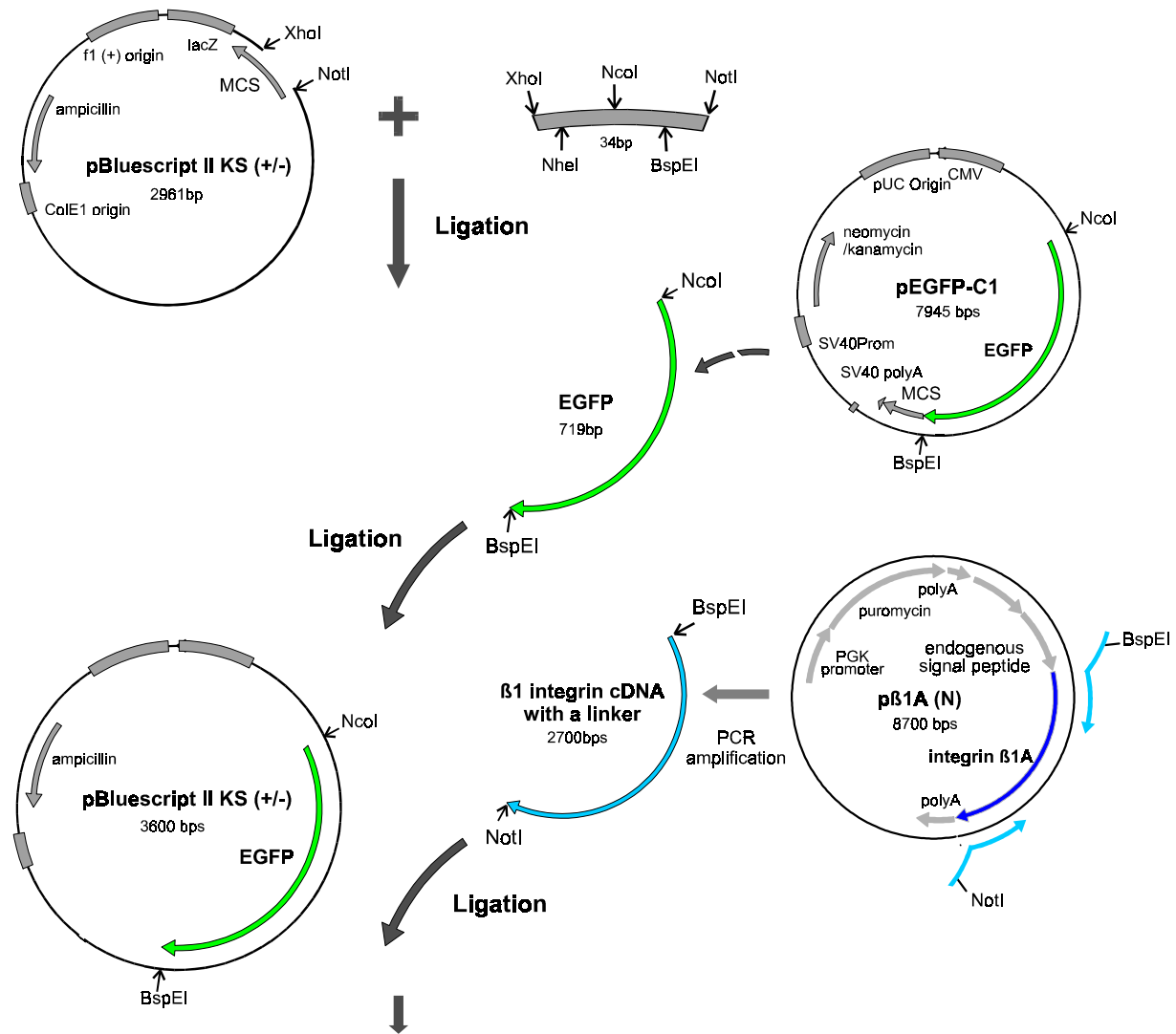


Figure 2.3: Cloning steps of the signal peptide-EGFP- β 1 integrin fusion construct. All the broken arrows represent digestion with restriction enzymes. (i) an oligonucleotide with several restriction sites for the later use was ligated into a multiple cloning site of a plasmid, pBluescript. (ii) cDNA for EGFP without its stop codon was isolated from pEGFP-C1, then ligated into the plasmid from (i) between NcoI and BspEI. (iii) cDNA of β 1 integrin excluding its endogenous signal peptide was PCR amplified using p β 1A (N) as a template, which created a BspEI site followed by a linker at the amino-terminus, and then a NotI site after its stop codon. The PCR product was ligated into the plasmid from (ii) behind EGFP. The next figure illustrates the last steps.

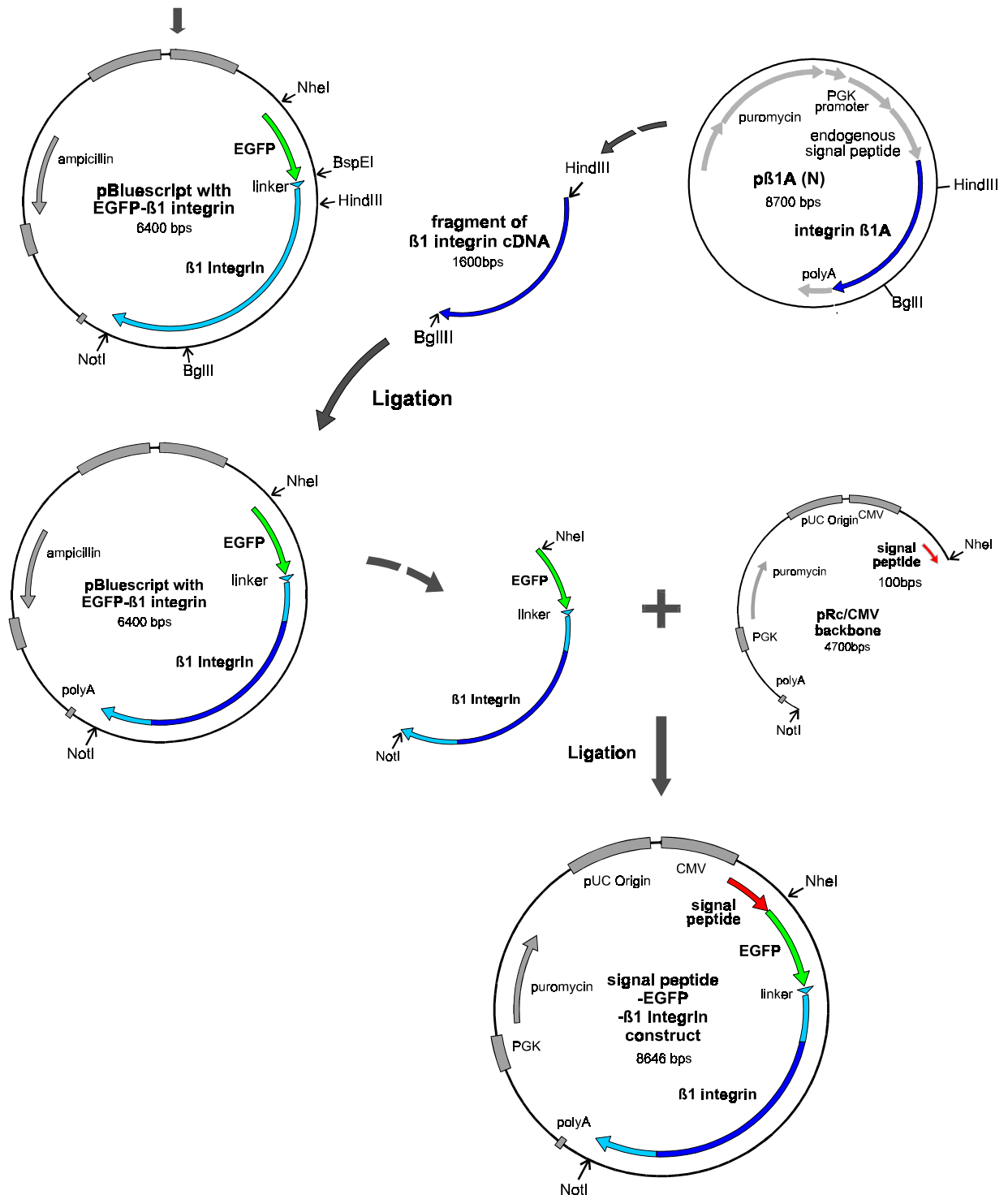


Figure 2.4: Continuation of the cloning procedure from the previous figure in constructing the signal peptide-EGFP-β1 integrin. (iv) cDNA of β1 integrin was isolated from pβ1A (N) between HindIII and BglIII sites, and replaced the ligated PCR product in the plasmid from (iii). (v) The sequence EGFP-β1 integrin in the plasmid from (iv) was excised and ligated into a eukaryotic expression vector that contains a signal peptide and a poly A, between NheI and NotI sites behind this signal peptide sequence. An identical steps were performed parallel also with ECFP.

the EGFP in the pBluescript. Large part of the PCR amplified β 1A integrin (approximately 1.6 kbps) was then replaced by the original cDNA from the plasmid p β 1A(N) between HindIII and BglII sites. The remaining PCR amplified regions, one before HindIII and one after BglII sites, were sequenced to confirm the integrity of the PCR product. The construct EGFP- β 1A integrin was then cleaved with NheI and NotI to insert into expression vector pRc/CMV between a signal peptide sequence and a poly A signal at NheI and NotI sites. The pRc/CMV employed here consisted of previously ligated cDNA for puromycin, poly A and signal peptide sequence. An identical construct was also made with ECFP.

2.2 Cell culture

2.2.1 Fibroblasts

For most of the experiments in present studies, mouse fibroblast, GD25 and GD25- β 1A cells were employed. Fibroblasts are connective tissue cells in which large focal adhesion complexes are often found, that consist of more than 20 different molecules. In connective tissues, the ECM is generally more plentiful than the cells determining the tissue's physical properties [1]. At the interface between an epithelium and connective tissue, the matrix forms a basement membrane (described in the previous chapter) that also plays an important role in defining cell behavior.

The mouse cell line, GD25 cells lack the β 1 family of integrin subunit through null mutation, whereas GD25- β 1A is established by stable transfection with cDNA encoding cytoplasmic splice variant of murine integrin subunit β 1A [28][89]. A gene trap vector was used to obtain targeted disruption of β 1 integrin alleles in a mouse embryonic stem cells [28]. The differentiated β 1 integrin-deficient cell line was established by infecting the embryonic stem cells with recombinant retroviruses that transduced the SV-40 large T antigen followed by ring cloning. Both GD25 and GD25- β 1A cells express restricted integrin heterodimers which allow controlled study of cell-matrix interactions. Immunoprecipitation of surface-iodinated cells using antibodies specific for various integrin subunits has shown that GD25 cells express α v β 3, α v β 5 and a small amount of α 6 β 4. GD25- β 1A cells are found to additionally express α 3 β 1, α 5 β 1 and α 6 β 1 [89].

The GD25 and GD25- β 1A cells were cultured in DMEM with glutamax (Gibco BRL, Eggenstein, 31966) supplemented with 10% fetal calf serum (FCS). The cells were harvested regularly by trypsin-EDTA treatment and resuspended in serum-containing medium to inactivate the trypsin.

2.2.2 Primary neuronal cell culture

Neurons were dissociated from the hippocampi of Wistar rats (Thomae, Biberach) at 18 days gestation [85]. The cells were directly plated on silicon chips (prepared as described in the following section) placed in a 35 mm Falcon dish. 0.5 ml of cell suspension was plated on silicon chips with additional 2 ml of DMEM/glutamax I (Gibco BRL, 61965) with 10% fetal bovine serum (FBS)

(Gibco BRL, 10270) and 1% penicillin/streptomycin (Gibco BRL, 15146) to a final concentration of 100×10^3 cells/ml. After settling for 2 hours, the medium was removed to eliminate cell debris from the preparation and exchanged with fresh medium without penicillin/streptomycin. The cells were further cultivated for approximately one day at 37°C and in 10% CO_2 before they were transfected with the fusion constructs.

2.2.3 Substrates

The substrates for all the experiments, silicon chips, glass plates and coverslips, were silanized with dichlorodimethylsilane in toluol (volume 2:100). After sterilizing them by illuminating with UV light, the substrates were coated with ECM protein of interest. The protein adsorbed from solution onto solid surface is found to resemble the *in vivo* environment of cells [63]. Coating with ECM protein was done by incubating the silicon chip placed in a 35 mm diameter petri dish with PBS containing 5-10 $\mu\text{g/ml}$ of the protein overnight at 4°C . The coated silicon chips were washed twice with PBS, blocked with 1% bovine serum albumin (BSA) in PBS for 2-3 hours and washed with PBS before plating the cells. Previous studies have shown that BSA adsorbed surfaces result in elimination of cell attachment [51][88], thus serves to cover silicon oxide surface that are still free from ECM protein after incubation and to avoid nonspecific binding.

2.2.4 Transient transfection

Both fibroblasts and neurons were transiently transfected by chemical methods a few days prior to experiments were performed in order to attain a high expression efficiency of the fusion construct. Figure 2.5 illustrates this procedure.

Fibroblasts

A few hours before a transient transfection of the fibroblasts was carried out, the cells were supplied with fresh culture medium. With calcium phosphate-DNA coprecipitation method, a precipitate containing DNA, calcium phosphate and HEPES-buffered saline solution was prepared and incubated at room temperature for 20 minutes. The mixture was then introduced to the cells (0.1 ml per ml of medium) for 16 hours to one day. After exposing to the DNA precipitate, the cells were washed with PBS and further incubated in fresh culture medium until high expression efficiency of the fusion protein was attained. With lipofectamine transfection method, a mixture of lipofectamine reagent (Gibco BRL, Life Technologies, 18324) and DNA solution at volume proportion of 3:7 was prepared and incubated at room temperature for 10-15 minutes. During the incubation, the cells were washed three times with DMEM without FCS and then kept further in the medium without serum. The DNA-lipofectamine suspension was slowly added to the cell culture, at 0.1 ml for every 3 ml of medium. The cells were incubated further up to one day before the medium was exchanged with fresh culture medium containing 10% FCS. Prior to experiments, the GD25/GD25- β 1A cells were treated with trypsin/EDTA, resuspended in serum-containing

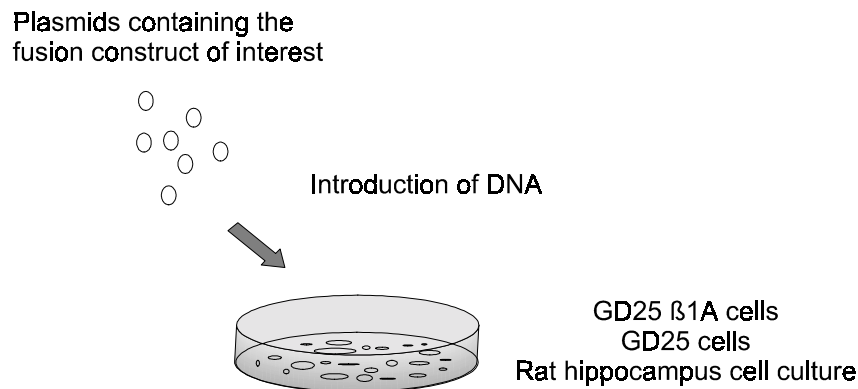


Figure 2.5: The plasmids containing the fusion construct of interest were introduced to the cell culture (GD25 β1A/GD25 or rat hippocampus) by calcium-phosphate transfection method or lipofectamin transfection.

medium to inactivate the trypsin and further washed twice in PBS by centrifugation. This step of washing the cells in PBS was for the purpose of avoiding the possibility of serum-derived factors altering the surface chemistry prior to cell attachment. For measurements, the cells were subsequently incubated at 37°C in serum-free medium on silicon chip coated with ECM protein as a substrate.

Primary cell culture

The culture in a 35 mm dish with a silicon chip was transfected with the fusion protein of interest by calcium-phosphate-DNA coprecipitation method. Before transfection was carried out, the culture medium was taken up and kept in the culturing condition in the incubator in order to apply to the cells after the transfection. The cells were washed twice with DMEM/glutamax I without serum and then kept in the 1 ml of the same medium. 100 μ l of the precipitate as prepared in the same manner as for the fibroblasts was added to the culture and incubated for 80-90 minutes. At the end of the incubation, the serum-free medium containing DNA precipitate was removed, and the original medium which was meanwhile kept in the incubator was applied to the cells. The cells were further incubated for approximately one day before the measurements.

2.3 FLIC microscopy

Fluorescence interference contrast (FLIC) microscopy was performed as presented in the previous work [53][10][11] [12]. Theory behind the technique and its analysis discussed in these works will be repeated in the following sections. In this method, the cells are seeded on microprocessed silicon chip surface with a thin layer of silicon dioxide in four different thicknesses, coated with ECM protein as illustrated in figure 2.6. The cells stained with membrane fluorescent marker, DiIC₁₈ [6] are observed under a microscope. Identical experiments were performed also using

confocal FLIC microscopy which is described in [10].

Principles of FLIC microscopy

The basic principle behind the technique will be first summarized in this section.

The silicon surface under a layer of oxide behaves as a mirror. In front of the mirror, incident and reflected lights interfere with one another, thus establish standing modes of electromagnetic field. The fluorescent dyes embedded near the outer surface in the cell membrane are positioned in proximity to the silicon surface. Their transition moments of excitation and emission are parallel to the cell membrane [5]. The fluorescent dyes are excited by the standing wave of incident and reflected lights. The emission of fluorescent dyes embedded in the lower membrane is also detected as an interference of reflected and non-reflected light.

In this setup, the separation between the silicon and the dye molecules embedded in the lower cell membrane consists of oxidized silicon layer, ECM and fluid (culture medium). The length of pathway through this separation modulates both the intensity of excitation and emission of fluorescent dyes positioned close to the reflecting silicon surface. A set of oxide steps on the silicon brings the membrane of an adhering cell to different distances from the mirror, given by the known thickness of the oxide d_{ox} plus the unknown distance d_{cleft} between the lower membrane and the oxide, as illustrated in figure 2.6. Due to differences in the pathway length of the lights at the four surfaces with different oxide thicknesses, four different fluorescence intensities are detected in front of corresponding surfaces.

The fluorescence intensities are evaluated and plotted versus the height of the four steps which are identified by the contrast in reflected light (figure 3.1, right) using an objective with small aperture. The distance between the oxide layer and the lower membrane d_{cleft} common over all four known oxide thickness is determined by using theoretical curves that describe the dependence of fluorescence intensity on the position of excited dyes relative to silicon (mirror). The employed electromagnetic theory takes into account: i) the absorption and emission spectra of the dye, ii) the orientations of dyes transition moments and iii) all directions, polarizations and wavelengths of the excited and detected light.

2.3.1 Theory

The optical theory employed in this technique will be discussed in several steps in this section.

Excitation

Dye molecules in membrane in front of the silicon dioxide is excited by the interference between lights incident and reflected against silicon. Relative field strength at the position of dyes, E_{in} is obtained by characteristic transfer matrix methods [9][41].

In a layer system, a product of transfer matrix of each layers between the interfaces j and $j + 1$

defined as:

$$M = \prod_{j=0}^{N_i-1} M_{j+1}^k = \prod_{j=0}^{N_i-1} \begin{pmatrix} m_{11j}^k & m_{12j}^k \\ m_{21j}^k & m_{22j}^k \end{pmatrix} = \prod_{j=0}^{N_i-1} \begin{pmatrix} \cos \theta_j & i \frac{1}{p_j^k} \sin \theta_j \\ i p_j^k \sin \theta_j & \cos \theta_j \end{pmatrix} \quad (1)$$

allow determination of a relationship between the tangential fields U and V at the layer $j = 0$ and $j = N_i - 1$, so that

$$\begin{pmatrix} U_0 \\ V_0 \end{pmatrix} = M \begin{pmatrix} U_{N_i-1} \\ V_{N_i-1} \end{pmatrix}$$

The components of the matrix further define the Fresnel coefficients at layer $j = 0$. The effective indices are given by $p_j^{TE} = n_j \cos \mu_j$ and $p_j^{TM} = \frac{\cos \mu_j}{n_j}$ for non-normal incidence, $k = TE; TM_p; TM_n$ and

$$\theta_j = \frac{2\pi}{\lambda_{in}} n_j d_j \cos \mu_j$$

The final Fresnel coefficients,

$$r = \frac{h_1 - h_2}{h_1 + h_2} \quad t = \frac{2p_0}{h_1 + h_2} \quad (2)$$

with

$$h_1 = i m_{11}^k + m_{12}^k \zeta p_N \zeta p_0 \quad h_2 = m_{21}^k + m_{22}^k \zeta p_N$$

are calculated for both above and below the layer with dye (i.e. membrane). Thus in the case of FLIC microscopy, r_{below} with $N = \text{silicon}$, and r_{above} with $N = \text{medium}$ (above upper membrane), and with $p_0 = p_{\text{membrane}}$, are evaluated for both TM and TE. The characteristic matrices for the layers depend on the optical properties of the assembly and on the position of the dye molecule determined by the thickness d_{ox} of the oxide and the distance d_{left} between membrane and support.

The interference term of r_{below} and r_{above} defined as if , is then calculated for the layer with the dye molecule:

$$if^k = \frac{q}{1 - j r_{\text{above}}^k} \frac{1 + s^k r_{\text{above}}^k e^{i d_c} = d}{1 - i r_{\text{above}}^k r_{\text{below}}^k e^{i'}} \quad s^k = f_{1;1} g \quad \theta_j = \frac{4\pi}{\lambda_{in}} n_j d \cos \mu_j \quad (3)$$

For the incoming electrical field E_{in}^{*0} described with a wavelength λ_{in} , an angle of incidence μ_{in} (with respect to the normal) and an angle of polarization θ_{in} (with respect to the plane of incidence), the local field strength E_{in}^* can be expressed as:

$$E_{in}^* = \begin{pmatrix} if_{TE} & 0 & 0 \\ 0 & if_{TM_p} & 0 \\ 0 & 0 & if_{TM_n} \end{pmatrix} E_{in}^{*0} \quad (4)$$

where

$$E_{in}^{*0} = \begin{pmatrix} E_{TE}^0 \\ E_{TM_p}^0 \\ E_{TM_n}^0 \end{pmatrix} = \begin{pmatrix} \sin \theta_{in} \\ \cos \theta_{in} \cos \mu_{in} \\ \cos \theta_{in} \sin \mu_{in} \end{pmatrix}$$

The probability per unit time P_{ex} for excitation of a dye molecule is determined by integrating the following components over the wavelength λ_{in} :

- i) the intensity of illumination $I(\lambda_{in})$ (quanta per area, time and wavelength interval),
- ii) the extinction coefficient of the dye $\epsilon(\lambda_{in})$ and
- iii) the modulation of excitation by the interface.

The modulation is expressed as a square of the local electrical field E_{in}^* projected onto the direction of the transition dipole expressed as:

$$e_{ex}^* = \frac{E_{TE}^0}{E_{TMp}^0} = \frac{\cos \mu_c \sin \hat{A}_c}{\sin \mu_c \sin \hat{A}_c} \frac{E_{TMn}^0}{E_{TE}^0} \quad (5)$$

where μ_c is the angle of the chromophore to the membrane normal and the dipole of the chromophore with a rotation angle is \hat{A}_c . First, $\int jE_{in} \cdot e_{ex}^{*2}$ is integrated over orientations of the dye, \hat{A}_c , and over all directions and polarizations of the incident light within the aperture of the microscope, ω_{in} . Finally the total probability of excitation per unit time is given as:

$$P_{ex} = \int d\lambda_{in} I(\lambda_{in}) \epsilon(\lambda_{in}) \int \int jE_{in} \cdot e_{ex}^{*2} \quad (6)$$

Emission

The emission of chromophore is described similarly to excitation owing to the symmetry between excitation and emission as discussed in [52] and [10]. The detection system instead defines a light wave with λ_{out} along a plane of incidence at an angle μ_{out} with respect to the normal, and an angle of polarization θ_{out} . The probability of spontaneous emission into a certain mode of the electrical field is proportional to the probability of excitation of the same molecular transition by the same mode.

The probability per unit time P_{em} to detect an emitted quantum from an excited molecule is given then by integrating over the wavelength λ_{out} , with dependence on:

- i) the quantum yield $\Phi_{det}(\lambda_{out})$ of the detector,
- ii) the fluorescence spectrum $f(\lambda_{out})$ (quanta per wavelength interval) of the dye,
- iii) the relative strength E_{out} of the local electrical field of that mode that accepts the emitted photon and
- iv) the direction e_{em} of the transition dipole of emission.

Similar to P_{ex} , P_{em} is obtained first by averaging $\int jE_{out} \cdot e_{em}^{*2}$ over all directions and polarizations of the detected light within the aperture of the microscope, ω_{out} , and the orientations of the dye in the plane of the membrane, \hat{A}_c . Integrating over the wavelengths of detection, λ_{out} :

$$P_{em} = \frac{Z}{d_{s,out}} \Phi_{det}(s_{out}) f(s_{out}) h \nu_{out}^* \epsilon^* e_{em} j^2 i \quad (7)$$

Detected intensity

An average flow J_{fl} of quanta per unit time from a dye molecule is detected under stationary illumination. It depends on the probability that the molecule is in its excited state and on the probability of emission to be detected per unit time, P_{em} . The population of the excited state depends on the probability of excitation per unit time, P_{ex} , and the variation in quantum efficiency near the silicon surface. Incorporating the correction for the quantum efficiency q_0 of the dye as presented in [53] and [10], the fluorescence intensity is calculated with:

$$J_{fl} = q_0 \epsilon P_{ex} \epsilon P_{em} \quad (8)$$

Optical model

For the analysis of the data, five homogeneous isotropic layers are assumed with: i) bulk silicon, ii) silicon dioxide ($d_{ox} = 10\text{-}150\text{nm}$), iii) extracellular medium, d_{cleft} , iv) cell membrane ($d_{mem} = 4\text{nm}$) and v) cytoplasm. Optical parameters for each layer were employed as described earlier with refractive indices $n_{ox} = 1.460$, $n_{cleft} = 1.333$, $n_{mem} = 1.450$, $n_{cyt} = 1.37$. The complex refractive index of silicon (refractive index n_{si} , attenuation index \cdot_{si}) was taken also as previously described [11]. The refractive index of silica with $n_{ox} = 1.460$ at 632.8 nm of the thermally grown oxide was used to determine the thickness of the oxide by ellipsometry.

With the 100 \times objective employed with either mercury or xenon lamp, the angle of aperture in water were 47.3 $^\circ$ for excitation at 546 nm and 48.6 $^\circ$ for emission at 580-640 nm, corresponding to numerical apertures 0.985 and 1.0 of the objective, respectively. The lower aperture for excitation was assigned on the basis of systematic measurements of fluorescence interference with supported lipid membranes [53]. The evaluation was based on the values with monochromatic excitation at $s_{in} = 546\text{nm}$ producing an emission spectrum $f(s_{out})$ used as measured in a 1 $^{-1}$ M ethanolic solution with a maximum at 565 nm. The spectrum of the quantum yield of detection $\Phi_{det}(s_{out})$ was given by the data sheet of the camera and the transmission of the dichroic mirror and the optical filter [11]. As specified in [10], with confocal FLIC microscopy, 60 \times objective was used. Its numerical apertures for excitation and emission were 0.68 and 0.72, respectively.

Fit of data

The intensity data obtained from the FLIC micrographs are fitted with three parameters:

i) the unknown distance d_{cleft} of the extracellular cleft between the cell and silicon chip, which affects mainly the phase of the wave $J_{fl}(d_{ox})$ of detected fluorescence,

ii) a scaling factor a of the fluorescence intensity, which determines the amplitude of the wave of detected fluorescence and

iii) a constant increment b ; which accounts for background fluorescence, originating in large part due to the upper side of the cell which was out of focus.

The values of the scaling factor and of the background were calculated from the data analytically. Then d_{cleft} is fitted with the function:

$$F(d_{\text{ox}}; d_{\text{cleft}}) = P_{\text{ex}}(d_{\text{ox}}; d_{\text{cleft}})P_{\text{em}}(d_{\text{ox}}; d_{\text{cleft}})$$

given by the optical theory for any setup which describes the observed photons per unit time according to [11][12][53]:

$$J_{\text{fl}} = a \cdot F(d_{\text{ox}}; d_{\text{cleft}}) + b \quad (9)$$

The regression algorithm of Powell adopting the estimate of the standard deviation of d_{cleft} from the Marquardt algorithm was employed for fitting [11].

Prerequisites, nature and evaluation of the method

The evaluation of the distance d_{cleft} requires homogeneous staining of the membrane and illumination, and assessment of homologous regions of cell adhesion on all four steps. The estimated precision of the averaged distance d_{cleft} due to systematic and stochastic errors is around 1 nm independent of its absolute value [11][12]. The technique attains lateral resolution of approximately 400 nm. Since the relevant modes of standing waves level out due to the large numerical aperture of the microscope, any perturbations by the upper membrane are negligible if its separation is larger than 0.5λ from lower membrane. Therefore, perturbations by the upper membrane is not negligible at flat regions of the cells such as lamellipodia. At the cell periphery, the upper membrane appears as fringes of alternating intensities.

A complete distance map can be evaluated on selected terraces by solving equation (9) for d_{cleft} after determining a and b on homologous sub-squares [12]. This process is most precise at high values of the slope,

$$dF(d_{\text{ox}}; d_{\text{cleft}}) = dd_{\text{cleft}} \quad (10)$$

The contrast with respect to height inverts with the sign of this slope; if it is positive, increased intensity corresponds to increased distance, otherwise increased intensity corresponds to decreased distance. This inversion in contrast enables the distance evaluation to be separated from a possible but improbable intensity variation from dye angle or inhomogeneous staining.

Chips

The chips used to harvest cells were prepared by microprocessing polished, n-doped (4-8 Ωcm) four-inch silicon wafers (100 surface). After cleaning the wafers by the standard RCA procedure, a homogeneous layer of silicon dioxide with a thickness of about 145 nm was grown thermally

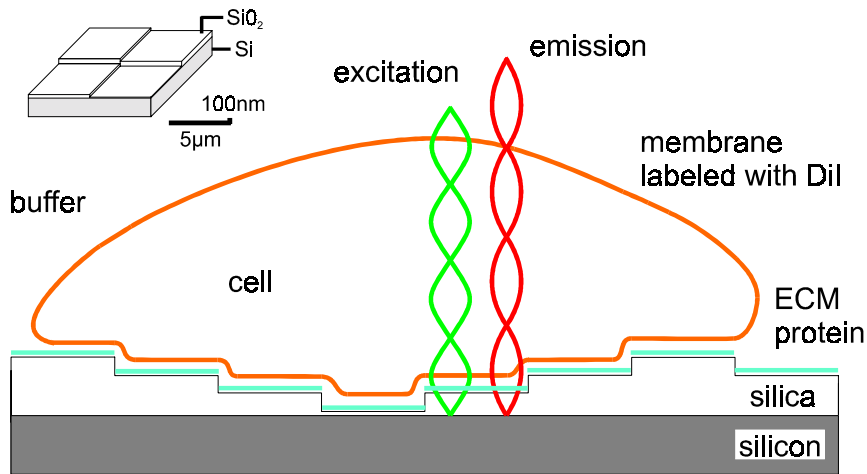


Figure 2.6: Schematic illustration of fluorescence interference contrast (FLIC) microscopy of a cell on checkered silicon chip (not on scale). A cell grows across microscopic terraces of silica coated with ECM protein. The height of the steps is about 50 nm, their width is 5 μm . The cell membrane is stained with a fluorescent dye, DiI₁₈. The fluorescence intensity depends on the position of the dye embedded in the cell membrane with respect to the standing modes of light.

in an oven at 1000 \pm C (E1200 Lab, Centrotherm, Blaubeuren). Photolithography was performed with a metal mask with stripes of 5 μm width at 10 μm interval. The silicon dioxide surface free of photoresist after development was etched in fluoric acid down to around 86 nm. The second photolithography was done by rotating the mask by 90 \pm followed by removal of oxide around 43 nm. The resulting wafer with a pattern of repeating squares with four different silicon dioxide thickness was cut into chips (3:4cm \times 1:0cm). The heights of the four oxide square layers of each side at 5 μm thus resulted to approximately 10-150 nm at equal intervals, as shown in an insert in figure 2.6. Before usage, individual chips were cleaned by immersing in H₂SO₄ and H₂O₂ (5:1) for 15 minutes and then rinsed by Quick dump rinsing. After drying, they were silanized with dichlorodimethylsilane in toluol. The final thickness of silicon dioxide layer was measured by an ellipsometer (SD 2000, Plasmos, München) using a refractive index $n_{\text{ox}} = 1:460$ at 633 nm. A quadruple of reference squares with a size 500 μm \times 500 μm arranged on the chip at a separation of 1 cm were used for this measurement.

Dye and photometry

A homolog of the amphiphilic trimethin-indocarbocyanine dye S27/DiI₁₈ (figure 2.7, left) was used which is a common dye employed as membrane marker [6]. Shortly before the measurement, stock solution of dye at 2.5-5 mM in ethanol was diluted in 0.05 M Tris-buffer solution (pH 7.4) to approximately 1 μM . The cell culture medium was exchanged with the solution containing DiI₁₈ dye, and the stained cells were examined immediately under fluorescence microscope up to 30 minutes after staining.

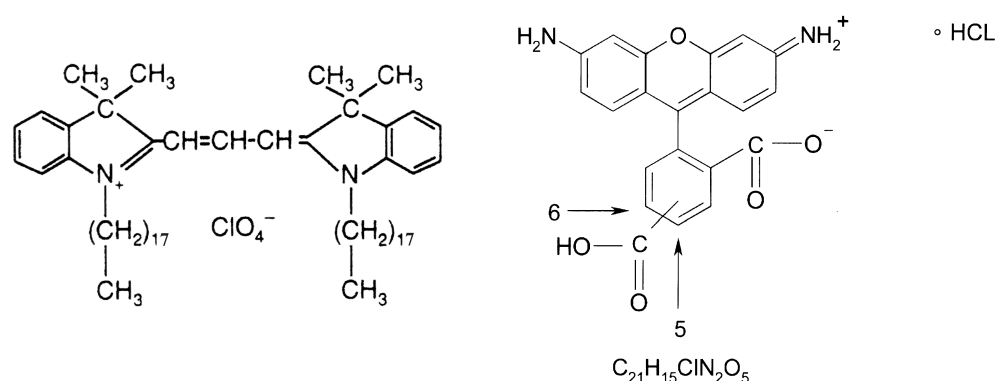


Figure 2.7: Left: Structure of DiIC₁₈ used to mark the cell membrane for FLIC microscopy. Right: Structure of the Rhodamine Green used in TIRAF microscopy.

The stained cells were observed with a water immersion objective (100 \times , numerical aperture 1.0, Axioskop, Zeiss, Oberkochen) using mercury/xenon lamp (Zeiss). DiIC₁₈ was excited monochromatically at 546 nm through a dichroic mirror (Q565LP, AHF Analysentechnik, Tübingen) and a bandpass filter (546/10 nm, 546FGS, Andover, Salem, NH). Its emission was detected at around 610 nm through a dichroic mirror and a bandpass filter (610/70 nm, AHF). EGFP was excited through a dichroic mirror (Q495LP, AHF) and a bandpass filter (HQ470/40, AHF) and observed through a bandpass filter (HQ510/20, AHF) which eliminated any emission by DiIC₁₈. The fluorescence images were obtained with a CCD camera with 752 \times 582 pixels (Sony chip ICX039AL, HRYX, Theta System, München).

Confocal FLIC microscopy was performed using the setup presented in [10]. DiIC₁₈ and GFP were excited by the laser beam at 488 nm and their emissions were simultaneously detected by 60 \times objective (numerical aperture 0.9 W, Olympus) through two separate channels with appropriate filters (610/70 and HQ510/20, respectively, AHF).

2.4 Total internal reflection aqueous fluorescence microscopy

Total internal reflection aqueous fluorescence (TIRAF) microscopy was performed as described in [32]. In this setup, the extracellular aqueous volume is stained with rhodamine green (Molecular Probes; Eugene, USA) (figure 2.7, right), which is excited by evanescent light generated under the condition of total internal reflection (figure 2.8). This condition is attained if a light beam in an optically dense medium strikes an interface to a medium of lower refractive index at an angle of incidence, μ_i , which exceeds a critical angle, μ_c .

2.4.1 Theory

Here the analysis is confined to the theory described in detail in [37] for the plane s-polarized wave traveling through a glass penetrating into a layer of water as evanescent wave. A beam of such light in glass (with a refractive index n_{glass}), incident at an angle μ_i encounters a planar boundary with water of index n_{water} . μ_i and the angle of transmission μ_t are related by Snell's law:

$$n_{\text{glass}} \sin \mu_i = n_{\text{water}} \sin \mu_t \quad (11)$$

As the angle of incidence increases, a critical angle, μ_c is reached where the angle of transmission is 90° . The critical angle is determined by rearranging Snell's law for $\mu_t = \frac{\pi}{2}$:

$$\mu_i = \mu_c = \sin^{-1} \left(\frac{n_{\text{water}}}{n_{\text{glass}}} \right)$$

Since $n_{\text{water}} < n_{\text{glass}}$, μ_t becomes imaginary for $\mu_i > \mu_c$, where

$$\sin \mu_t = \frac{n_{\text{glass}}}{n_{\text{water}}} \sin \mu_i$$

and in the expression for phase factor of the transmitted light becomes:

$$\cos \mu_t = \sqrt{1 - \left(\frac{n_{\text{glass}}}{n_{\text{water}}} \right)^2 \sin^2 \mu_i}$$

Thus reflectivity at the glass/water interface reaches unity as the incident angle μ_i approaches the critical angle, μ_c , and the light emerges in a direction tangent to the boundary. This way total internal reflection occurs at angles greater than μ_c , where no light enters the second medium but all light reflects back into the first medium. However, the electromagnetic-field in the second medium does not disappear, but instead appears as evanescent field as some of the incident energy penetrates through the interface. This evanescent wave propagates parallel to the surface in the plane incidence as a harmonic wave in the low-index medium. Since its energy decays exponentially with the distance from the interface, emission from fluorescent molecules dissolved in the second medium can be stimulated by the evanescent wave in a very restricted zone with a penetration depth:

$$d = \frac{1}{4k} \left(n_{\text{glass}}^2 \sin^2 \mu_i - n_{\text{water}}^2 \right)^{1/2} \quad (12)$$

Transfer of the electrical energy to the dyes in a thin layer in a multilayer system of a cell cultured on a glass substrate is considered in the following section.

Transmitted light through a multilayer system

Mathematical expressions for the electrical energy in the cell-glass gap from Maxwell's equations under conditions of total internal reflection illumination are described in detail in [37]. They have discussed all the conditions likely to arise at the cell contacts assuming a layer system as

illustrated in figure 2.9. Among the four situations presented, we have considered the two cases; (a) the waves in all the layers above the glass substrate are evanescent (decaying) and (b) the wave is continuous (propagating) in membrane and again evanescent in cytoplasm. The squared amplitude of calculated $E(z)$ is proportional to electrical energy at a particular depth, z in the water gap, thus the stimulated fluorescence is proportional to the local electric field energy. Thus $j E(z) j^2$ can be expressed according to the simple exponential. The detected fluorescence from underneath a cell is given by a general expression:

$$F(d_{\text{cleft}}) = \frac{A_i}{\cos \mu_{d_1}} \int_{d_2}^{\infty} \hat{A}(z) \hat{\otimes}(z) c(z) j E(z) j^2 dz \quad (13)$$

and of the background fluorescence at a nearby area without a cell:

$$F_1 = \frac{A_i}{\cos \mu_0} \int_0^{\infty} \hat{A}(z) \hat{\otimes}(z) c(z) j E(z) j^2 dz \quad (14)$$

where $\hat{A}(z)$ is the quantum efficiency of the fluorophore, $\hat{\otimes}(z)$ and $c(z)$ are molar extinction coefficient and concentration of the fluorophores. $\frac{A_i}{\cos \mu}$ is the interfacial area of illumination written in terms of the cross-sectional area of the incident beam A_i . The analysis of our experiments bases on the following assumptions;

- i) no fluorescence is stimulated from the aqueous medium beyond the cell,
- ii) the quantum efficiency and the extinction coefficient of the fluorophore are independent of the proximity to the totally reflecting interface and spatial orientation, i.e. $\hat{A}(z) \hat{\otimes}(z) = \hat{A} \hat{\otimes}$;
- iii) the fluorophore distribution between the limits is homogeneous, $c(z) = c$.

The assumptions ii) and iii) constitute an ideal case, ignoring spatial variations in fluorescence emission resulting from fluorophore orientation with respect to the incident beam, fluorophore proximity with respect to the substratum interface, and molecular aggregation of fluorophore molecules. Thus the expressions (13) and (14) simplify to:

$$F(d_{\text{cleft}}) = QMSI(d_{\text{cleft}})$$

$$F_1 = QMSI(1)$$

and the relative fluorescence would be:

$$G(d_{\text{cleft}}) = \frac{I(d_{\text{cleft}})}{I(1)} \quad (15)$$

Numerical derivation of the cell-substrate distance

Although the exponential expression for the amplitude of the transmitted electric field and the integral for the fluorescence emission at the dielectric interface are exact solutions to the field equations, the expressions are cumbersome to apply to determine the cell-substrate separation. In most cases, an approximation is made by simplifying the model layer system or expressions for the fluorescence [14][13]. The values of the decaying evanescent field closely follows a general

form:

$$T(z) = T_{\text{eff}}(0) \exp(-jz/d_{\text{eff}})$$

which can be substituted into the integrals (13) and (14) for $j E(z) j^2$ [72]. In a case with membrane marking, a fit of membrane fluorescence can be performed by assuming that the effective values for the transmitted interfacial amplitude squared, $T_{\text{eff}}(0)$, and the depth of penetration, d_{eff} , are independent of water gap thickness. This assumption is however, not valid for the case of fluorescence in water gap, since $T_{\text{eff}}(0)$ and d_{eff} vary with water gap thickness.

An exact evaluation of this value is presented in [43], where the true field distribution is obtained numerically. For quantitative evaluation, we have observed cell adhesion under TIRAF for incident light with the electric vector parallel to the surface (s-polarized), and determined cell-substrate distance based on their algorithm. The s-component was chosen to minimize birefringent effects by restricting the excitation radiation to TE polarization that is parallel to the net membrane molecular orientation, since the optical axis of lipid membranes is normal to the membrane surface. The equation (15) for the ratio $G(d_{\text{cleft}})$, of the fluorescence from the layer between lower cell membrane and the substrate, $I(d_{\text{cleft}})$, to that from the whole evanescent wave I_1 cannot be rearranged to yield d_{cleft} . Here, measured ratio, GM , is fitted to theoretically determined ratio G as described in [37], in order to obtain d_{cleft} by numerical evaluation. Employing the algorithm from Heavens:

IF $GM - G > 0$ THEN $d_{\text{cleft}} = d_{\text{cleft}} + 10$

IF $GM - G < 0$ THEN $d_{\text{cleft}} = d_{\text{cleft}} - 1$

IF $GM - G > 0$ THEN $d_{\text{cleft}} = d_{\text{cleft}} + 0.1$

an estimation of d_{cleft} with an accuracy of 0.1 nm can be attained. This process seeks for a theoretical value G closest to the measured ratio by varying the parameter of interest, d_{cleft} . A set of values of I_1 for each image was used to extrapolate accurate values at each position $I(d_{\text{cleft}})$, by fitting a Gaussian curve that takes into account the aperture correction. We have obtained G either for the cases (a) or (b) presented in [37] depending on the model layer system used.

Fluorophore, substrates, photometry

Fibroblast cells prepared under the same condition as for FLIC microscopy were cultivated on glass slides (24mm \times 60mm \times 1mm) coated either with fibronectin or laminin. These glass slides were cleaned and silanized in advance as described for silicon chips. After incubating the cell culture for several hours, the culture medium was exchanged for PBS with rhodamine green, a membrane impermeable molecule (figure 2.7, right) dissolved at 50 μ g/ml and maintained at 37 \pm C shortly before measurements.

In order to quantitatively analyze the cell-substrate distance, the experimental setup for a stationary TIRAF as described in [32] was employed. An air-cooled argon-ion laser (PS, AR, Model

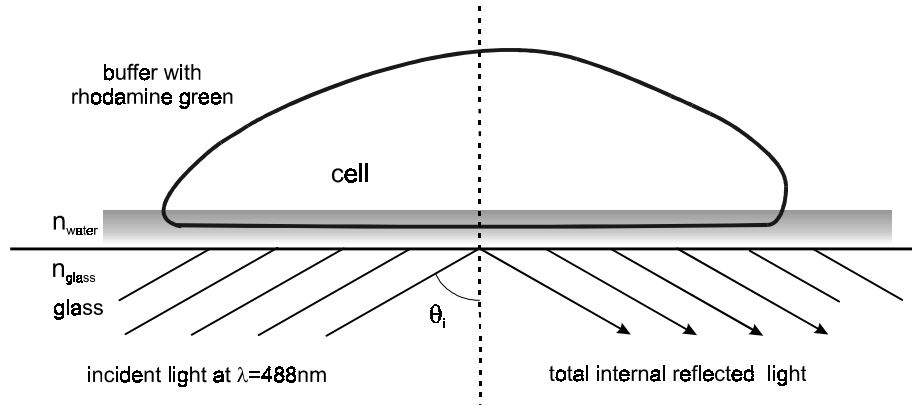


Figure 2.8: Schematic drawing of a cell adherent to the glass interface that is illuminated by the evanescent wave of a total internal reflected light beam.

532, Omnicrome, USA) was used at output power of 11 mW. The generated coherent light at 488 nm was linearly polarized and passed through a set of neutral density filters (Newport GmbH, Germany) in order to set the correct irradiation intensity. The laser beam was further guided by highly reflecting mirrors and with a reduced area of illumination produced with a help of a converging lens (Newport GmbH, Germany) directed into an inverting prism (BK7, Spindler & Hoyer, Germany) so that incident angle is 68.285^\pm . We coupled a glass slide with index of refraction at $n = 1.52224$ to a prism (BK7) with oil. With this setup, the decay length estimated according to the equation (12) for depth of penetration estimates to 82.6 nm with $n_{\text{glass}} = 1.52224$ and $n_{\text{water}} = 1.337$. The fluorescence signal collected through an infinity-corrected oil immersion objective (60 \times) with a numerical aperture 1.4 was passed through a tube lens with a focal length f ($f = 200; 250; 300; 400$; Spindler & Hoyer, Germany). The image was focused onto a CCD chip of a camera system with 12-bit dynamic range and a readout frequency of 12.5 MHz (CCD, Visicam 1280, Visitron Systems GmbH, Germany) after passing through a long-pass interference filter (Andover Corp. Lot/GmbH, Germany) for separating fluorescence from scattered incident light. Spatial resolution of the microscope attained in this setup is described in [32]. Briefly, the object resolution, RL in terms of the numerical aperture NA is given by:

$$RL = \frac{0.61 \lambda_{\text{ex}}}{NA}$$

from which $RL = 212:6$ at laser wavelength of $\lambda_{\text{ex}} = 488\text{nm}$ and a numerical aperture $NA = 1:4$ of the objective is obtained. Taking into account Nyquist's sampling theorem, the total microscope magnification M of a diffraction-limited image is given by:

$$M = \frac{2(\text{pixel size})}{RL}$$

from which $M = 63$ is obtained with above RL and $6:7^1\text{m} \in 6:7^1\text{m}$ as pixel size of the CCD chip.

2.5 Interference reflection microscopy

Since introduced by Curtis [21], interference reflection microscopy (IRM) or reflection interference contrast microscopy (RICM) [93] has been mainly used to study cell motility and cell-substrate contacts [7][8][76]. In this technique, images are formed by the interference among the reflection of light at interfaces between media of different refractive indices.

2.5.1 Theory

In a multilayer system, incident light at each interface of changing index of refraction is partially reflected. From the second interface, the incident light is the transmitted light from the previous interface, whose strength depends on the optical property of the previous layer. The reflection of transmitted light repeats for each interface which reaches the detection layer as a superposition among all the reflected light rays. A multilayer system used in this study is illustrated in figure 2.9. The computation to describe interference among the reflected light rays consists of forming the vector sum for all waves in medium n_{glass} that have been reflected from the different interfaces of the multilayer above. We have calculated the interference for layered homogeneous multiple thin films based on the optical theory described previously for FLIC microscopy. As stated in [9] and [41], all the waves present within each layer can be described by transfer matrix obtained in terms of the other interfaces. Using a model for the multilayer system with known thicknesses and refractive indices of each film, the reflection coefficients are determined by multiplying all the transfer matrices, M_j (defined by equation (1) in the previous section for FLIC microscopy) of each layer above the glass surface (detection layer):

$$M = \prod_{j=1}^{N_i-1} M_j = \begin{pmatrix} m_{11} & m_{12} \\ m_{21} & m_{22} \end{pmatrix}$$

Effective Fresnel coefficients of the light ray emerging into the glass substrate is determined by:

$$r = \frac{(m_{11} + m_{12} \zeta p_{\text{medium}}) \zeta p_{\text{glass}} - (m_{21} + m_{22} \zeta p_{\text{medium}})}{(m_{11} + m_{12} \zeta p_{\text{medium}}) \zeta p_{\text{glass}} + (m_{21} + m_{22} \zeta p_{\text{medium}})}$$

for both TE and TM, with the elements of the transfer matrix and p_r as described also for FLIC theory. Setting the incident light intensity as I_0 , the detected light becomes:

$$I(\mu; \zeta) = I_0 \zeta \int_j r^{\text{TE}} j^2 + j r^{\text{TM}} j^2 \mu$$

which is integrated in the glass over the aperture for each ray independently to obtain the total intensity of the reflected light:

$$I(\zeta) = \int_0^{\mu_M} I(\mu; \zeta) W(\mu) d\mu$$

where $\mu_M = \sin^{-1}(NA=n_{\text{glass}})$, based on a rectangular profile function as described in [70]. To take into account the fact that relatively more light reaches the focus of the objective from larger

angles, and also to convert from a two-dimensional distribution to a cone of incident light, an aperture weight function $W(\mu) = \sin \mu$ is employed as discussed in [38] and also described for FLIC theory. In the analysis, the relative intensity between the reflected light at the region with and without cell, I_{cell} and $I_{\text{background}}$ was employed:

$$\frac{I_{\text{cell}}}{I_{\text{background}}} = \frac{R_0^{\mu_M} \int_0^{\pi} j r_{\text{cell}}^{\text{TE}} j^2 + j r_{\text{cell}}^{\text{TM}} j^2 W(\mu) d\mu}{R_0^{\mu_M} \int_0^{\pi} j r_{\text{background}}^{\text{TE}} j^2 + j r_{\text{background}}^{\text{TM}} j^2 W(\mu) d\mu} \quad (16)$$

The relative intensities from chosen model systems were calculated setting the optical parameters as listed in figure 2.9.

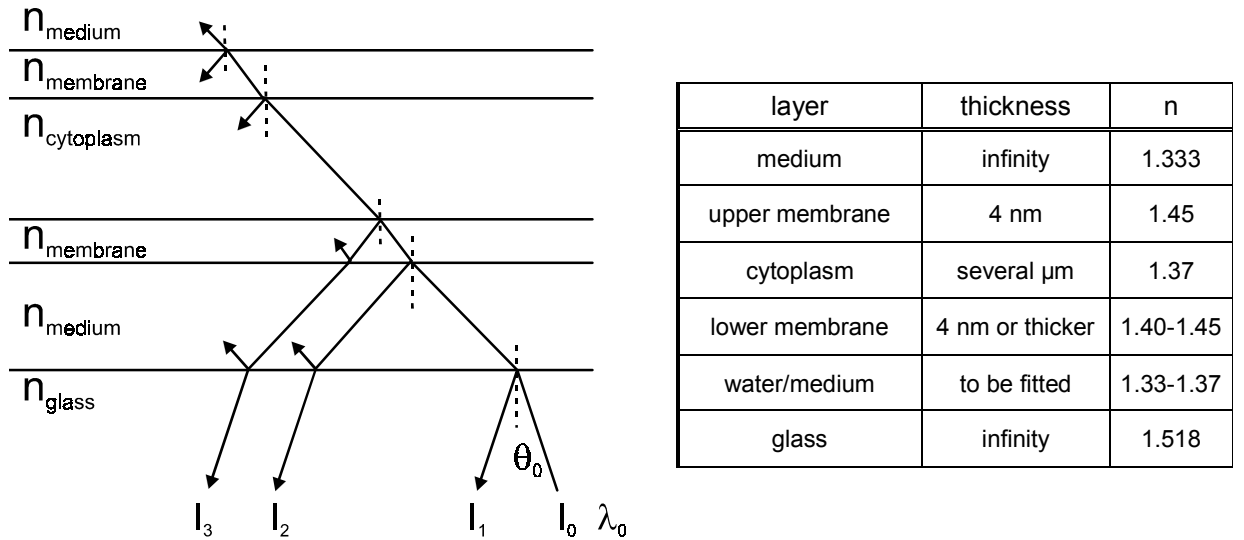


Figure 2.9: Left: A multilayer system used for all the optical techniques. For FLIC microscopy, glass is replaced by a silicon with thin layer of oxide. In IRM, interference among all the reflected lights from each interface with changing index of refraction that emerges into the glass substrate is detected. Right: Parameters for the multilayer system used for the analysis of cell-substrate distance.

2.6 TIRAF-IRM-fluorescence microscopy

A direct comparison of the two techniques, TIRAF and IRM, was done by obtaining images of the cells expressing ECFP-vinculin with the both techniques sequentially. For this purpose, we used an inverted microscope (Zeiss Axiovert 100, Germany) equipped with a reflector slider antiflex with integrated polarization/analyzer system, a technique based on the principle of reflection contrast, to separate stray light from detected light [68][70]. Fibroblasts transfected with ECFP-vinculin a few days in advance were prepared as described in the previous section. For the experiments, the cells were cultured in a plexi-ring fixed on a glass coverslip

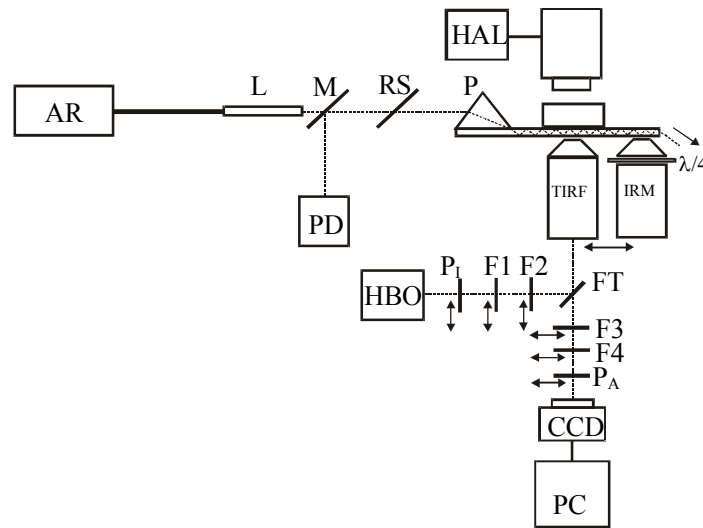


Figure 2.10: Microscope setup used for TIRAF-IRM-fluorescence microscopy. For TIRAF microscopy; AR: argon-laser, L: fiber optics, M: mirror, RS: rotary stage, P: prism, PD: photodiode, F3: longpass filter (LP520). For IRM; HBO: mercury arc lamp, P_1 : polarizer, F1: interference and color glass filter, FT: beam splitter, P_A : analyzer. For CFP-vinculin fluorescence microscopy; F2: bandpass filter (425/40), FT: dichroic mirror (460LP), F4: bandpass filter (470/30). (adapted from Geggier and Fuhr, (1999))

(24mm \times 60mm \times 0:17mm) which were cleaned, silanized and coated with fibronectin or laminin. Shortly before the measurement, the culture medium was exchanged with PBS containing 50 μ g/ml of rhodamine green maintained at 37 \pm C.

First, a cell expressing ECFP-vinculin was selected under fluorescence microscope through an objective with a magnification 63 \times and a numerical aperture 0.8. An image was made with a white light illumination for the purpose of recognizing the cell again for subsequent TIRAF microscopy. Then the 488 nm laser beam was directed into a prism coupled onto one side of the glass coverslip beside the plexi-ring with the cell culture and TIRAF image was captured. Subsequently, the objective was exchanged with an oil immersion ANTIFLEX objective (Plan-Neofluar 63/1.25 Oil Ph3 Antiflex) and the sample was illuminated with a mercury arc lamp (HBO 50W) in order to obtain an IRM image. Monochromatic light of $\lambda = 577:0\text{nm}$ was isolated by a combination of an interference and a colored glass filter (03 FIM 008 and OG 570, Melles Griot). The light passes through an integrated polarizer and reaches the sample through $\lambda/4$ plate on top of the objective as circular polarized light. The interference of the reflected light becomes again linear polarized through the $\lambda/4$ plate, thus selectively observed through a beamsplitter and then an analyzer [68][70]. Subsequently, a ECFP-vinculin image at the identical focus position was made using a filter combination of a bandpass filter (HQ 425/40) for ECFP excitation and a dichroic mirror (Q 460LP, AHF) to separate the excitation and emission, and a bandpass filter (HQ 470/30) to detect the emitted fluorescence. A schematic diagram of the experimental setup is shown in figure 2.10.

Chapter 3

Cell-substrate separation

Cell-substratum distances of fibroblast cells cultivated on silicon chips coated with various ECM proteins were determined using FLIC microscopy. Most culture dishes contained to a certain extent, mixed population of various cell shapes even when they were plated on the substrate coated with the same protein. Cultured in medium without serum, the cells however exhibited distinct adhesion properties depending on the coating. This explicit morphological characters facilitated by the attachment to various ECM proteins confirm the specificity of cell-ECM interactions. The average cell-substratum distances from FLIC microscopy calculations for each ECM protein are shown in table 3.1. There were large deviations among the cells in the measured distances as well as in the morphologies in each culture sample as seen in a histogram of figure 3.15.

3.1 Fibronectin

On fibronectin, the cells were pinned out developing smooth contour line along the cell periphery, and adhered on the surface with homogeneous lower cell membrane. Both fibroblasts and cells in neuronal cultures separated at around 50 nm from the substrate. In GD25- β 1A cells, fibronectin preferentially bind to integrin α v β 3, but also to α 3 β 1 and α 5 β 1.

Fibronectin facilitated broad spreading of the cell body, which enhanced much larger attachment area than on laminin. Almost no structure like lamellipodia was found among these cells. The cells were already spread out smoothly 30 minutes after plating on the substrate as shown in figure 3.3 (left). Most cells extended very smooth contour around the cell body with some sparse long and thin filopodia-like extensions. Many cells remained flat and smooth against the substrate during the first few hours of cultivation in medium without serum (figure 3.1). Some of the cells with smooth contour exhibited very little filopodia.

The cells cultivated for longer time on fibronectin often formed parallel membrane ruffles (figure 3.3, right). Some of these structures developed between the substrate and the membrane appeared like vesicles budding away from the cell membrane. Many cells also began to develop very short hairy protrusions along the cell periphery and also rather irregular cell shapes. Most cells during the first few hours of cultivation were pinned out in all directions as if the cell bodies were stretched out with these forces at equilibrium. After certain length of incubation time, there

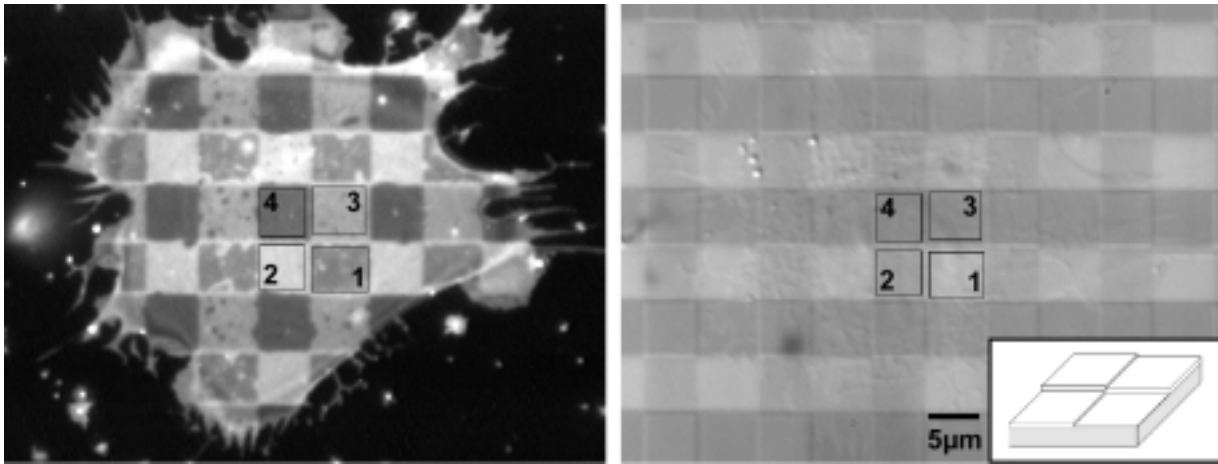


Figure 3.1: An example of a GD25- β 1A cell attached to fibronectin-coated silicon chip for about 1.5 hours. Left: FLIC micrograph of the cell stained with DiI $_{C18}$. The areas used to measure fluorescence intensities for distance calculation are labeled with boxes and corresponding microscopic oxide terraces (heights from 1-4; 17.0 nm, 57.0 nm, 1057 nm, 147.9 nm). Right: Reflection micrograph with closed Abbe condenser used to distinguish and assign the terraces 1, 2, 3 and 4 as sketched in the insert. Theoretical curve fitted to the data points are illustrated in the next figure. The cells attached to fibronectin in general appeared like a cloth pinned out on a flat surface.

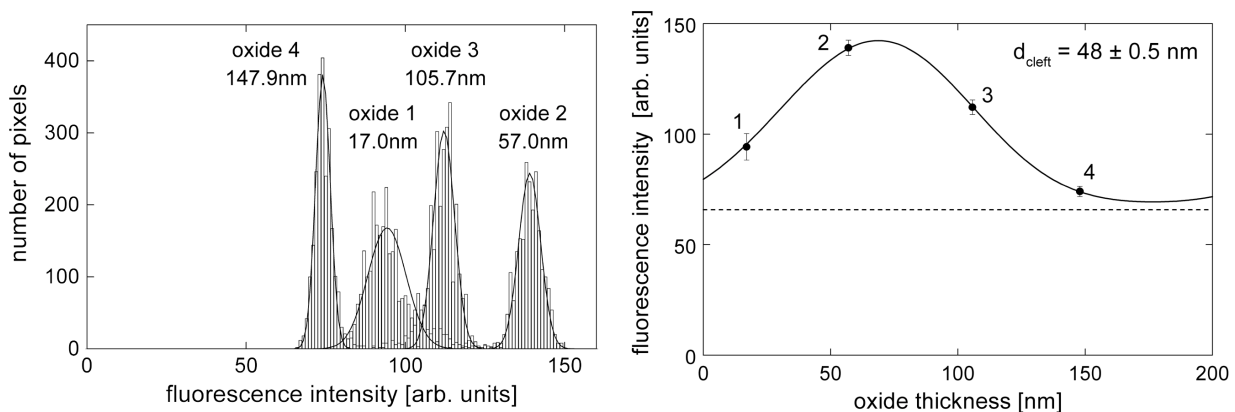


Figure 3.2: FLIC theory of the cell shown in the previous figure. Left: A theoretical curve with an average distance between membrane and substrate $d_{\text{cleft}} = 48 \pm 0.5 \text{ nm}$ is fitted to the fluorescence intensities measured at regions on each oxide step as labeled with boxes in the previous figure. Right: Histograms of the fluorescence intensities within each of the labeled boxes 1, 2, 3 and 4 fitted by Gaussians.

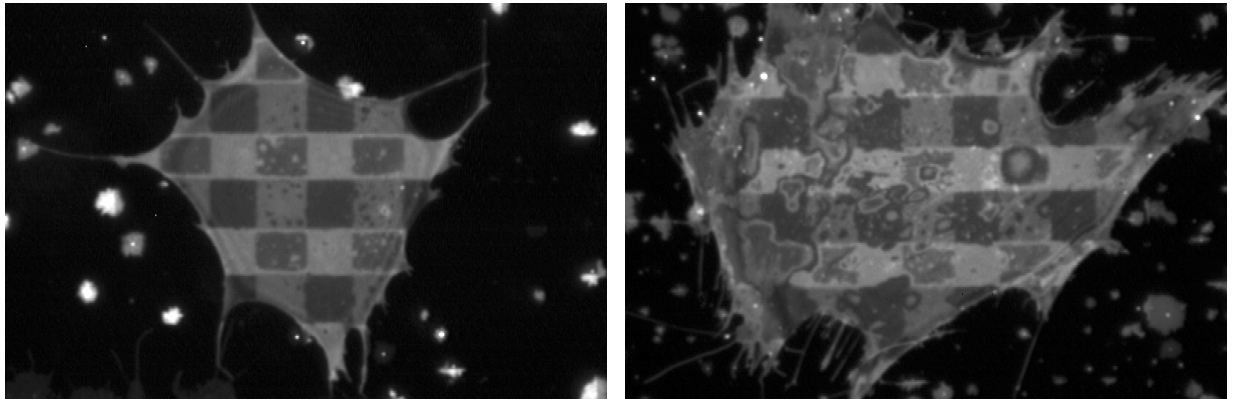


Figure 3.3: *GD25-β1A cells plated on fibronectin-coated silicon for 30 minutes (left) and 3 hours (right) after resuspending in medium without serum. The interaction with fibronectin clearly enhances prominent cell spreading relative to laminin. After a few hours of incubation, the cells on fibronectin also lost smooth attachment and began to develop regions of larger cell-substrate distance, often over the whole membrane surface.*

were notably many cells which lost the balance of stretching forces and began to develop patches of detachment. These cells gave the impression of motile cells, where the reorganization of cytoskeletal structure may be responsible for the perturbation of the spanned smooth membrane. These ruffles aligned parallel to one another throughout the cell attachment surface, often seen after longer incubation may be due to the pulling and stretching thought to take place in cell migration. In contrast, the distance measurement by FLIC microscopy of cultures after various length of time showed neither significant difference in the width of distribution nor in the mean value. However, in many cases it became difficult to perform FLIC analysis of the distance because of the rough membrane after longer incubation.

Reducing the fibronectin molecule by constructing a recombinant module of cell adhesion domains 7-10 unexpectedly did not change the cell-substrate separation (left histogram in figure 3.4). Further, the cell morphology alone appeared unaffected in spite of the absence of second cell attachment domain near the carboxy-terminus of the molecule (figure 1.1). However, if the recombinant molecule contained a mutation in the RGD sequence that is considered to be recognized by integrins in cell attachment to fibronectin, there was an apparent change in the membrane structure. Although many cells indeed were able to adhere to the silicon chip coated with the recombinant molecules with a mutation, the ventral cell membrane was not spanned as smoothly as on the wild-type recombinant module or the full fibronectin molecule.

Variation in separation distances among the substrates could arise from specific integrin subunits involved in the interaction between the cell membrane and the ECM molecules. For instance, attachment of GD25-β1A cells to laminin is mediated mainly by $\alpha 6\beta 1$ integrin heterodimer, whereas both $\beta 1$ and $\beta 3$ integrin subunits are involved in the interaction with fibronectin. A

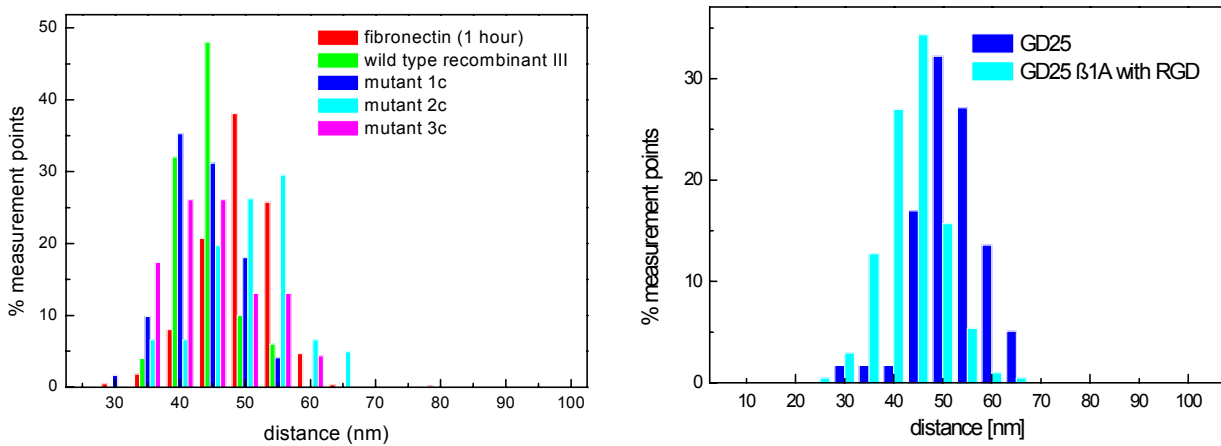


Figure 3.4: *Left: Histogram of GD25-β1A cells cultivated on fibronectin, recombinant of fibronectin module III 7-10 wildtype and its mutants, 1C, 2C, 3C. No obvious difference among the distances from the recombinant modules were found. Right: Distances measured for GD25 cells cultivated on fibronectin and for GD25-β1A cells also on fibronectin, but in the presence of RGD peptide; i.e.: comparison between β3 and β1 integrin subunit binding to fibronectin.*

comparative experiments between the attachment of GD25 cells to fibronectin, which lack β1 integrin subunit expression, and the attachment of GD25-β1A cells to fibronectin in the presence of RGD peptides were performed. The RGD peptides preferentially bind to β3 integrin subunit, thus enables isolation of the integrin β1-fibronectin interaction in GD25-β1A cells. This way, a comparison was made between the distances stretched by β3 integrin-fibronectin (in GD25) and β1 integrin-fibronectin (in GD25-β1A with RGD peptides) interactions. No apparent difference between the distances spanned by β1 and β3 integrin subunits was observed (right histogram in figure 3.4).

3.2 Laminin

In the case where the cell attachment was through interaction with laminin, the cell-substrate separation measured was on average 100 nm for both fibroblasts and neuronal cultures [12]. In order to avoid the effect of multiple molecular stacking of laminin between the cells and the substratum, FLIC microscopy was repeated with lower laminin coating concentrations. There was no change in the distances among cultures on laminin coated at various concentrations (left histogram in figure 3.5). Optical measurement of adsorbed laminin thickness performed in the condition without cells and in a dried state has yielded approximately 3-4 nm. The cell-substratum distance was subsequently measured using the same laminin-coated silicon chip after rehydration, which still yielded around 100 nm [12].

On laminin adsorbed silicon chip, GD25-β1A cells stretched thin, needle-like filopodia but hardly any lamellipodia during the first hour. The cells were able to attach to the laminin-coated sili-

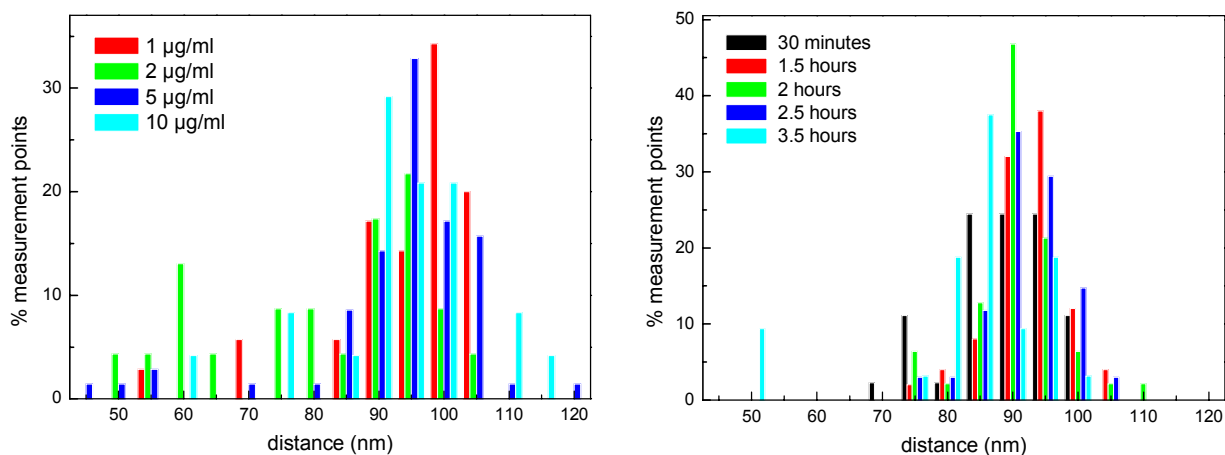


Figure 3.5: Histograms of distances measured by FLIC microscopy with GD25- β 1A cells plated on laminin-coated silicon at various laminin concentrations (left) and cells plated for various lengths of time (right). The laminin concentrations depicted are the concentration at which the silicon chip was incubated overnight in PBS with laminin. The cells were prepared as described previously and cultivated in medium without serum mostly for approximately one hour till they were observed by FLIC microscopy, unless otherwise stated as in the case of experiments in determining the time-dependency (right histogram).

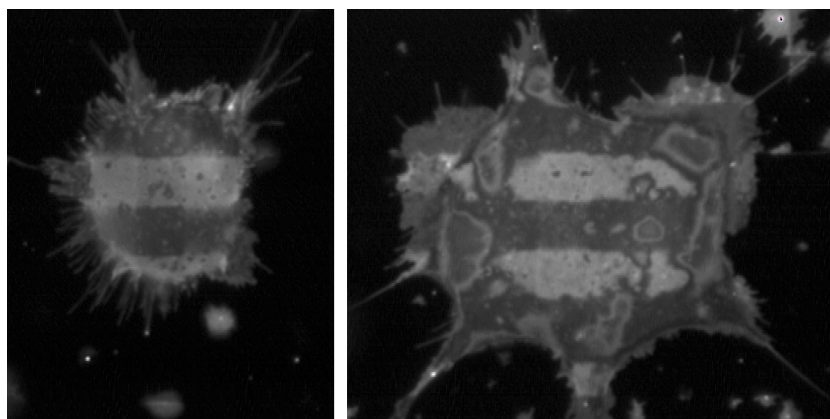


Figure 3.6: GD25- β 1A cells allowed to adhere on laminin for 30 minutes (left) and 3 hours (right) after resuspending in medium without serum. During the first hour the cells attached with flat membrane on the surface before spreading. In the cell culture incubated for longer than a few hours already contained many cells with rough structures specially at the cell periphery.

con within half an hour of incubation, however many were still rounded, typically appeared unspread as shown in figure 3.6 (left). During the first one hour of cultivation, they attached to the substrate with smooth membrane surface (figure 3.7). Cells cultivated on laminin for longer than one hour began to possess very rough membrane structure, first in the vicinity of cell periphery, leaving the center of the cell body rather flat on the substrate surface. The ventral surface often

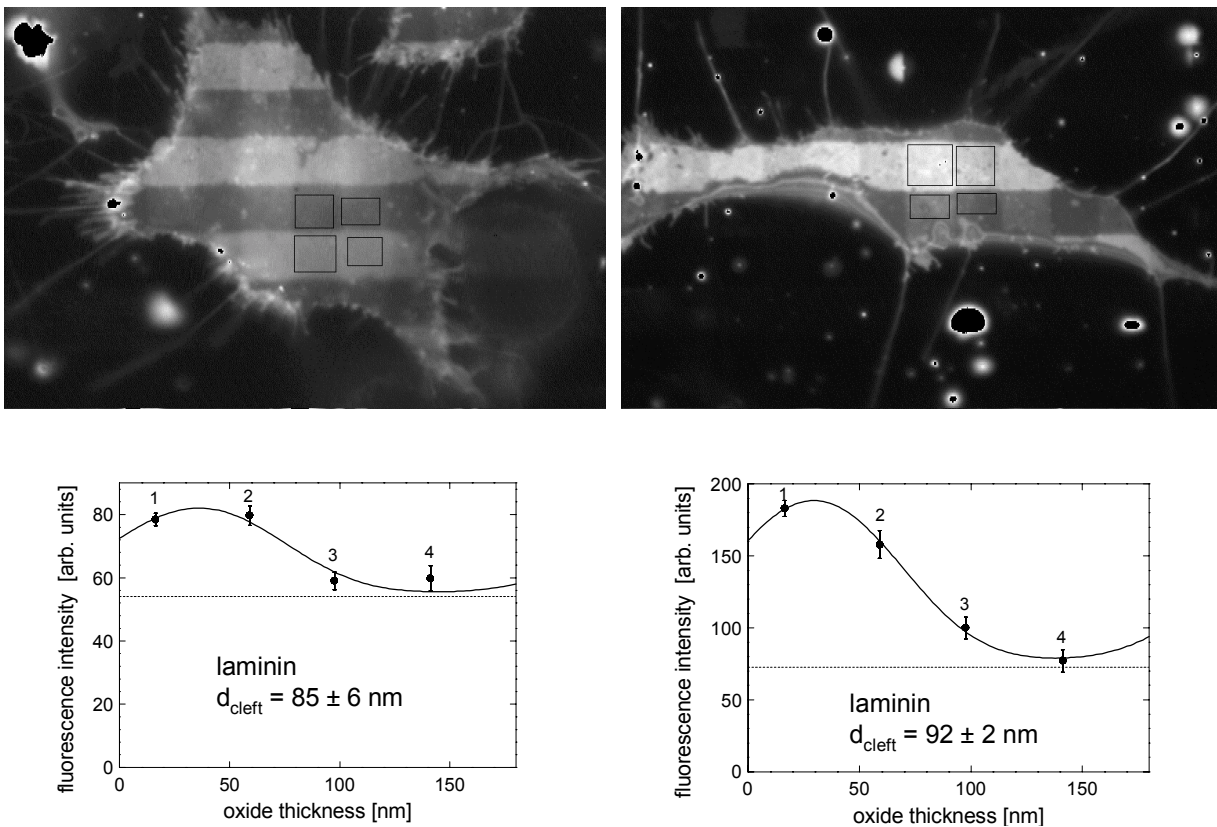


Figure 3.7: Typical GD25- β 1A cells attached to laminin-coated silicon chip (top). Analysis of distances for the corresponding cells are done based on the fluorescence intensities within the four rectangular regions fitted to the theoretical curves (bottom). The fluorescence from DiI C_{18} are the brightest on oxide 1 and 2 when the dye molecules embedded in the membrane are around 100 nm away from the silicon.

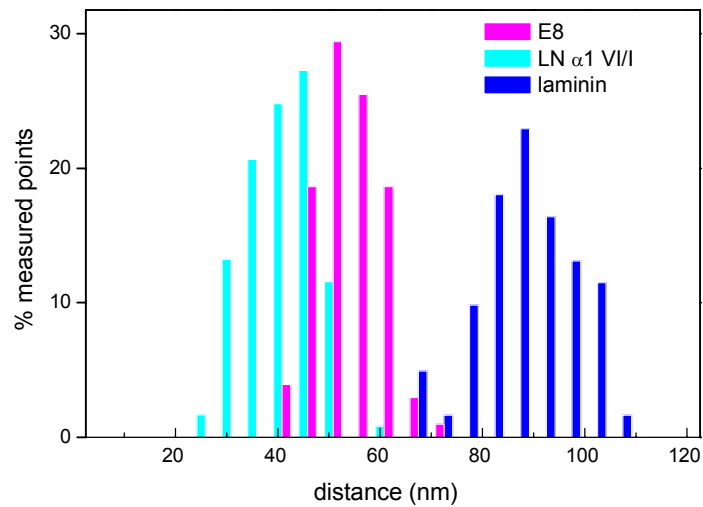


Figure 3.8: FLIC microscopy performed on GD25- β 1A cells cultivated on laminin and its fragments, E8 and LN[®]1 VI/V. The distance was considerably reduced when the cells were plated on only a fragment of the whole laminin molecule, to the values corresponding to the fragment size.

became no longer flat throughout the adhesion area, instead it formed ruffles and often patches of larger separation from the substrate. Such inhomogeneous membrane structure along the cell periphery around the smooth attachment area at the center of the cell bodies eventually formed lamellipodia-like structures (figure 3.6, right). After longer incubation than 2-3 hours, some cells began to lose the flat adhesion area even at the center. In spite of the morphological changes after longer incubation, the cell-substratum distance was still maintained at around 100 nm as shown by the right histogram in figure 3.5.

Reducing the laminin molecules down to smaller fragments retaining their cell adhesion property have yielded considerably smaller cell-substratum separation (figure 3.8). Attachment to a cell growth and adhesion promoting elastase fragment of laminin, E8, which consist of the carboxy-terminus long arm from all three laminin chain resulted in average separation of 52 nm. On a fragment obtained from the [®] chain of laminin, LN[®]1 VI/V, the distances were slightly smaller at around 40 nm. The cells were able to attach with homogeneous surface on the substrate coated with such fragments of laminin molecule, but most of them did not spread a large attachment area (figures 3.9 and 3.10). Some long filopodia similar to that of cells cultivated on full laminin molecules were still present on laminin E8 and LN[®]1 VI/V. Also, many short filopodia-like protrusions were found along the cell periphery. On E8 fragment, the cell body possessed strange round overall shape, however, the cells had surprisingly smooth ventral membrane surface. The cell periphery appeared quite thin due to the extensive lamellipodia, indicating that the upper and lower membrane were almost glued together. The cells attached to LN[®]1 VI/V had many short hair-like protrusions at regular intervals along the periphery, but hardly any lamellipodia was observed. Most cells were attached with very smooth membrane except for some distinct

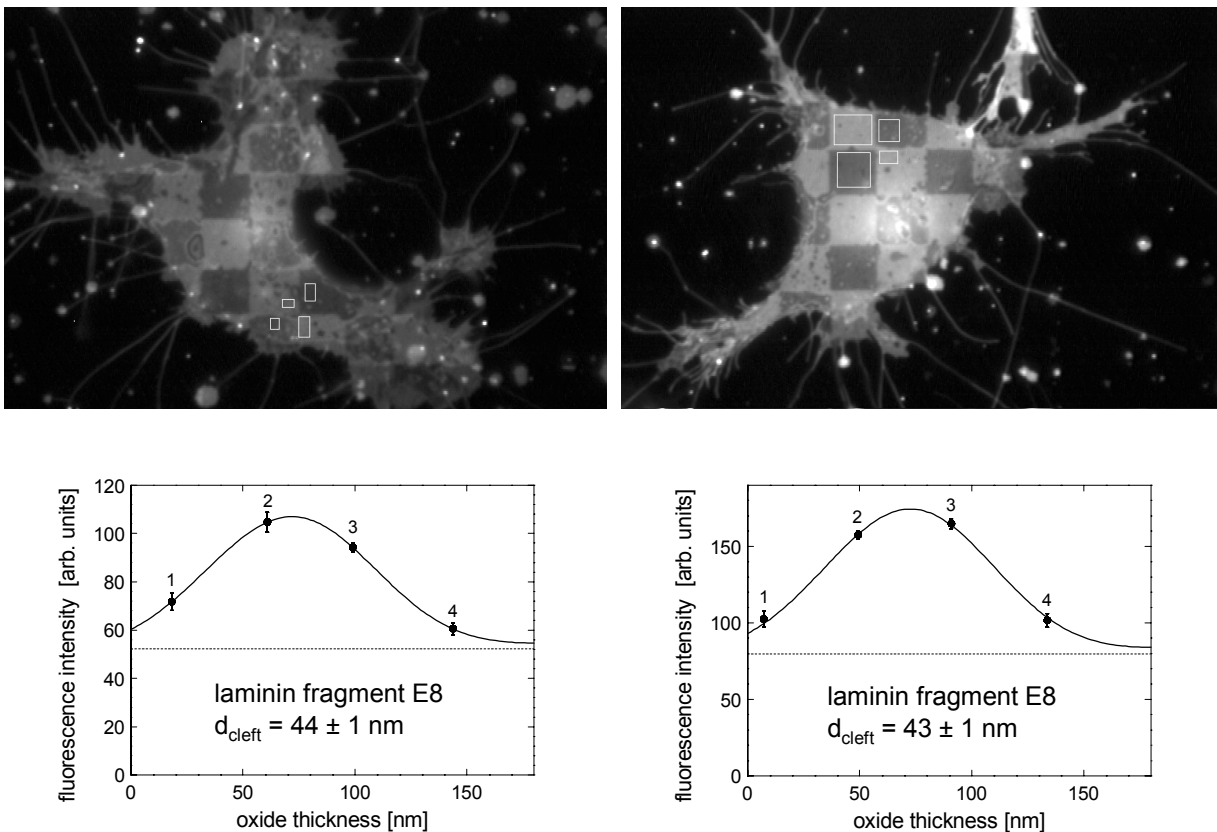


Figure 3.9: Typical morphology of GD25-β1A cells cultivated on laminin fragment E8 (1 hour) in medium without serum (top). Corresponding distance analysis by FLIC microscopy are shown underneath each figure. The ventral membrane surface is much closer to the substrate than that of the cells on whole laminin molecule. Now, the regions on oxide 2 and 3 are the brightest, which correspond to distances in the range around 50 nm.

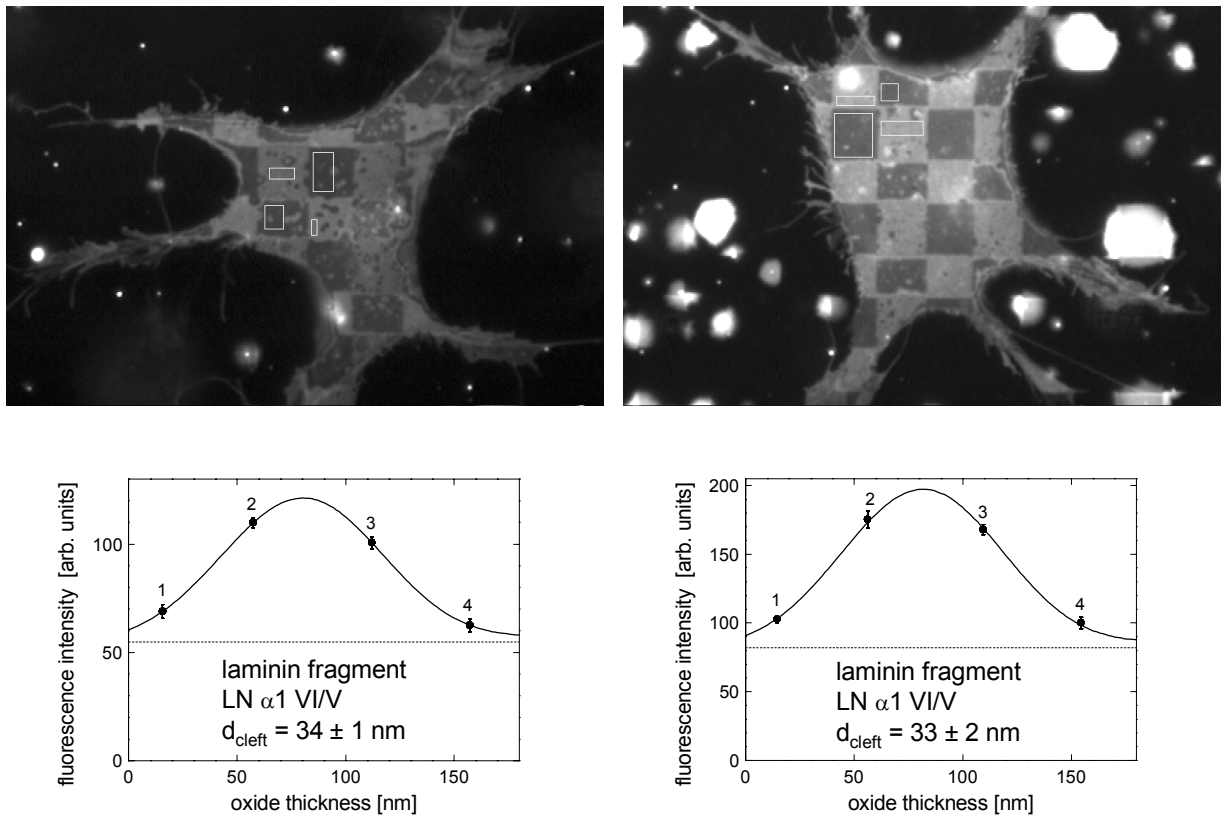


Figure 3.10: *GD25- β 1A cells attached to the laminin fragment, LN α 1 VI/V for 1 hour (top). Not only the distance, but the appearance of cells also changed, most likely due to absence of other domains of the native molecule where interaction with cells takes place. The corresponding analysis of distance by FLIC microscopy at the marked regions are shown below each figure.*

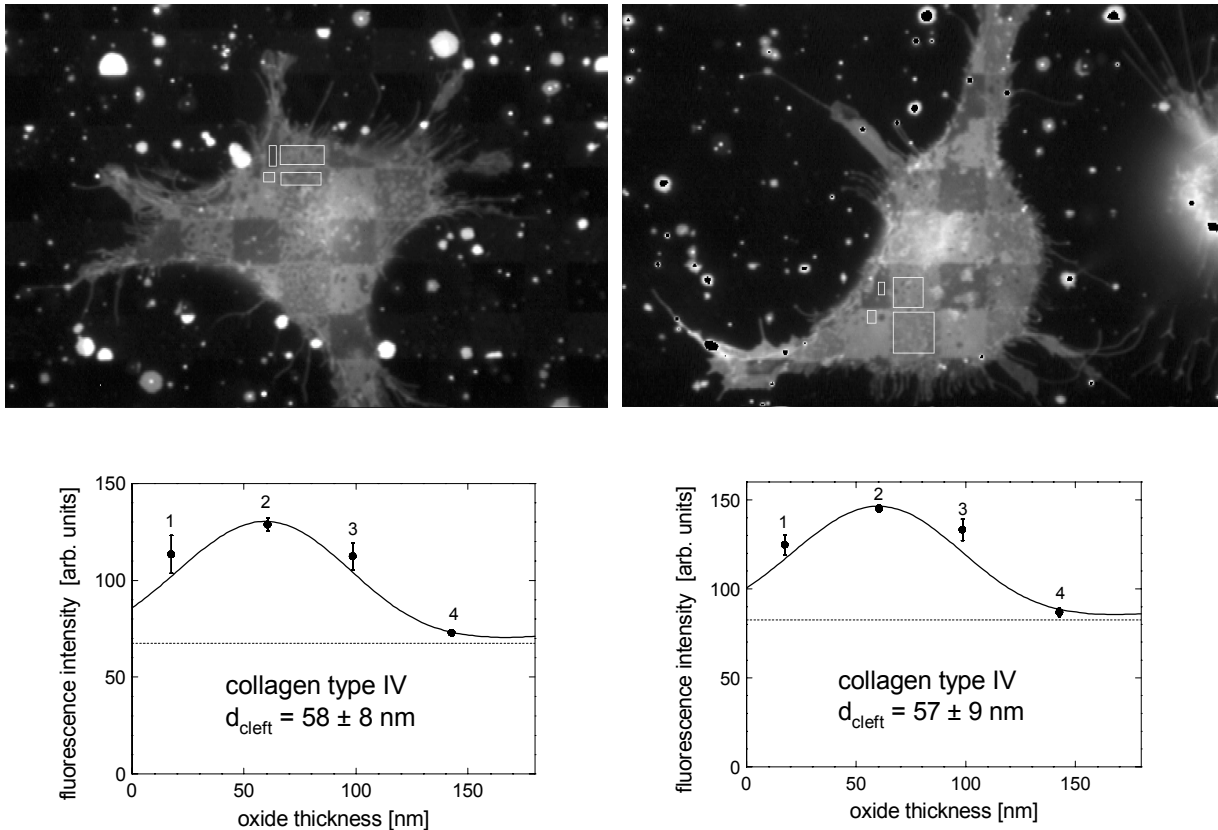


Figure 3.11: *GD25-β1A* cells cultivated on silicon chip coated with collagen type IV. Top: Typical fibrous membrane can be observed by staining with DiIC₁₈. Bottom: Corresponding analysis of cell-substratum separation shows a large uncertainty in fluorescence intensities at each oxide thickness due to inhomogeneity. The rough membrane made it difficult to determine the representative fluorescence intensity at each oxide area.

dot patterns. In most cases they adhered with simple round cell shape without distinguishable contour.

3.3 Collagen Type IV

Although collagen molecules are considerably larger than any other ECM proteins, FLIC measurements with collagen of type IV have yielded distances around 55 nm with a large deviation, most likely due to flexibility in its tertiary structure. Attachment to collagen type IV promoted formation of fibrous and inhomogeneous lower cell membrane surface. Unlike on fibronectin, cell body did not seem to spread on the substrate but instead, simply attached to the solid surface and extended filopodia-like structures similar to the cells on laminin (figure 3.11). The *GD25-β1A* cells bind to collagen type IV only through integrin α₃β₁ which recognizes the RGD sequence. The fibrous surface of the membrane made it difficult to select the representative local fluorescence intensity of the membrane embedded DiIC₁₈ dye molecules in determining the

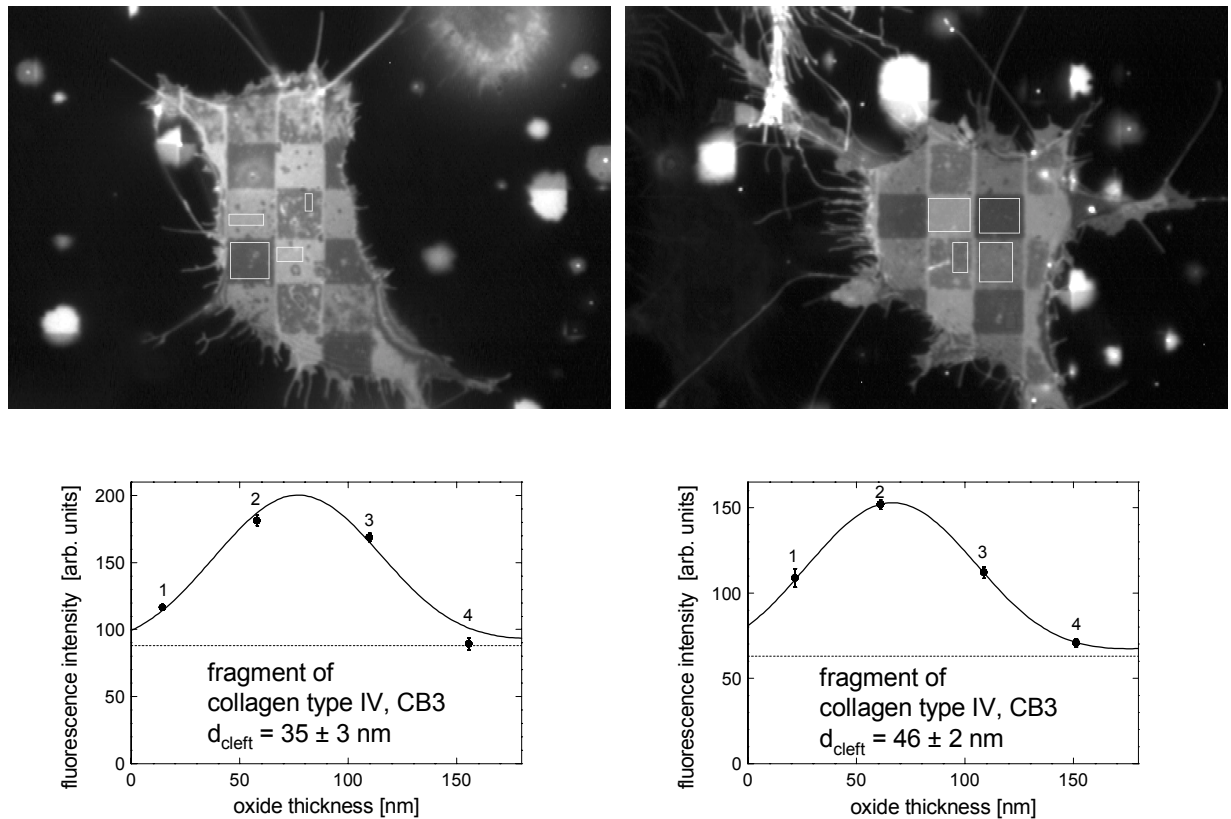


Figure 3.12: *GD25-β1A cells attached to fragment CB3 for 1 hour (left) and 2.5 hours (right). The isolation of cell attachment domain has induced a noticeable change in cell morphology. The cells adhered to CB3 seemed to lose the cytoskeletal reorganization seen as fibrous membrane of the cells adhered to full collagen molecule. Unlike the cells on fibronectin or laminin, these cells maintained the same cell morphology even after longer period of incubation.*

cell-substrate separation. Contrast to the cells on fibronectin and laminin, there was no apparent change in cell morphology after several hours of cultivation on collagen type IV.

Isolation of a cell adhesion fragment CB3 from collagen type IV, which is approximately 40 nm long has reduced the cell-substratum distance only by around 10 nm as shown by a histogram in figure 3.13. Many cells attached to the fragment CB3 developed circular deformation of around 0.5 μm in diameter away from the substrate towards cytoplasmic side (figure 3.12, left). Apart from these distinct structures, the cells attached with a very smooth membrane to the surface resembling the cell culture on fibronectin. However, many cells protruded short filopodia-like structures all along the cell periphery giving a hairy appearance. The cells also did not give the impression of spreading or spanning like the cells attached to fibronectin and the adhesion area was notably smaller. Unlike in the case of cultures on laminin and fibronectin, the cells did not change their appearances even after 3 hours of incubation (figure 3.12, right). No ruffles were developed, and the cells stayed attached flat on the substrate.

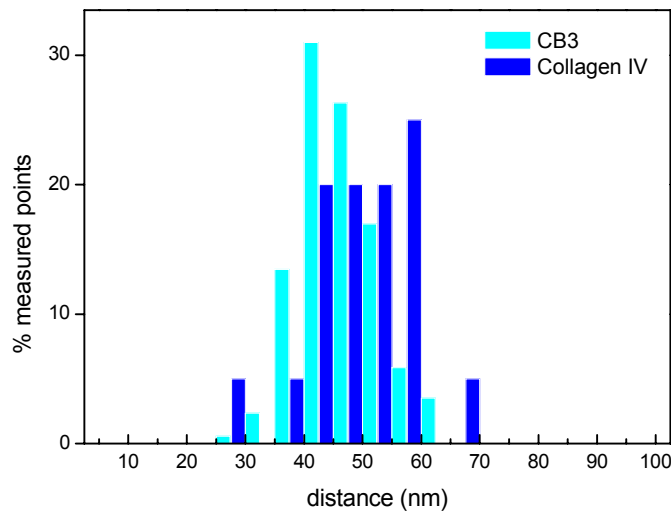


Figure 3.13: Histogram of FLIC microscopy performed with GD25- β 1A cells cultivated on collagen type IV and its fragment CB3. Unlike in the case of laminin, reducing the molecular size of collagen down to a fragment of around 40 nm long did not affect the cell-substrate distance, but at most, reduced on average by 10 nm.

3.4 Vitronectin

The fibroblasts exhibited similar morphology when plated on fibronectin and vitronectin. The figure 3.14 (left) represents a typical cell cultured on vitronectin. The cell-substrate separation was around 40 nm, slightly less than the distance on fibronectin.

3.5 Polylysine

The distance measurements with cells seeded on polylysine represents the case of nonspecific cell-substratum attachment, established solely through an electrical interaction between the negatively charged lipid membrane and the positively charged polymers. Here, the distances were determined to be around 10-20 nm.

In contrast to ECM substrates, the cells adhered to polylysine coated silicon chips showed no variation in appearance among the cultured population. Typical GD25- β 1A cell is shown in figure 3.14 (right). All the cells plated on polylysine coated silicon chip stayed round, appeared tightly and mechanically glued to the substratum surface. The dorsal membrane at cell periphery appeared often pulled flat towards the ventral side of the cell.

3.6 Discussion

These experiments with fibroblasts together with the previous studies with neuronal cell culture [12] suggest that the absolute values of separation between the cell and substratum arise neither

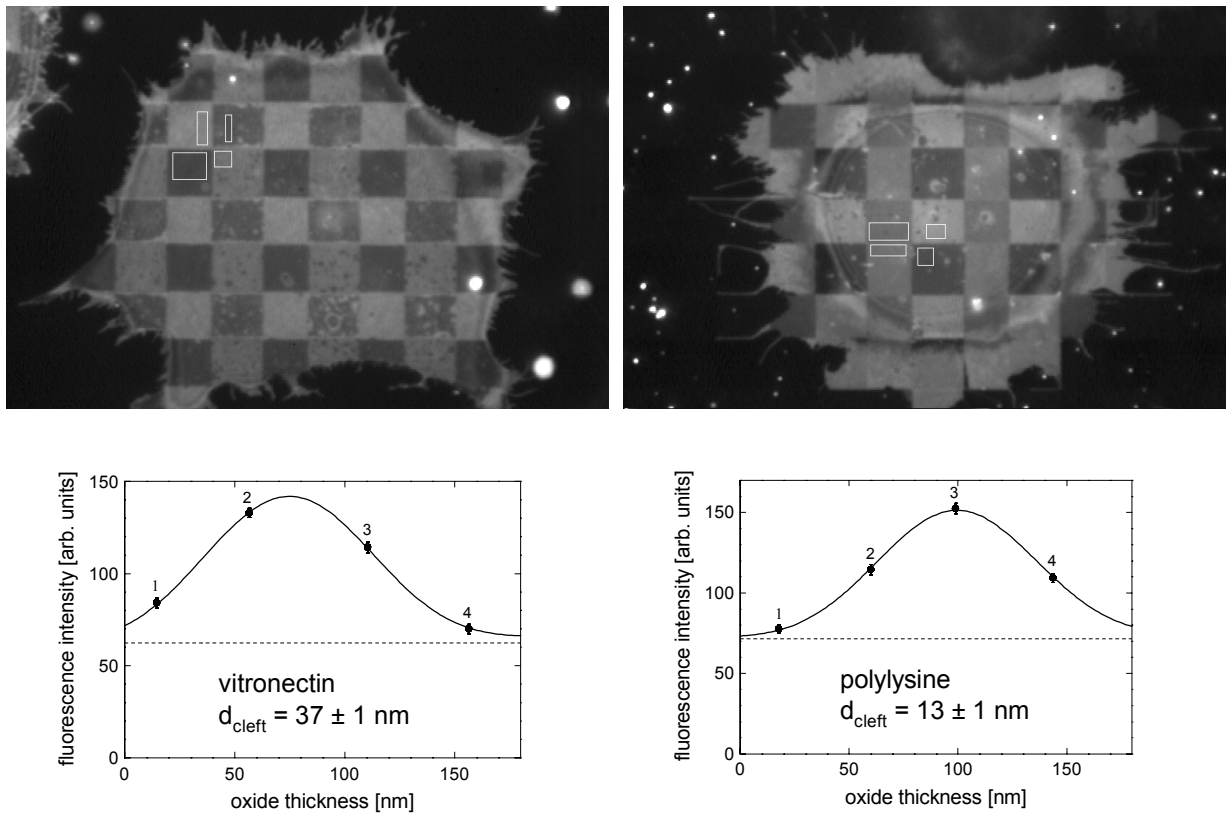


Figure 3.14: *GD25-β1A* cells plated on vitronectin (left) and on polylysine (right) for 1 hour. The appearance of the cells adhered to vitronectin was not distinguishable from the cells on fibronectin. The cells attached to polylysine appeared all quite similar to each other. At the cell periphery, top and lower membrane seemed glued together due to the electrical attraction towards the polylysine-coated substrate.

from the cell type nor from the transmembrane receptor. Rather the distance seem to depend on the conformation of the adsorbed ECM molecules which mediate the cell adhesion to solid surface. Single laminin molecule extends to around 110 nm and fibronectin molecules are approximately 120-160 nm in length according to electron micrographs with rotary shadowing technique [74]. Structural studies of integrin molecules approximate the extracellular length of the stalk to be 12-20 nm. In order to maintain a space of 100 nm between the membrane and the substratum, this implies that the laminin molecules cannot simply be lying flat on the solid surface as measured in a dried state upon binding to the transmembrane receptors. The actual molecular configuration of laminin and fibronectin upon binding to cell membrane must be investigated in order to understand for instance the cause of the large difference between the cell-substratum separations induced by these two ECM proteins of similar lengths. From the studies done on fibronectin molecule by electron microscopy, it is known that the dimer has flexibility in extension as well as in bending [27]. On the other hand, the rigidity of laminin structure can be suggested by the combined the knowledge in molecular structures from previous studies and the present measurements of absolute cell-substratum distances.

| cell | substrate | integrin subunits | mean values (nm) | conditions |
|----------|----------------------------|-------------------|------------------|-------------|
| GD25-β1A | laminin | α6β1, α3β1, α6β4 | 91 ± 16 | |
| GD25-β1A | fibronectin | αvβ3, α5β1, α3β1 | 50 ± 6 | |
| GD25-β1A | vitronectin | αvβ3, αvβ5 | 42 ± 4 | |
| GD25-β1A | collagen type IV | α3β1 | 55 ± 12 | |
| GD25-β1A | polylysine | - | 18 ± 6 | |
| GD25-β1A | E8 laminin fragment | α6β1, α7β1 | 52 ± 6 | |
| GD25-β1A | LN α1 IV/V | α3β1 | 40 ± 8 | |
| GD25-β1A | CB3 (collagen IV fragment) | α3β1 | 43 ± 7 | |
| GD25-β1A | fibronectin | α5β1, α3β1 | 43 ± 6 | RGD peptide |
| GD25 | fibronectin | αvβ3 | 52 ± 7 | |

Table 3.1: Average values of cell-substratum separation distance measured with FLIC microscopy. GD25-beta1A/GD25 cells express distinct integrin heterodimers which interact specifically with ECM proteins. The cells were resuspended twice in PBS in order to wash away serum and other adhesion molecules produced by the cells themselves. Following the wash, the cells were cultivated in medium without serum on various ECM proteins. The results shown in the table are measurements from cells cultivated for around one hour.

There are numerous studies done on cell adhesiveness to matrix substrates by cell attachment assays [89]. These investigations show how well the substrates mediate in retaining the cells adhered to a solid surface in terms of percent cells withstanding a mechanical stress applied by washing the samples with buffer solution. Together with the adhesiveness determined by such studies, the absolute distances measured by FLIC microscopy shows that the laminin molecules bind cells tightly, at the same time retains them away from the substrate surface with a large separation. There are also quantitative studies done on the actual strength of the cell-substrate binding [31]. They report that cell adhesion strength increases linearly with α5β1 integrin and

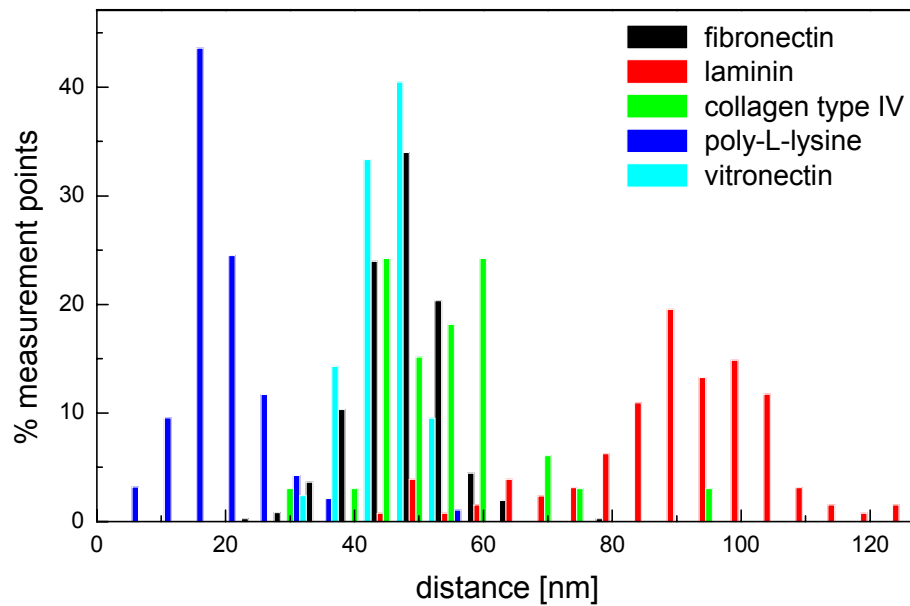


Figure 3.15: Histogram of FLIC microscopy performed with GD25- β 1A cells cultivated on various ECM proteins. The cell-substratum distance was measured at one or more small selected area in each cell attached to ECM-coated silicon chip. The frequency count was done with data from several experiments to confirm the consistency of the obtained values.

fibronectin surface density; i.e. change in adhesion strength is proportional to number of integrin-fibronectin bonds. Here, we could conclude that the strengthening of the cell attachment to the substrate does not change the cell-substrate separation, since the distance is independent of the amount of ECM proteins coated on silicon and most probably, even of the number of integrin-fibronectin bonds.

Serum

Cells cultivated in the presence of serum appeared in general fibrous with rough membrane-substrate attachment surface, regardless of the type of protein coated on the silicon. In such conditions, cells adhere to the substrate through nonspecific interactions in the presence of various ECM components produced by themselves as well as adhesion molecules contained in the serum.

Focal contacts

The topography of the cell-substratum separation distance constructed from the FLIC microscopy measurements show no focal plaque which should be present as regions of plasma membrane sharply approaching to the silicon dioxide surface down to 10-15 nm [48][55]. The profile analysis displayed either homogeneous gap throughout the cell body or inhomogeneity that did not resemble the structure of previously described focal plaques from the observations made with IRM.

A similar study was done on growth cone adhesion to various ECM coating using IRM [40]. They have investigated the growth cone-substrate association also by observing substrate-associated membrane. Their IRM analysis have yielded cell-substrate distance for laminin and polylysine to be greater than that for fibronectin and collagen IV. They have found that growth cones associate with laminin and polylysine less than with fibronectin and collagen IV based on their observation of membrane association with the substrate. There, they interpreted these regions of membrane that remain adhered to the substrate after detachment of the growth cones as site of close contacts, since they appear as dark interference patterns in IRM images. With FLIC microscopy, studies that provide additional information on the molecular interaction at the cell contact site to the distance measurement must be performed to understand the difference between the results from these techniques.

Chapter 4

Distance maps and vinculin

In order to visually localize the molecular events of cell adhesion to solid surface in living cells, the green fluorescent protein (GFP) from the jellyfish *Aequorea victoria* was used to tag vinculin, a protein found to be present at the site where the cells develop an adhesion structure, focal contact. DNA-sequence manipulations allow to express the protein of interest with the GFP tagged either at its carboxy-terminus or amino-terminus without interfering with the expression and functions of the native protein. For the purpose of present investigation, retention of the intact expression and transportation of vinculin was a critical factor after the construction of the fusion chimera. Immunostaining of the native protein was employed as reference to confirm the expression of the fusion constructs.

As already discussed in introduction, vinculin is an actin-binding protein well accepted as an identification of focal contacts, as it is usually located at membrane insertion sites of microfilament bundles [62]. The molecule is a single 115 kDa polypeptide consisting of three structurally and functionally distinct domains; a 90 kDa compact head, a proline-rich hinge region and a 29 kDa rod-like tail [19]. It is a major and ubiquitous component of adhesion plaques and cell-cell junctions [29]. The molecule plays a key role in stabilizing the linkage between the microfilaments and the transmembrane receptors of the cadherin and integrin families. Microfilaments are major cytoskeletal components involved in determining cell shape, dynamics and adhesion of eukaryotic cells.

4.1 Fibroblasts

Correlation studies were performed between FLIC microscopy and GFP-vinculin with fibroblasts cultured on either fibronectin or laminin. GD25- β 1A cells showed quite different expression pattern of GFP-vinculin depending on the ECM proteins. A brief experiment with HEK293 cells showed no reaction of the fusion protein upon attachment to either fibronectin or laminin.

4.1.1 Fibronectin

Vinculin expressed in GD25- β 1A cells adhered to fibronectin were reorganized into classical pattern of stripes which has been understood as focal adhesion plaques. Immunostaining of vinculin in the cells transfected with the GFP-vinculin fusion construct confirmed the validity of GFP-

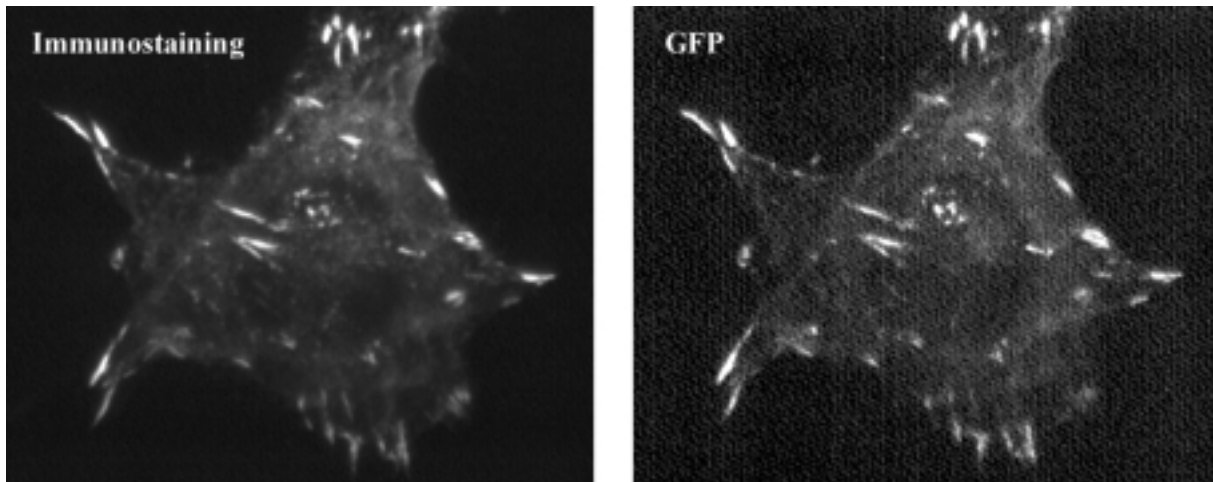


Figure 4.1: *GD25-β1A cells transfected with GFP-vinculin construct was seeded on fibronectin in medium without serum, and fixed with paraformaldehyde after 2 hours of cultivation. Left: Fluorescence of immunostaining with anti-vinculin followed by Cy3. Right: GFP-vinculin fluorescence of the same cell. Immunostaining of vinculin was taken as a reference in order to confirm that the expression pattern of GFP-vinculin precisely represented the distribution of entire vinculin expression in the cells including the endogenous vinculin.*

vinculin fluorescence in showing the complete vinculin expression in these cells (figure 4.1). Also the expression pattern of the fusion protein was closely compared with the previously performed anti-body staining of vinculin in GD25-β1A cells in order to exclude any possibility of the chimera interfering the general expression and reorganization of vinculin [89].

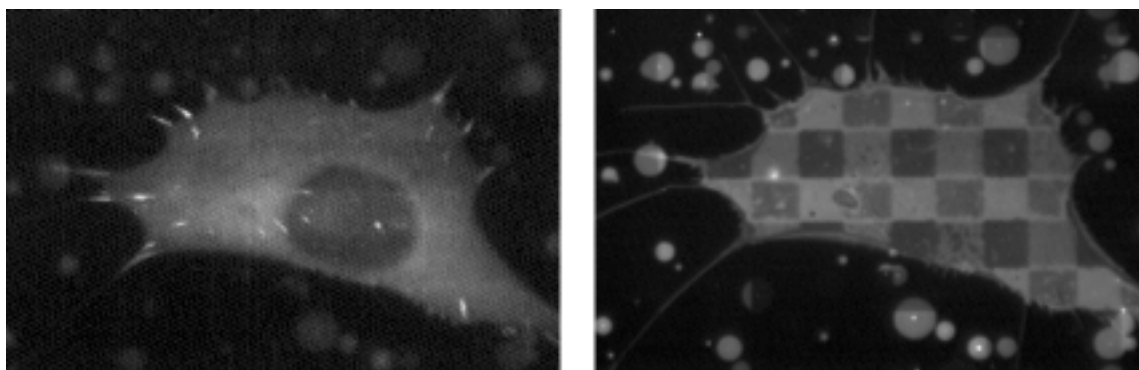


Figure 4.2: *A GD25-β1A cell transfected with GFP-vinculin construct. The cells were plated on fibronectin-coated silicon chips for 1.5 hours and observed under microscope. Most cells have recruited the fusion protein to cell periphery but only into thin stripes. The membrane was still smooth as shown by DiIC₁₈ staining. Left: GFP-vinculin expression, Right: FLIC microscopy.*

The cells normally recruited vinculin at the cell periphery during the first one hour (figure 4.2). After a few hours, thick stripes of vinculin clustering began to appear throughout the cell body.

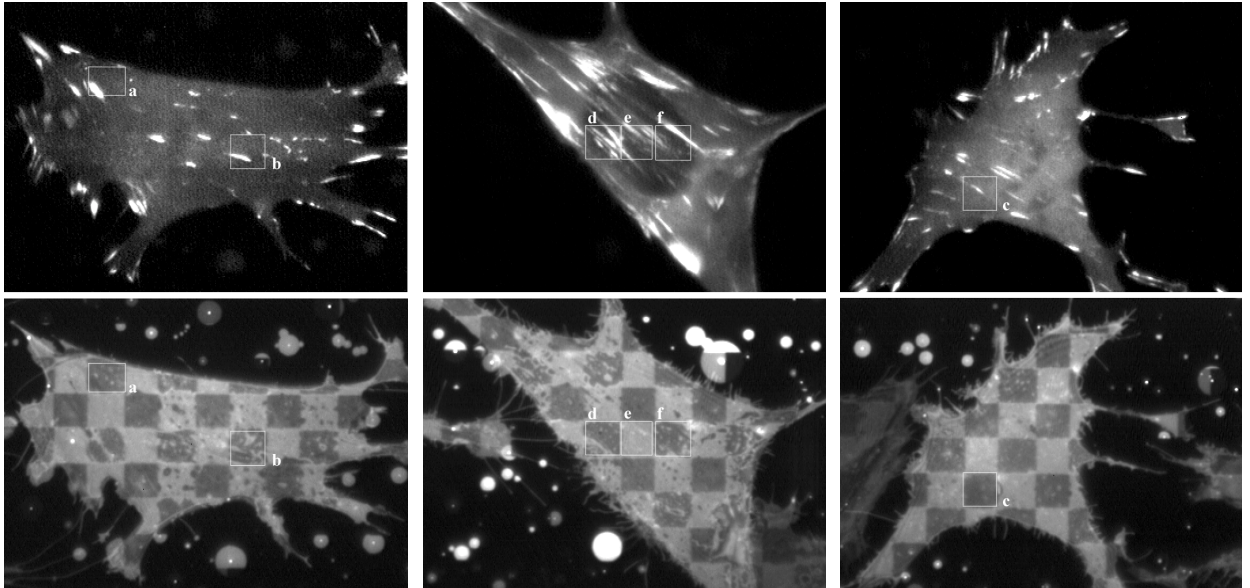


Figure 4.3: *GD25-β1A cells expressing GFP-vinculin. The cells were cultivated on fibronectin for 3-5 hours in serum free medium. Top row: GFP-vinculin expression. The cells recruited vinculin into pattern of stripes identical to focal adhesion plaques. Bottom row: FLIC microscopy. Ventral membrane of the corresponding cells were observed by staining with DiIC₁₈ for cell-substrate separation analysis.*

The GFP-vinculin images from such culture showed typical pattern of focal adhesion which have also been observed in IRM images. These stripes of vinculin were often parallel to one another. This clustering appeared to induce formation of membrane ruffles which also aligned in the same orientation as the vinculin stripes. Precise analysis of cell-substrate distance at and around the focal adhesion molecule, vinculin, was done by constructing a topography of selected small regions of FLIC microscopy image and its corresponding GFP-vinculin fluorescence image (figure 4.4).

The profile analysis was done as described in the materials and methods section in chapter 2. The regions suited for constructing a cell-substrate distance profile along with the corresponding typical vinculin pattern were limited due to several factors. First, on fibronectin, cells are on average around 50 nm away from the silicon oxide surface. This leads to the fluorescence intensity values of DiIC₁₈ emission only on oxide 1 and oxide 3 along the slope of the fitted curve (equation (10)), where the fluorescence intensity is sensitive enough to the changes in the dye position, i.e., to the cell-substrate separation. Secondly, the fluorescence detected from the GFP emission is also affected by the interference with the reflection (an approximation of the position of GFP relative to the silicon oxide surface based on its random orientation and using this interference effect is discussed in a separate chapter). The effect of interference is most visible in the GFP pattern of the middle cell in figure 4.3. It is clear that the fluorescence detected over oxide 3 and oxide 4 are very weak due to destructive interference, and bright over oxide 1 and oxide 2 due to constructive interference. These factors resulted in limitation of such comparative profile

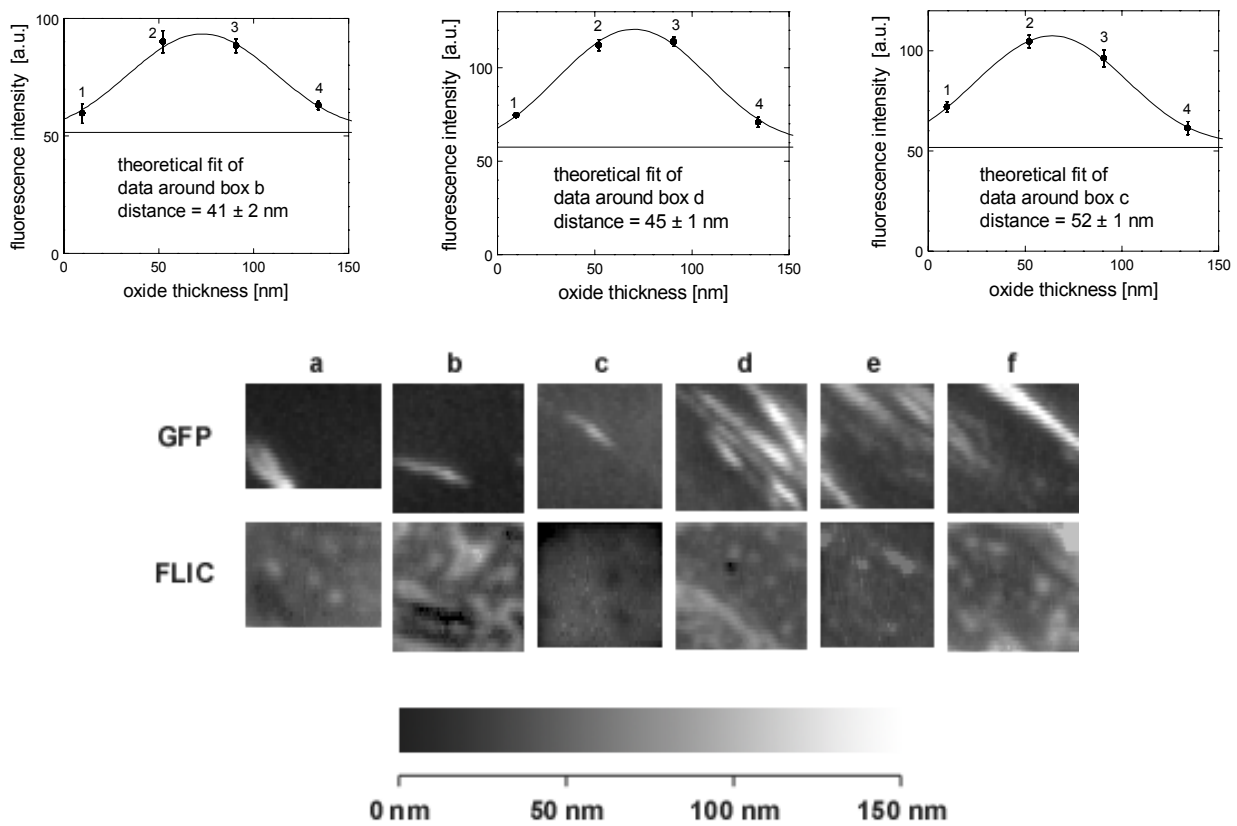


Figure 4.4: Top row: Fluorescence intensity of the cell membrane stained with DiI₁₈ around the labelled regions (in the previous figure) versus the thickness of silicon dioxide, fitted with a theoretical curve for distance around box b: 41 nm, box c: 45 nm, box d: 52 nm. Second row: GFP-vinculin expression and corresponding profile of the distances at the labeled regions. The gray scale representing the cell-substrate distance is shown at the bottom.

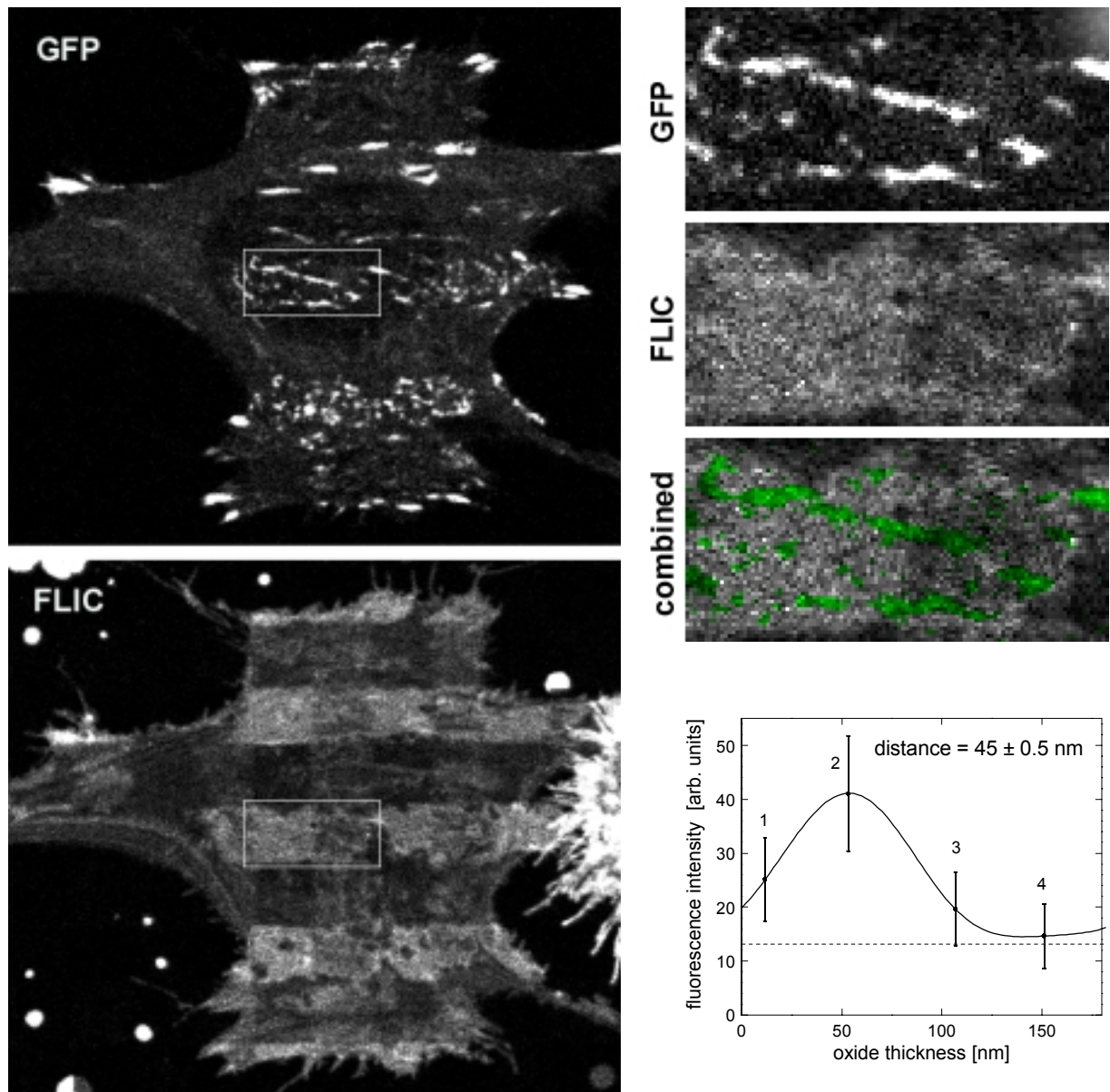


Figure 4.5: Confocal microscopy of GFP-vinculin transfected GD25-β1A cell on fibronectin. At the right, close up of the region labeled with a box is shown. The third box is the same close up of FLIC micrograph with the presence of vinculin depicted as green .

analysis to region over oxide 1. Several examples of representative correlation studies are shown in figures 4.3 and 4.4.

There was no defined structure of close association between the substrate and basal region of the cells at exact position of focal adhesion clusters (figure 4.5). The membrane regions corresponding to strong GFP-vinculin patterns usually developed ruffles parallel to the vinculin stripes rather like a folding of the membrane than a dent approaching the substrate. The pattern of membrane deformation in the vicinity of focal contacts recognized by the GFP-vinculin fluorescence was often more complex than the pattern of these biochemically defined focal adhesion plaques. The membrane deformation consisted of lipid membrane folded either towards the cytoplasmic side or towards the substrate. In most cases rows of folded membrane were formed both at and around the GFP-vinculin aggregates as seen around box d in figure 4.4. Additionally, dot-like structures of around 500-800 nm in diameter were occasionally formed in the neighborhood. These dot-like membrane structures approaching the substrate were found nearby vinculin aggregates without apparent general rule in terms of its relative position to the vinculin aggregates (boxes a and d in figure 4.4). The GFP-vinculin aggregates appeared also as densely distributed dots in some cells. However such protein clustering seemed not to directly induce membrane deformation as expected. There was no difference observed when the same experiments were done with the GD25 cells.

4.1.2 Laminin

On the other hand, attachment to laminin induced vinculin clustering only weakly in these cells. The fusion protein was mostly expressed diffused without distinct pattern of focal adhesion (figure

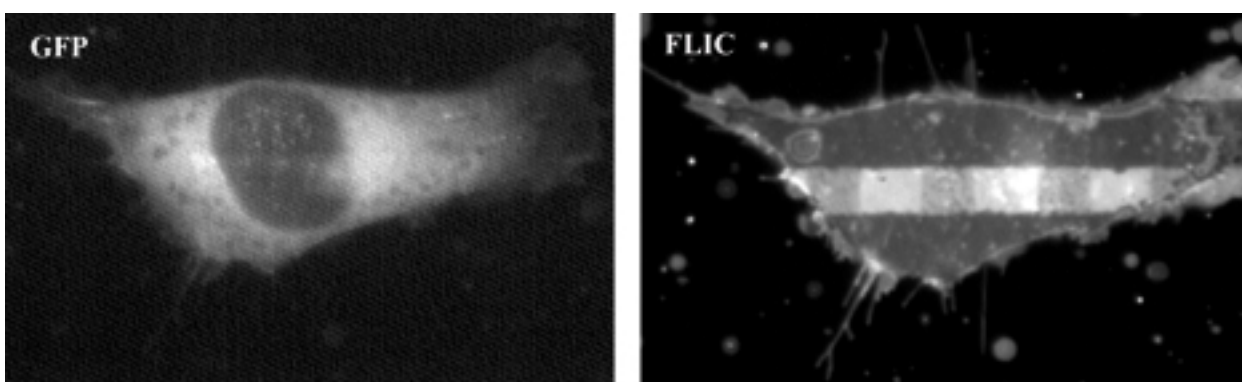


Figure 4.6: *Left: GFP-vinculin expression in GD25- β 1A cells cultured on laminin (2 hours). Typically the fusion protein was present diffused in the cytoplasm as shown in this figure. Right: Fluorescence of DilC₁₈ embedded in the ventral cell membrane. Regardless of whether the cell attached with smooth membrane as in this case or with rough membrane, the expression of GFP-vinculin was not reorganized into any pattern in the cells adhered to laminin.*

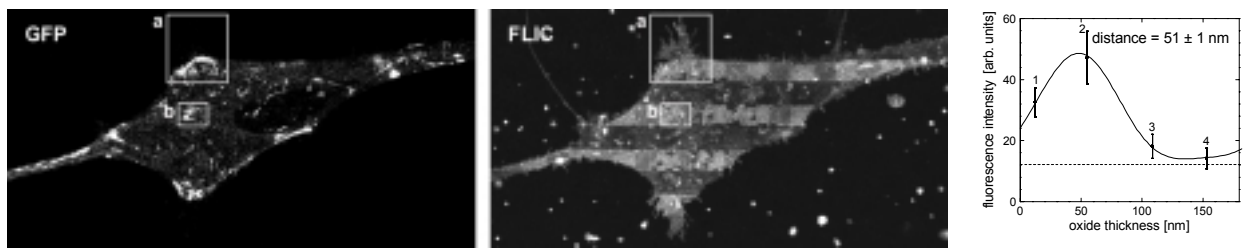


Figure 4.7: Confocal microscopy of a neuronal culture on fibronectin-coated silicon chip, transfected with GFP-vinculin. Left: Fluorescence microscopy of GFP-vinculin fusion protein. Vinculin clusters were found concentrated at the roots of filopodia and lamellipodia. Right: FLIC microscopy of the corresponding cell shows the filopodia and lamellipodia extending further than the position of vinculin clusters.

4.6). Cultivation up to approximately 6 hours in the medium without serum did not change the distribution of the fusion protein. This observation indicates that the early stages in attachment of these fibroblasts to laminin does not involve vinculin reorganization. Only after around 10 hours of cultivation in this condition, some cells began to recruit vinculin into patterns of thin stripes. The corresponding FLIC microscopy showed development of rough ventral membrane often with fibrous surface. Due to this inhomogeneous membrane structure, quantitative analysis of the distance was not possible. Similarly GFP-vinculin was expressed diffused in HEK293 cells transfected with the same fusion construct. These cells did not react either to fibronectin nor to laminin.

4.2 Neuronal culture

The level of GFP-vinculin expression was much lower in the case of cells in primary neuronal culture prepared from rat hippocampus. Occasionally diffused expression in the cytoplasm was present, but at much lower level than observed in GD25/GD25- β 1A cells. The expression patterns between the cells cultured on fibronectin and laminin were not distinguishable. This is in contrast to the large difference in cell-substrate distances, where for fibronectin is on average 50 nm and on laminin, which is 100 nm. This indicates that the variation in the distances may be irrelevant to the expression pattern of vinculin at the cytoplasmic side. The results presented in this section are all from experiments with confocal FLIC microscopy.

4.2.1 Fibronectin and laminin

The GFP-vinculin was mainly recruited at the cell periphery and at the tips of filopodia, consistent with previous findings [3]. Some cells with smooth contour expressed the fusion protein selectively along the contour, as shown in figure 4.10. There were also such GFP-vinculin expression with filopodia- or lamellipodia-like structures extending from the contour line (figure 4.13, box c). In some cases, vinculin aggregates were found to concentrate at the roots of filopodia and

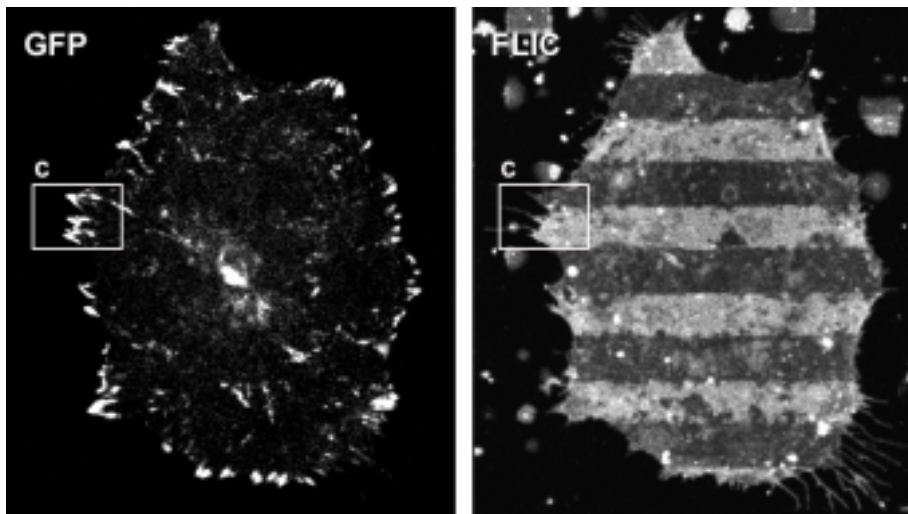


Figure 4.8: Neuronal cell culture on fibronectin observed by confocal microscopy. Left: GFP-vinculin expression in a glia cell. Mostly adhesion pattern of vinculin was observed along the cell periphery. Right: FLIC microscopy. Despite of sparse vinculin distribution, the membrane shows roughness.

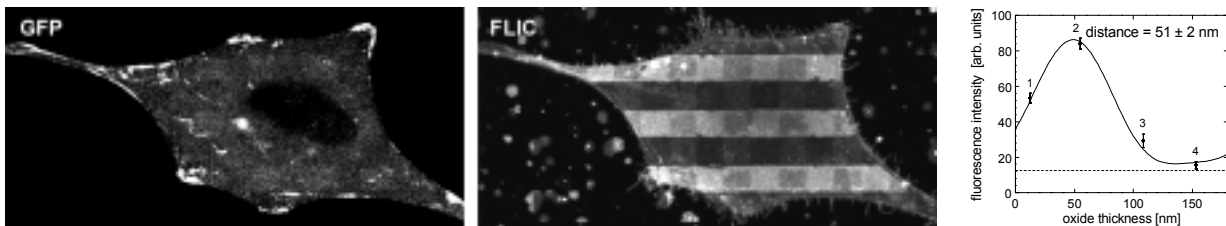


Figure 4.9: An example of smooth cell adhered on fibronectin. Left: Vinculin expression is restricted to cell periphery. The level of diffuse expression is much lower compared to that in fibroblast cells. Middle: FLIC micrograph shows its smooth membrane. Right: Theoretical curve is fitted to the measured fluorescence intensities from confocal microscopy to estimate the cell-substrate distance. Distance = 51 ± 2 nm.

lamellipodia (figure 4.7 and figure 4.13, box a). This is in agreement with the darker patterns behind the extended brighter mottled band of lamellipodium observed in the IRM images, matching the indirect immunofluorescent staining for vinculin [22]. Other cells clustered focal adhesion molecules into stripes aligned parallel to one another and oriented perpendicular with respect to the cell periphery, which were between 2-5 μ m long (figure 4.11 and figure 4.13, box d).

Previous studies have reported that neuronal cells lack focal contacts where astrocytes form both point contacts and focal contacts [81]. The occasional focal contact-like stripes found in our neuronal culture and this report suggest that the cell shown for example in figure 4.11 could be an astrocyte.

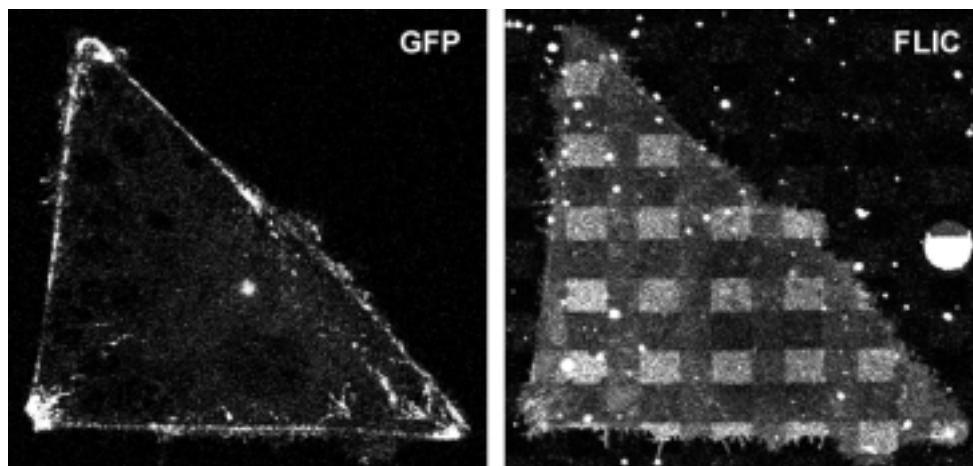


Figure 4.10: Primary neuronal culture on laminin. The culture was transfected with GFP-vinculin construct 1-2 days after its preparation. The cells were observed by confocal microscopy one day after the transfection. Left: GFP-vinculin expression. In most cells, the fusion protein expression was limited to the cell periphery. Right: FLIC micrograph made with confocal microscopy. In the absence of vinculin cluster, the cell membrane spanned a smooth surface against the substrate coated with laminin.

Many cells developed hairy filopodia which contained vinculin along the protrusion and at the tips (figure 4.8). An example is shown in a selected area labeled as box d of figure 4.13, where vinculin is present at the tips of filopodia as previously described with respect to the studies done in neuronal cultures [3].

In the cell body, only some stripes of vinculin clustering were found in agreement with their observation. Only rarely there were stripes aligned parallel to one another as observed in the fibroblast cells. In several cases, the membrane attached to fibronectin observed by FLIC microscopy indicated very rough cell-substrate interface where vinculin clusters were formed at cell periphery. However, the position of the protein aggregates and the membrane structure did not match directly as shown in the close up in the box b of figure 4.13. On laminin, clusters of vinculin did not seem to induce membrane roughness (figure 4.13, box e). The cells adhered to laminin exhibited extremely smooth ventral membrane as shown in figure 4.12.

All together, the cells from rat hippocampus cultured in DMEM supplemented with 10% FBS were attached to both fibronectin and laminin with rather flat ventral membrane surface, whereas cells cultivated in neurobasal exhibited much rougher surface. The vinculin aggregates such as radial recruitment induced rough membrane surface, however, the cell body itself often remained smooth (figure 4.9). There, the rough membrane structures made it difficult to decipher the exact distance to the substrate. There were many cases where the membrane was rough without any presence of vinculin, and in other cases, the membrane was smooth with the presence of vinculin clusters. There were some dots of vinculin which did not affect the distance at all. But in general,

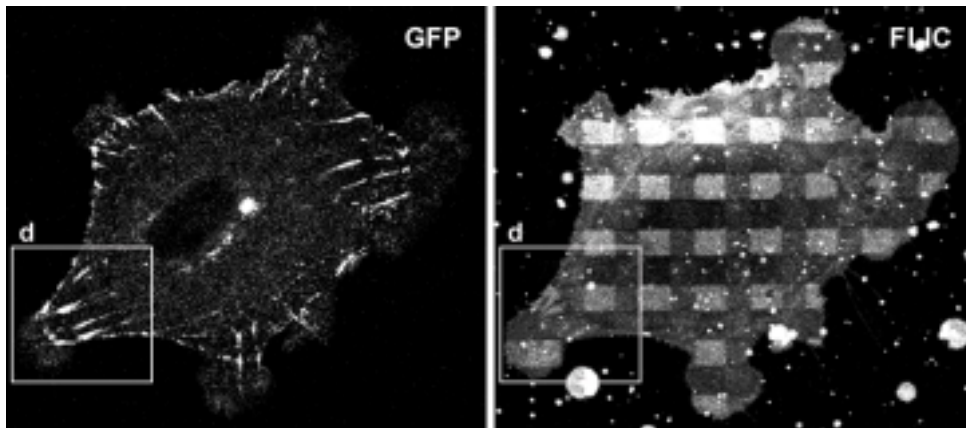


Figure 4.11: Confocal microscopy of neuronal cell culture prepared on laminin. The cells were transfected as already described. Left: GFP-vinculin expression showing radial pattern of clusters in an astrocyte. Right: FLIC microscopy. No apparent membrane structure related to the pattern of vinculin expression was found.

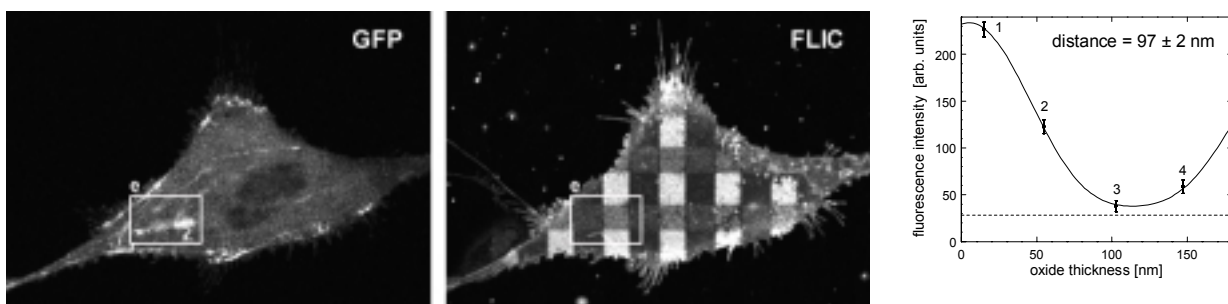


Figure 4.12: An example of smooth cells adhered on laminin. Some vinculin clusters are found in the region marked with box e (left). The corresponding FLIC micrograph (middle) shows no deformation in the membrane at this location. The cell-substrate distance is estimated to be 97 ± 2 nm (right).

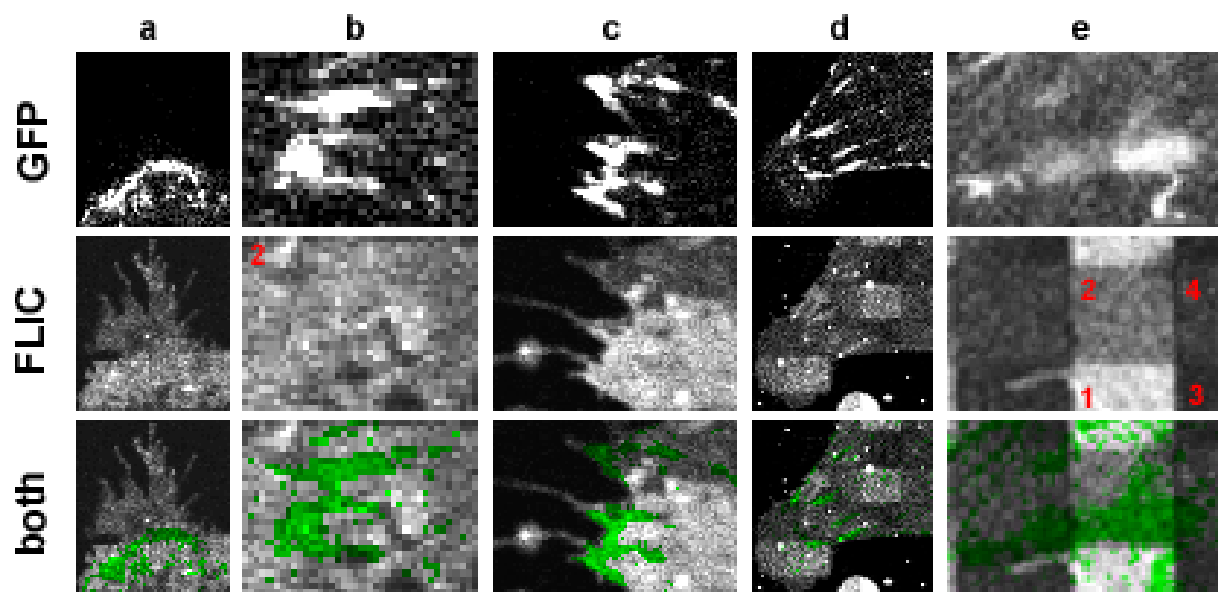


Figure 4.13: Close up of the areas marked in the previous figures. Top row: GFP-vinculin expression. Middle row: FLIC micrograph. Bottom: FLIC micrograph with overlay of GFP-vinculin distribution. GFP-vinculin fluorescence pattern above certain threshold level is marked in green, at the same time conserving the intensity gradient of FLIC micrograph. Box a: Vinculin is concentrated at the root of filopodia-like protrusions. Box b: Vinculin clusters do not correspond to the roughness of the membrane. The area is over oxide 2. Box c: Vinculin is highly localized at the tips of filopodia. Box d: Vinculin stripes are aligned parallel to one another and radially from the cell body. Box e: Despite of vinculin clusters, no deformation is observed in the membrane. The numbers in red represent the oxides.

strong aggregates of vinculin at the cell peripheries induced a region of rough membrane.

4.3 Discussion

According to previous studies on focal adhesions, sharp deformation of membrane approaching the substrate were expected precisely at the position where the vinculin molecules are clustered [4][48][71][79]. Here, the observation done by GFP-tagging of vinculin together with FLIC microscopy shows complexity in cell-substrate distance as a consequence of reorganization of adhesion molecules. In fibroblasts, the recruitment of vinculin into aggregations seemed to induce lipid membrane reorganization which appeared similar to the pattern of molecular clustering. The induced membrane deformation was however, in most cases, much more complicated than the classical stripes of focal contacts observed by IRM. The membrane also did not appear to be pulled towards the substrate. Instead it exhibited ruffles at and around the region of contact site by forming folding of the lipid membrane which was spread smooth otherwise. According to the analysis of FLIC measurement, the upward folds towards the cytoplasmic side of the membrane could be up to 30 nm above the rest of the ventral membrane. The downward folds could be close to the substrate approximately at 20 nm. These folds did not usually match the position of the vinculin aggregations.

Earlier immunostaining studies have indicated similarity among distribution of fibronectin labeling, expression pattern of cytoskeletal components such as vinculin and actin, and the dark streaks of IRM image [4][62]. For instance, double-label immunofluorescence experiments demonstrated coincidence and collinearity between actin and fibronectin in well-spread fibroblasts. Also when cultured in low serum medium, thereby arresting at G1 phase of the cell cycle, expression of vinculin in fibroblasts were similar to the pattern of fibronectin fibers at the substrate surface underneath the cells. This co-distribution was also found to be most prominent in the perinuclear region of the cell. These linear fibronectin and vinculin containing adhesion complexes appear collinear with the major ventral stress fibers, which are the locus of a major type of substrate adhesion complex of stationary fibroblasts. It has also been found that the fibronectin does not co-distribute with focal contacts in these cells cultured in medium containing more than 5% serum. Under such conditions, the cytoplasm is actively mobile, the stress fibers are not highly developed, and focal contacts are in a state of rapid flux.

The cells in the primary culture of rat hippocampus on the other hand expressed vinculin at limited level, mainly at and along the cell periphery. Some studies done earlier have indicated focal contacts in the absence of many cytoskeletal components such as vinculin, talin and p125^{FAK}. Point contacts are such commonly observed site of cell adhesion without involvement of cytoskeletal components in many neuronal cells. In PC12 cells, vinculin is found to only partially co-localize with such point contacts [3]. The localization of vinculin in the tips of filopodia is suggested as area of the strongest adhesion of cells to the substrate [92]. The membrane roughness found with-

out vinculin expression could well be the site functional not in cell adhesion, instead may have other roles in cell motility. Also, the attachment of fibroblast cells on laminin without vinculin aggregation may suggest another mechanism of cell adhesion which takes place without association with cytoskeletal proteins [20][90]. These two different expression patterns of vinculin in fibroblasts and neuronal culture implicate the two different functions residing in distinctly different interactions of fibronectin with receptor molecules in motile cells compared to non-motile cells.

In fibroblastic cells, two types of adhesive cell-substrate contact in culture are specifically described; the focal and close contacts [22]. Depasquale et al. [22] have postulated a precursor of focal contact formed by accumulation of F-actin at the membrane before the contact occurs. Here, they have followed the sequential events leading to the structural and molecular organization of the focal contact and associated adhesion plaque and stress fiber complex. They have observed that the focal contacts defined by dark pattern by IRM images are formed in the presence of these F-actin accumulations. In the leading lamellipodium, they have detected an F-actin rich rib, in the absence of vinculin and as bright band in the IRM image. They have interpreted such cases as a precursor of contact formation. During a time-lapse observation of IRM images, they have marked several dark patterns which after fixation, matched the F-actin but not necessarily the vinculin staining. This could explain our observation in FLIC images of rough membrane in the absence of GFP-vinculin. Distribution of contact sites without vinculin must therefore also be visualized in order to find out whether cells do in fact make close apposition at focal contacts.

Chapter 5

Distance maps and Integrin $\beta 1$

In order to locate directly the molecular docking site of the membrane to ECM proteins, $\beta 1$ integrin subunit was tagged with GFP. This subunit has been implicated as the largest family of integrins [48]. Mutagenesis studies have suggested that its cytoplasmic domain interact directly with the cytoskeleton [57][59]. In many cells, $\beta 1$ family of integrin is in particular found to play a central role in cell-substrate adhesion, by forming transmembrane links between ECM components and the actin-cytoskeleton. For example, $\beta 1$ -class integrins specifically have been shown to mediate neuronal attachment and process of outgrowth in response to several ECM proteins.

Ligation of GFP cDNA between a signal peptide and the amino-terminus of $\beta 1$ integrin cDNA after its endogenous signal peptide results in the expression of $\beta 1$ integrin with GFP hanging at the end of its extracellular domain. After the fusion proteins are folded and transported with an appropriate α -subunit partner to the cell surface with the help of the signal peptide, they are cleaved at right after the signal peptide.

In this section, membrane deformation observed by FLIC microscopy is compared to the GFP- $\beta 1$ integrin distribution, which are sites where the membrane form a link between substrate and cytosolic proteins that cause membrane trafficking. Fluorescence microscopy of the cells transfected with the fusion construct localize the distribution of the extracellular domain of $\beta 1$ integrin bound to ECM proteins as well as being transported to the final destinations.

5.1 Fibroblasts

All the experiments presented in this section are done by confocal FLIC microscopy. The GD25 cells lacking integrin $\beta 1$ expression was transiently transfected with the fusion construct of GFP and integrin $\beta 1$ as described for GFP-vinculin. The transfected cells cultured on silicon chips for the measurements were prepared also as described in the method section in chapter 2. The expression of the fusion protein in the cells were observed both in cultures on fibronectin and laminin.

5.1.1 Fibronectin

GFP- $\beta 1$ integrin was seen as dense mesh-like pattern and occasionally also as stripes and small dots. The larger aggregations often present around and excluded from the cell nucleus are most probably the fusion proteins on the way to the cell surface. At cell periphery, fluorescence was observed to the tip of filopodia and along the contour. If the cells were incubated for longer than one day, the fusion protein was recruited into thin stripes, often radially aligned from the center of the cell body (figure 5.4). The intricate grainy pattern of $\beta 1$ integrin expression matched the roughness of the membrane (figure 5.3). Close comparison between the GFP and FLIC micrographs (figure 5.8, boxes a-d) showed that integrin $\beta 1$ is present mainly in the areas where the membrane is separated from the substrate at around 50 nm, which is the average distance calculated (graph in figure 5.2). The regions of upward and downward ruffling of membrane were devoid of integrin $\beta 1$. Due to the interference effect, GFP was most visible on oxide 2 and 3.

Some retracted cells have left the fusion protein on the substrate where they were previously attached to. At the left side of the cell in figure 5.1, fluorescence of the GFP is present as a mesh-like pattern forming triangular areas. The fluorescence of membrane-embedded DiIC₁₈ shows that the cell has retracted to a slim shape leaving only a few thin filopodia-like protrusions at its left side. Previous observations indicate that an appreciable fraction of $\beta 1$ integrins are known to remain behind the cell through ripping process [71]. Cytoskeletal components however, do not remain behind with integrin. Consistent with these findings, we have also never found retracted cells leaving any GFP-vinculin behind.

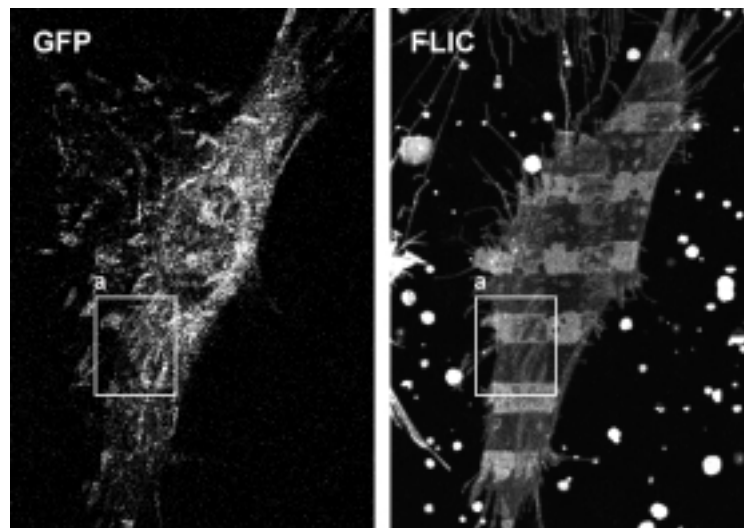


Figure 5.1: *At the left side of the cell, GFP- $\beta 1$ integrin is left behind on the substrate, indicating that the cell has been translocated. Since GFP molecule is expressed extracellularly at the amino-terminal of the $\beta 1$ subunit, it is not clear whether the entire subunit stayed behind, attached to fibronectin, or only the extracellular domain is ripped off from the β -subunit.*

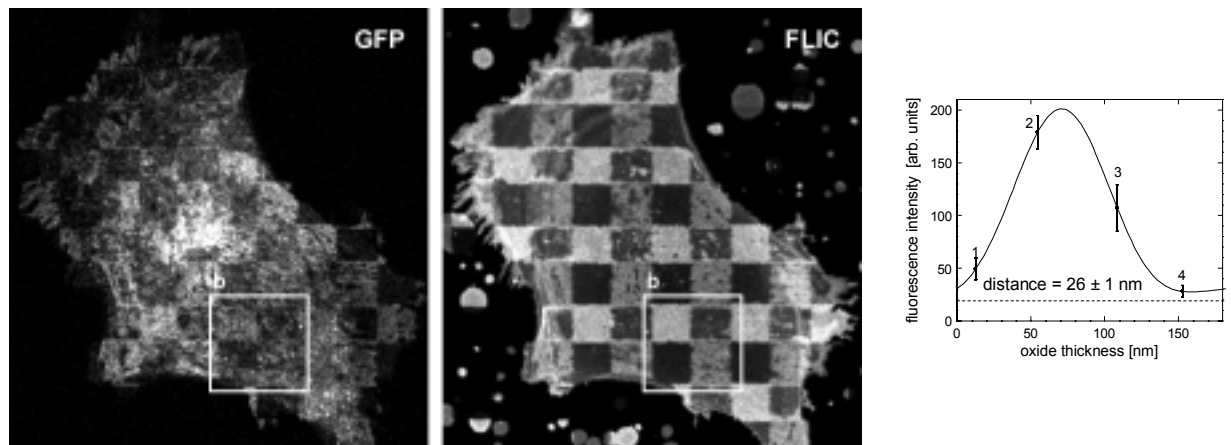


Figure 5.2: An example of well-spread fibroblast cultured on fibronectin (2 hours). GFP-β1 integrin shows grainy distribution with occasional small dots. The position of GFP relative to silicon (mirror) induces an interference effect of the incident and the emitted light that appear as checker board of repeating dark and light squares.

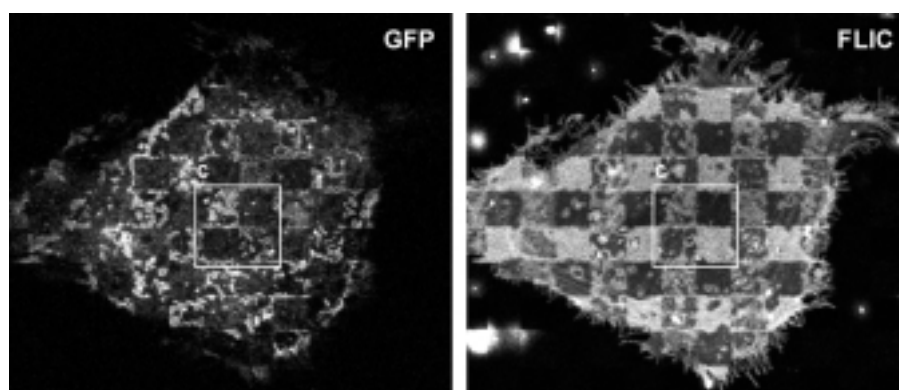


Figure 5.3: An example of fibroblast with rough membrane. Although cultured under the same condition on fibronectin, this cell exhibited complicated pattern of adhesion. GFP-β1 integrin expression echoes somehow the membrane deformation.

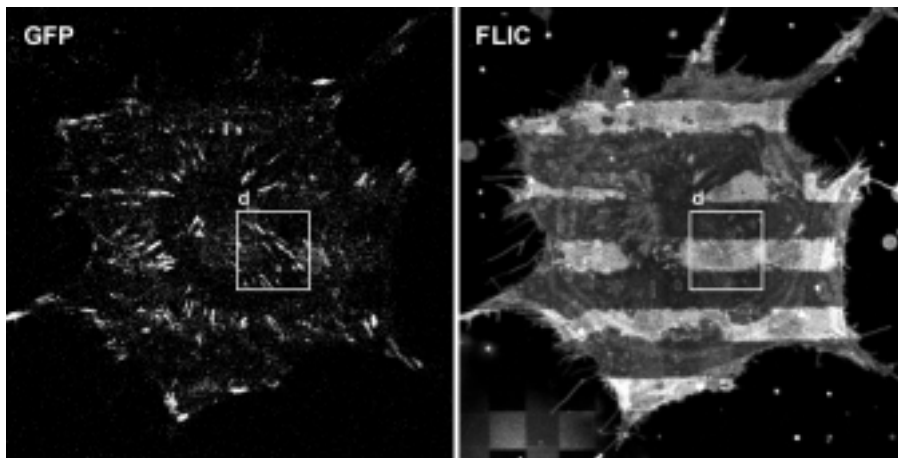


Figure 5.4: GD25 cell with GFP- $\beta 1$ integrin adhered to fibronectin overnight. The fusion protein appears in stripes aligned radially from the center of the cell body. This cell still shows relatively smooth membrane despite of a long cultivation period.

5.1.2 Laminin

The GFP- $\beta 1$ integrin transfected GD25 cells were plated also on laminin and the expression of the fusion protein was observed after various length of incubation time. Introduction of GFP- $\beta 1$ integrin allowed the originally $\beta 1$ integrin deficient cells to bind to laminin through integrin heterodimer, $\alpha 6\beta 1$ [89]. In most cases, the cells required much longer time before the GFP-integrin $\beta 1$ was recruited to exhibit any clusters. On laminin coated substrates, the GFP- $\beta 1$ integrin fusion protein appeared sparsely during the first hour as dots (figure 5.5) and eventually began to

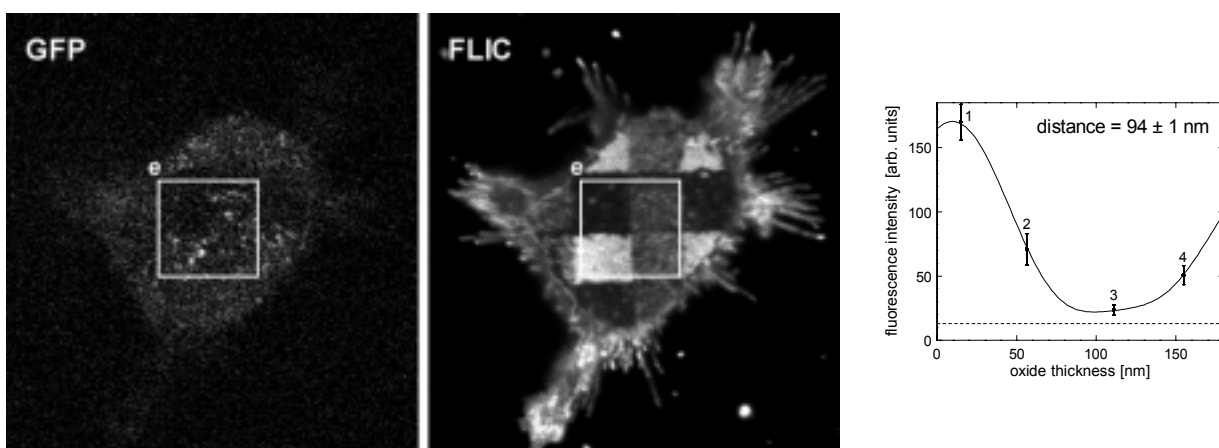


Figure 5.5: The early stage of GD25 cell attachment to laminin (1 hour). GFP- $\beta 1$ integrin is distributed in diffuse points. The membrane is smooth, approximately 94 nm away from the substrate as estimated by FLIC microscopy (right). The cell stretches filopodia-like protrusions.

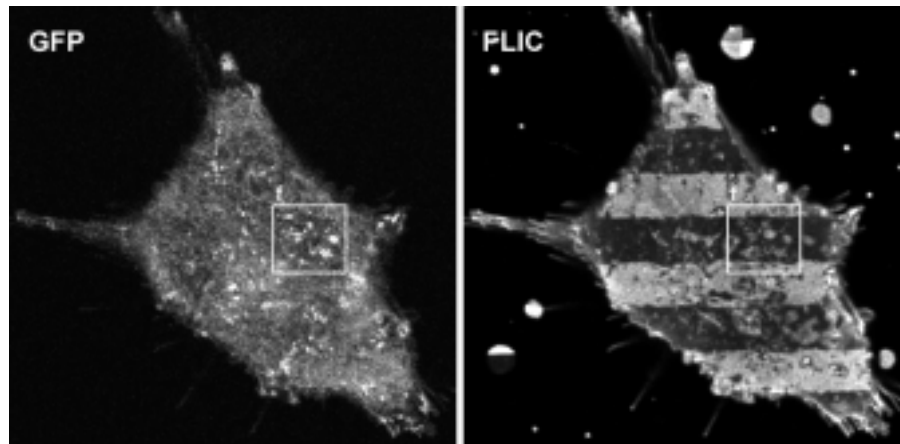


Figure 5.6: *GD25 cell expressing GFP- β 1 integrin, cultured on laminin for 2.5 hours in medium without serum. The fusion protein is distributed in fine points and dots throughout the cell body. There are some correlating membrane roughness as shown on the right, in the labeled box f.*

distribute throughout the cell body several hours after the cells were seeded in medium without serum (figure 5.6). There were no cells which had diffused expression as observed with the GFP-vinculin expression in the cells cultivated on laminin. This suggests that the GD25 cells attach to laminin through α 6 β 1 integrin heterodimer without inducing aggregation of vinculins. Whether reorganization of other focal adhesion molecules such as talin and paxillin is also absent in these cells attached to laminin must be investigated further. After overnight cultivation in the same medium (figure 5.7), the fusion protein was recruited to form thin, often parallel stripes throughout the cell body. The expression pattern became similar to that of GFP-vinculin and also

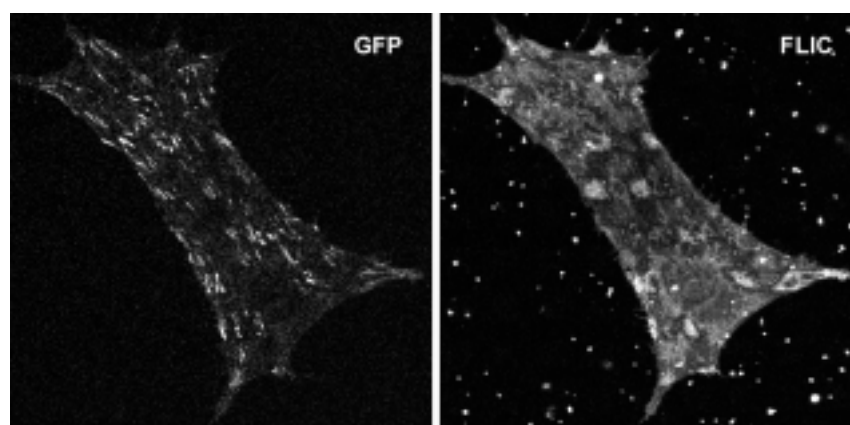


Figure 5.7: *GD25 cells transfected with GFP- β 1 integrin cultured on laminin, overnight in medium without serum. The fusion protein formed aggregates into parallel stripes similar to vinculin. The membrane became too rough to recognize the oxide pattern of the chip, as shown in the FLIC micrograph at the right.*

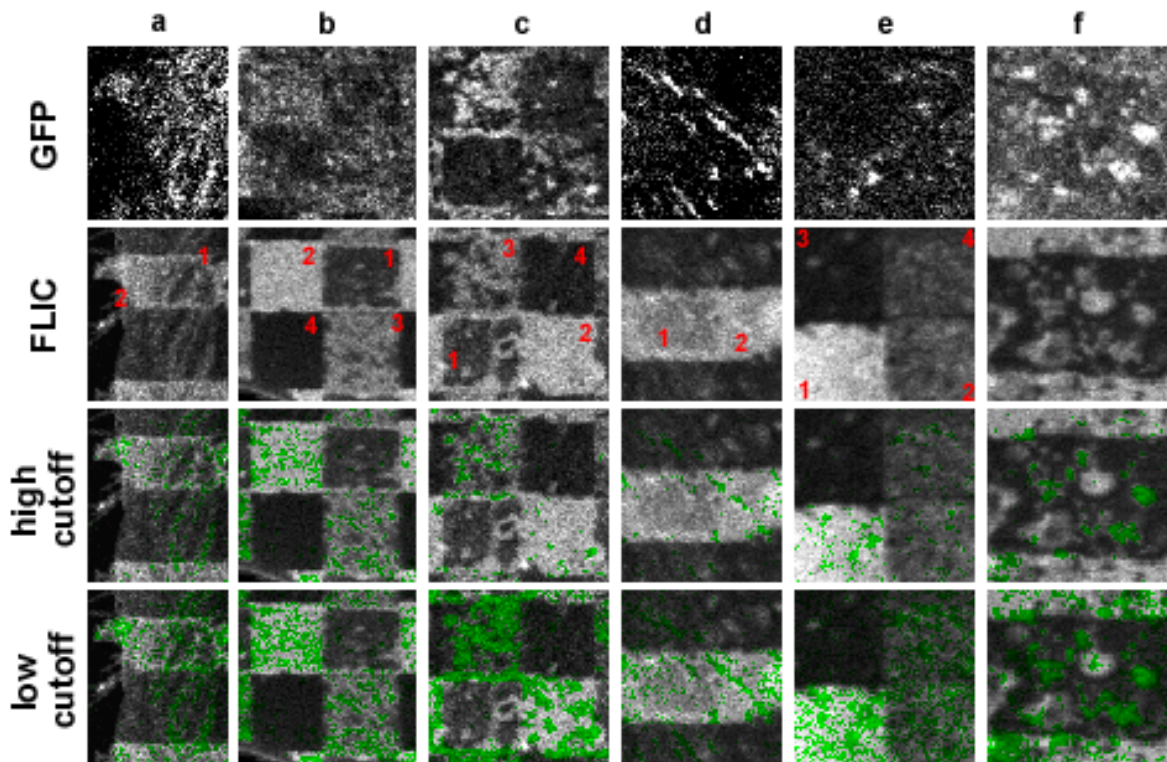


Figure 5.8: Close up of GD25 cells expressing GFP- $\beta 1$ integrin fusion protein. Boxes a-d are sections from cells adhered on fibronectin and boxes e and f are that on laminin (taken from the previous figures of the whole cells). The images at the two bottom rows are obtained in the same manner as explained for the images of neuronal cells transfected with GFP-vinculin. Box a: Membrane ruffling shown in FLIC micrograph matches the stripes of GFP- $\beta 1$ integrin (top). Due to the upper membrane effect at the cell periphery, membrane-substrate distance cannot be determined. Box b: GFP- $\beta 1$ integrin is present mostly where the membrane-substrate separation is homogeneous. Box c: On oxide 1, almost no fusion protein is visible due to destructive interference between the incident and reflected emission of GFP. However, the membrane is rough. On oxide 2, the membrane shows little deformation, but there is a dense cluster of integrins. On oxide 3, integrin is visible at regions corresponding to certain fluorescence intensity of the membrane labeling, i.e., to a certain membrane-substrate distance. On oxide 4, GFP fluorescence is not visible again, due to the destructive interference, and the fluorescence of membrane labeling is also insensitive to the membrane-substrate distance. Box d: Parallel stripes of fusion protein align with the membrane ruffling. Box e: Dots of GFP- $\beta 1$ integrin clusters do not correlate to the membrane structures. Box f: Close up of oxide 4 in the case of laminin.

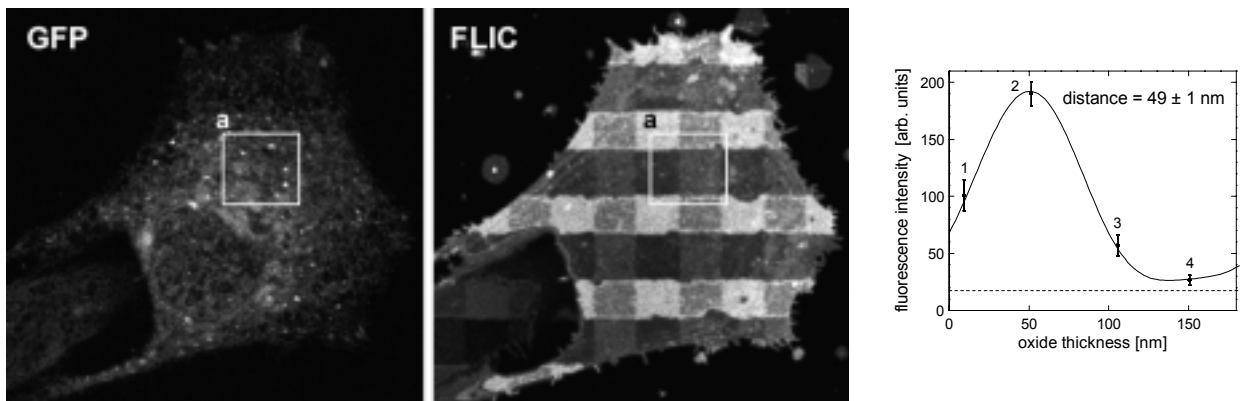


Figure 5.9: An example of a cell in primary culture of rat hippocampus on fibronectin. The culture was transfected with GFP- $\beta 1$ integrin fusion construct by calcium-phosphate transfection method one day after its preparation and one day before the images were made. Even on fibronectin, the cells in most cases exhibited smooth ventral membrane. FLIC micrograph and its fit to theory shows that the cell is around 50 nm away from the substrate.

GFP- $\beta 1$ integrin on fibronectin. However, these stripes were much thinner than the typical focal adhesion pattern formed by GFP-vinculin in the cells adhered to fibronectin.

5.2 Neuronal culture

The expression of GFP- $\beta 1$ integrin fusion protein was also investigated in neuronal cultures. Various expression patterns were present among the mixture of different types of cells in the primary cultures prepared from rat hippocampus. There was no noticeable difference in the expression of $\beta 1$ -integrins between the cultures on fibronectin and laminin. Most cells were again smooth with distance of around 50 nm on fibronectin and 100 nm on laminin. The experiments presented here were also done with confocal FLIC microscopy.

5.2.1 Fibronectin and laminin

The neuronal culture on fibronectin-coated substrate also exhibited very dense expression of GFP- $\beta 1$ integrins. Occasionally cells also formed parallel stripes of protein clustering (figure 5.11). As shown in figure 5.9, mostly the fusion proteins were present as small densely distributed dots throughout the cell body. At the center, large dot-like aggregates were also formed, as depicted in box a of figure 5.13. As shown in the bottom two boxes in the figure for this close-up section, these dots did not induce membrane deformation. Box b in figure 5.13 is an example of clusters which are formed into stripes at the roots of filopodia similar to vinculin clusters.

Similarly, in many cells cultured on laminin, the fusion proteins were distributed into a dense mesh-like patterns (figure 5.15) with occasional appearance of thin stripes and large dots (figure

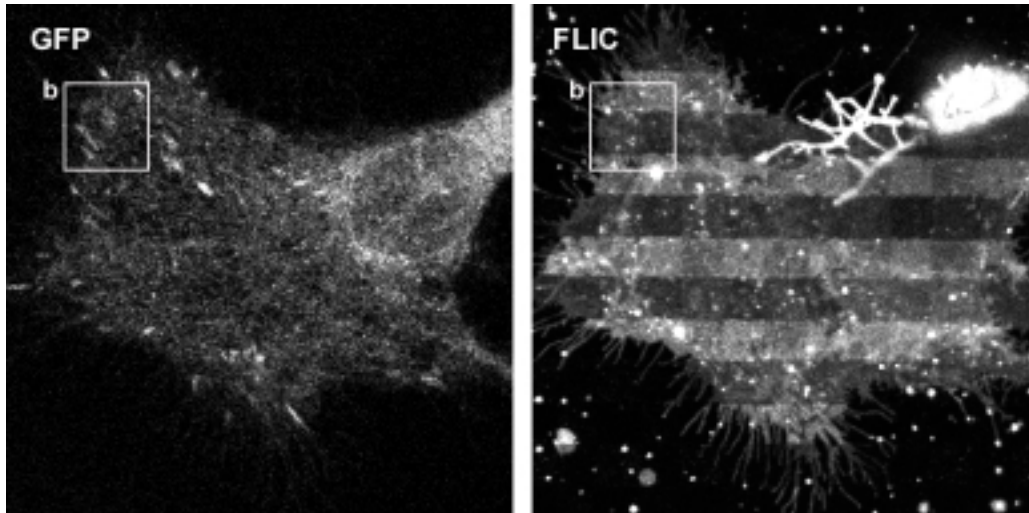


Figure 5.10: A growth cone projecting onto a glia cell. Both cells are expressing GFP- $\beta 1$ integrin fusion protein. Grainy expression pattern dominates the distribution of this fusion protein in neuronal culture.

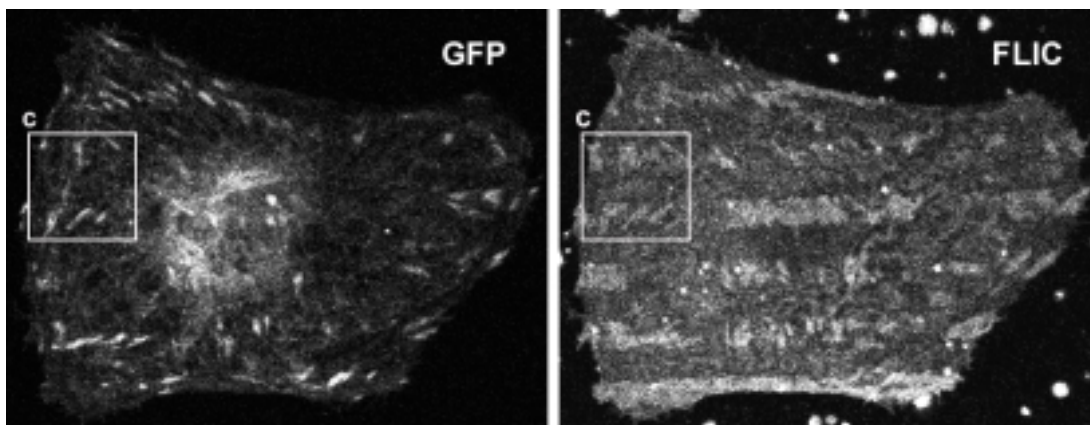


Figure 5.11: An example of a cell in neuronal culture with integrin $\beta 1$ subunits clustered into pattern of stripes, correspondingly with rough membrane.

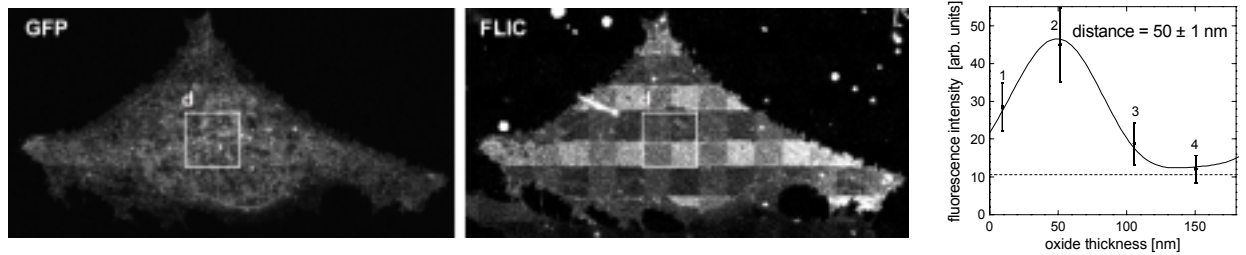


Figure 5.12: A cell in neuronal culture on silicon chip coated with fibronectin. The cell expresses the GFP- $\beta 1$ integrin in mesh-like pattern with several dot-like clusters. The membrane observed by FLIC microscopy appears smooth, separated by 50 nm from the substrate.

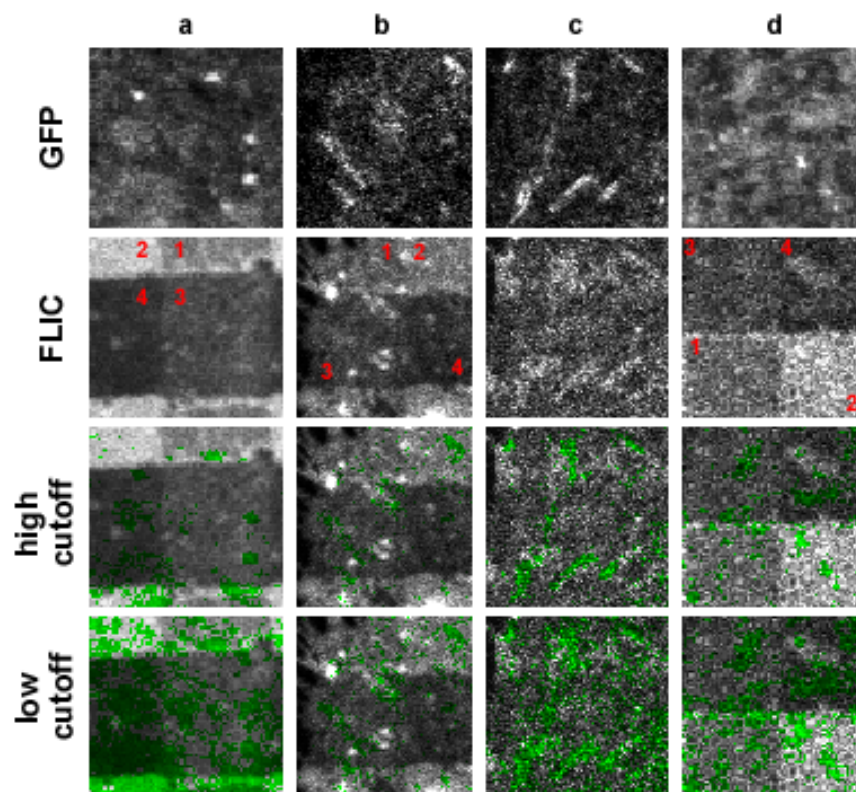


Figure 5.13: Close up of correlation studies (with neuronal culture on fibronectin) between GFP- $\beta 1$ integrin expression and membrane-substrate distance map from FLIC microscopy. The combined images of the two bottom rows are obtained as described in the previous section. Box a: Large dots do not induce any membrane deformation. Box b: $\beta 1$ integrin cluster at cell periphery. Box c: Rough membrane matching the $\beta 1$ integrin clusters. Box d: Intricate mesh-like pattern of the fusion protein does not disturb the smooth membrane.

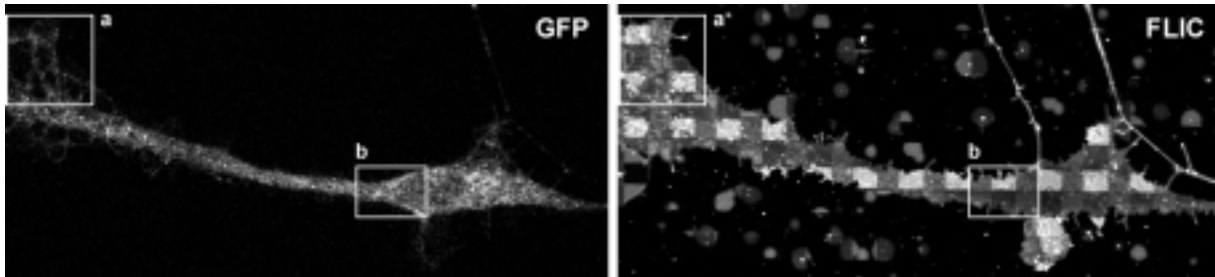


Figure 5.14: A cell in neuronal culture prepared on a laminin-coated silicon chip. There is a higher expression of GFP- $\beta 1$ integrin at the center of the cell body than at the periphery.

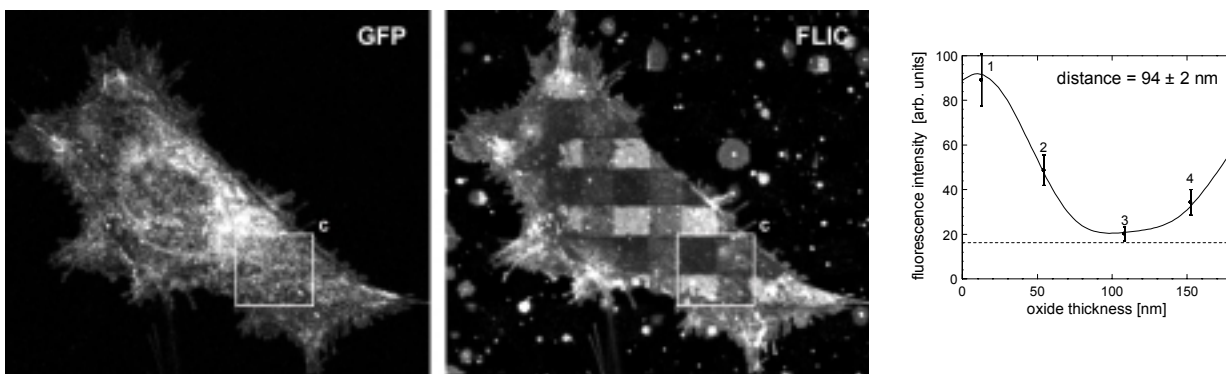


Figure 5.15: A cell on laminin. Many cells in neuronal culture show mesh like intricate distribution of GFP- $\beta 1$ integrin. Despite the presence of integrins, FLIC micrograph shows relatively smooth membrane. The fit to the FLIC theory yields cell-substrate distance of approximately 94 nm.

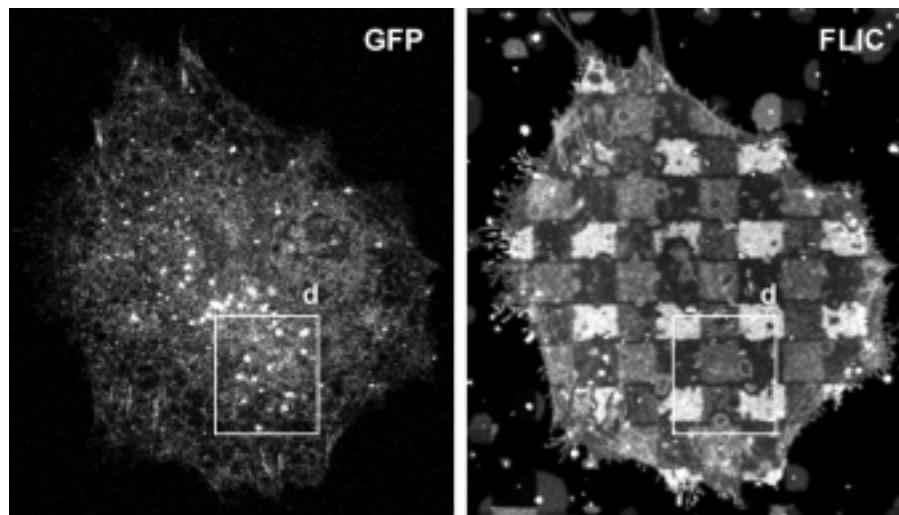


Figure 5.16: An example of a cell attached to laminin with some deformation in lower membrane. There are many distinct large dots of GFP-integrin $\beta 1$ clusters.

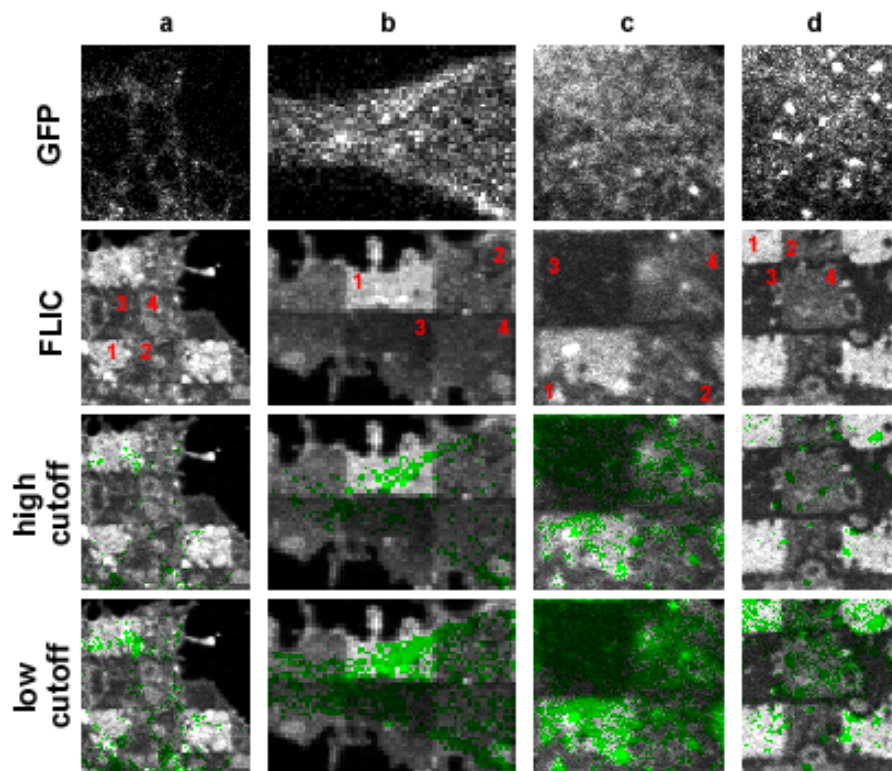


Figure 5.17: Close up of several sections of the adhesion pattern of cells in neuronal culture prepared on laminin. GFP- $\beta 1$ integrin expression at the top row is closely compared with the FLIC micrographs at the same position. As described in the previous figures, the positions where GFP is detected above certain fluorescence intensity is superimposed onto the FLIC picture of DiIC₁₈, where DiIC₁₈ intensity scale is shown in green instead of gray. Box a: GFP- $\beta 1$ integrin expression in dendritic structures on a glia cell. Box b: Fusion protein is not expressed in the protrusions. Box c: In some cases, mesh-like GFP- $\beta 1$ integrin distribution echoed the membrane deformation. Box d: Large dots of fusion protein do not correlate to the membrane roughness.

5.16) of molecular aggregations. There were also high expression of the GFP- β 1 integrin around the cell nucleus waiting to be transported to the cell surface. Many cell compartments which do not contain the fusion protein were visible as dark hollow regions. Most stripes were found at the cell periphery, whereas dots were often found in the cell body.

5.3 Discussion

As mentioned in introduction, cell adhesion is a complex cellular process. This process involves various molecules with specific functions present at specific stages and with intricate dependence on one another. In particular, through a variety of post-translational modifications including glycosylation, proteolytic processing, and changes in affinity for ligand binding [48][18], integrin heterodimers provide vast number of possible combinations of signal pathways that allow transmission of information between extracellular and intracellular environments.

In the following section, the observation from our experiments done with FLIC microscopy and GFP-tagging of both vinculin and β 1 integrin are discussed together with previous studies done on cell adhesion and integrins.

5.3.1 Cell-substrate distance at vinculin and integrin β 1

By comparing the expression patterns of vinculin and integrin β 1 in both fibroblasts and neuronal primary cultures, two different structures of cell adhesion are observed; the focal adhesion plaques found as vinculin clusters in fibroblasts on fibronectin, and the point contacts found as integrin β 1 clusters mostly in neuronal culture on both laminin and fibronectin, and in fibroblasts on laminin. The images from FLIC microscopy show that the focal adhesion plaques that contain vinculin induce parallel ruffling of the ventral cell membrane attached to ECM proteins. This roughness in the membrane could be explained by the organization of filamentous actin into bundles of uniform polarity lead by the aggregation of vinculin to the inner side of the ventral membrane [22]. Lack of vinculin clusters in the smooth cell body in neuronal culture contrast to the extensive vinculin aggregation in fibroblasts with rough membrane suggest that the membrane ruffling involves reorganization of the microfilaments and structuring of actin filaments that lead to establishment of focal adhesion plaques.

The point contacts on the other hand induced no membrane deformation in cells of the neuronal cultures, in agreement with previous IRM studies done with PC12 cells [3]. They have observed that these contact sites lack major cytoskeletal components such as talin and p125^{FAK}, and form only little microfilament bundling. The FLIC microscopy performed shows that the membrane of the cells in neuronal culture attach to the surface with the same separation as that of fibroblasts, but with a very smooth membrane.

In our experiments, the expression of integrin β 1 in fibroblasts on fibronectin exhibited patterns

closely correlated to roughness of the membrane. Estimation of cell-substrate distance by FLIC microscopy showed that presence of integrin $\beta 1$ maintains the membrane at the dominating distance (i.e. around 50 nm) when cultured on fibronectin. The regions where the membrane bulged either upward or downward lacked integrin $\beta 1$. Long incubation allowed formation of clusters both in stripes and occasionally in point forms, suggesting that focal adhesion plaques represented by vinculin clusters could well co-localize with integrin $\beta 1$ clusters at later stage despite of difference between expression patterns of these two proteins at the earlier stage. This could be explained by sequential processes consisting of dynamic contact involving only integrin and the ECM proteins, and the further development of stable contact that additionally involves vinculin and other microfilaments and cytoskeletal components. The latter contacts are therefore scarce in motile cells such as neuronal cells relative to the well attached fibroblast cells [15][73]. Also, fibroblasts attached to laminin are found to be motile and lack focal contacts [71] consistent with our observation (figure 4.6). Although in some cases point contacts in fibroblasts have been described as sites with close apposition to the substrate [64][80][81], these studies show that these point contacts are quite far away from the substrate. In fibroblasts on RGD peptides, the cell-substratum distance at point contacts were 90-200 nm, based on electron microscopy of vertical thin sections. They have defined point contacts as detergent resistant sites which contain little vinculin and microfilament [80]. $\beta 1$ integrin "macroaggregates" on laminin in motile fibroblasts described in [71] is a similar structure appearing only as faint gray patch in IRM images.

Smooth attachment of cells in the presence of integrin $\beta 1$ compared to development of membrane ruffling in the presence of vinculin stripes and integrin $\beta 1$ in fibroblasts on fibronectin suggest that,

- i) integrin $\beta 1$ binding to ECM proteins establishes a basic distance between the ventral cell membrane and the substrate, and
- ii) development of classical focal adhesion plaques containing vinculin induces ruffling of the ventral cell membrane.

Such membrane roughness on one hand is perhaps a result of tight attachment of fibroblasts to fibronectin, and on the other hand is a result of force required for movement at the cell periphery. The latter case is observed also as restricted but high vinculin expression at the cell periphery in cells from hippocampal culture, thus indicates involvement of cytoskeletal reorganization also at filopodia and lamellipodia. This is probably required at the leading edge of motile cells in order to produce the protrusive and the contractile forces described for cell body translocation [55].

Molecular aspect: focal adhesion, fibrillar adhesion and point contacts

Focal contacts are often described as "the best-known class of matrix adhesions in cultured cells", "visualized by electron microscopy or interference reflection microscopy" [50]. Recent compar-

ative studies between unimmobilized and immobilized (where it is covalently link to substrate) fibronectin-coated substrates, have indicated that the physical state of the ECM, not only its composition, plays a critical role in the regulation of differential assembly of adhesion sites [50][67][90]. Their results have lead to distinction of an additional type of integrin association with ECM that transmit cell-generated tension from focal contacts, which they have defined as fibrillar adhesions. Focal contacts and fibrillar adhesions differ from each other in their cytoskeletal association and in the composition of the submembrane plaque. These two structures are segregated at later stages, whose dynamics are presented in their subsequent studies [90]. They have found that in adhesion site of fibroblasts, $\alpha_5\beta_1$ is mainly bound to vitronectin or to immobilized fibronectin (thus nondeformable matrix), whereas $\alpha_v\beta_3$ is mainly bound to regular fibronectin coated surfaces. Both integrins are associated through different plaque proteins with actin filaments (F-actin). Since vitronectin provides a rigid substrate, the former does not move due to these contractile forces. Thus high tension develops, which results in the recruitment of proteins typical of focal contacts. On the other hand, the $\alpha_5\beta_1$ is bound to movable fibronectin matrix, thus is translocated in tensin rich fibrillar adhesion complexes.

Focal contacts

The focal contacts that are mainly associated with $\alpha_v\beta_3$ are found to exclude fibronectin and contain very little tensin. These sites anchor stress fibers [67] and contain a multitude of cytoskeletal molecules; there is a high level of phosphorylated tyrosine residues, enriched with paxillin, vinculin, α -actinin and FAK and they localize at the termini of actin stress fibers. Focal contact assembly depends on the formation of tension, regulated both by intrinsic cytoskeletal contractility and the properties of the extracellular substrate. They contain $\alpha_v\beta_3$ regardless of whether fibronectin is immobilized or unimmobilized [90]. Further more, they have observed that if fibronectin is immobilized, only little amount of fibrillar adhesions are formed, and $\alpha_5\beta_1$ associate also with classical focal contacts; i.e. $\alpha_5\beta_1$ can also in the absence of $\alpha_v\beta_3$, generate typical, highly phosphorylated focal contacts. Thus, $\alpha_5\beta_1$ is able to associate with two types of adhesions, depending on the degree of matrix "deformability" or "rigidity". Additionally, in the absence of $\alpha_5\beta_1$, $\alpha_v\beta_3$ is also able to assemble fibronectin [67]. These functional redundancies explain the indistinguishable attachment between GD25 cells and GD25- β_1A cells in the presence of RGD peptides, where $\alpha_v\beta_3$ is blocked by the RGD peptides from binding to fibronectin, i.e., between adhesion to fibronectin through $\alpha_v\beta_3$ and $\alpha_5\beta_1$. Integrin $\alpha_5\beta_1$ seems to be capable of switching roles, in order to functionally compensate for low level of integrin $\alpha_v\beta_3$ expression. A comparative results on $\alpha_5\beta_1$ and $\alpha_v\beta_3$ integrins, how β_1 -integrin influences fibronectin matrix assembly is presented in [91].

In general, focal contacts are found to predominantly contain integrin $\alpha_v\beta_3$ [67], originally found as vitronectin receptor. In primary fibroblasts, integrin $\alpha_v\beta_3$ has been shown to remain confined in focal contacts, for instance on immobilized fibronectin [50][90]. Astrocytes in neuronal cell

cultures are observed to form focal contacts which additionally contain integrin $\alpha 6\beta 1$ when cultured on laminin and $\alpha 5\beta 1$ on fibronectin [3][81]. In fibroblasts, also integrin $\alpha 1\beta 1$ is shown to accumulate in focal contacts [81].

Fibrillar adhesions

Fibrillar adhesions, which are associated mainly with $\alpha 5\beta 1$, bind fibronectin fibrils and align parallel to actin bundles and tensin. There, distribution of vinculin and $\alpha 5\beta 1$ are found to be largely mutually exclusive on regular fibronectin, possessing high levels of tensin but very little paxillin and vinculin. In fibroblasts, adhesive contacts in which cell surface integrins bind to fibronectin fibrils in fibrillar adhesions are maintained even when cell contractility is inhibited with specific drugs. They are characteristically elongated or beaded structures, located more centrally in cells. At the initial stage, integrin $\alpha 5\beta 1$ are assembled at one pole of classical focal contacts co-localizing with $\alpha v\beta 3$. Upon this ligand-mediated occupancy and receptor clustering, studies through immunohistochemistry has shown that they are actively transported along actin microfilament bundles towards the cell center [67][90]. In fibroblasts, integrin $\alpha 5\beta 1$ is implicated to be involved in matrix assembly by transmitting tension generated by cytoskeleton to ECM [67].

Point contacts

Point contacts are an adhesion structure which has already been extensively characterized in many cell types, specially in transformed fibroblasts and normal rat astrocytes cultured on RGD and laminin [81]. These sites do not contain major cytoskeletal components [3] and involve only little microfilament bundling. Lack of both protein clusters and close contact could explain the absence of dark spots at these sites in chick skeletal fibroblasts observed by IRM [71]. These macroaggregates or point contacts containing integrin $\alpha 5\beta 1$ are also often found in developing and regenerating peripheral neurons [3]. They observed that PC12 cells form point contacts with integrin $\alpha 1\beta 1$ and $\alpha 3\beta 1$, which only partially co-localize with vinculin.

According to previous studies, focal adhesions on fibronectin represented by vinculin do not necessarily contain $\beta 1$ integrins, but mostly $\beta 3$ integrins. This could explain the clear difference in distribution between vinculin and $\beta 1$ integrins in GD25/GD25- $\beta 1A$ cells on unimmobilized fibronectin-coated silicon, since $\beta 1$ integrin is found to co-localize with focal contacts only when fibronectin is immobilized on the surface.

Heterogeneous expression of integrin $\beta 1$ observed in neuronal culture of mixed cell types is probably due to dependence of $\beta 1$ heterodimer clustering on cell types; for instance, differences between fibroblasts and astrocytes are presented in [81]. As stated in the review [34], integrin-ECM interactions induce several types of intracellular responses. Cell membrane structure is one of the diverse responses of a particular cell type in a particular state to complex integrin-specific signalling triggered by a particular ECM-integrin interaction.

Chapter 6

GFP-substrate distance

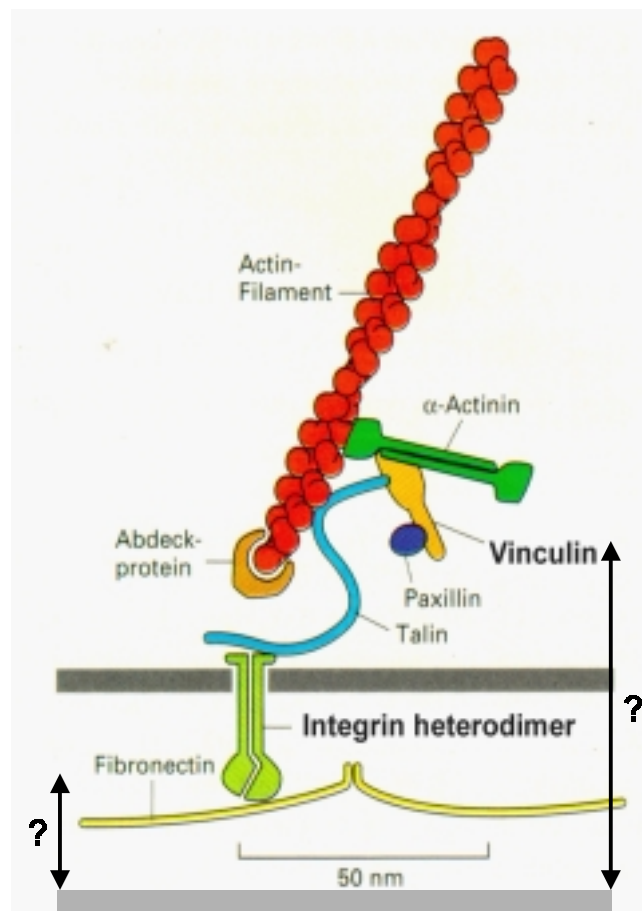


Figure 6.1: A simplified illustration of focal adhesion complex. (adapted from B. Alberts, et al. *Molecular Biology of the Cell*, 2nd ed., Garland Publishing, Inc., New York (1989))

In this chapter, analogies and differences between fluorescence of DiIC₁₈ and that of GFP in front of the reflecting silicon surface, which could enable and hinder an estimation of GFP-substrate distance are discussed. As mentioned in the previous chapters, detected fluorescence intensities of GFP hanging from both vinculin and $\beta 1$ integrin also exhibit the interference effect, to which FLIC theory can be applied. However, the accuracy is limited either because the requirements (as discussed in chapter 2) for the theory are not fulfilled or due to the difficulties as the following:

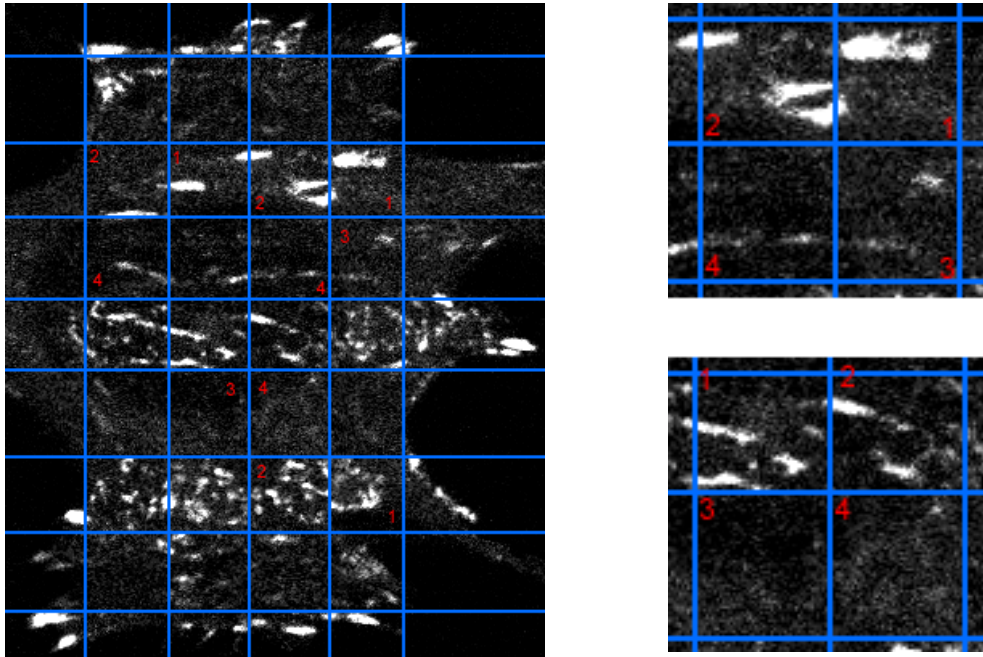


Figure 6.2: *Stripes of GFP-vinculin across two oxides could be used to obtain the ratio between fluorescence intensities on these oxides. The blue lines border the steps between the four oxides numbered in red. Destructive interference of the detected GFP in front of oxide 3 and 4, and constructive interference in front of oxide 1 and 2 can be observed in this example.*

(i) assessment of homologous regions of GFP present on all four steps is not possible, thus the detected fluorescence intensity becomes dependent also on an additional unknown parameter, the amount of GFP,

(ii) overall, it is not possible to define a representative detected intensities of GFP for all four oxides; only subjectively chosen data are available for the distance calculation.

Keeping these in mind, a preliminary attempt to make an estimation of distance from both GFP-vinculin and GFP- $\beta 1$ integrin to substrate (figure 6.1) will be briefly discussed in the next sections. An example of analysis to calculate the GFP-oxide distance for the case of GFP-vinculin in fibroblasts cultured on fibronectin will be presented.

6.0.2 GFP-vinculin to substrate

In principle, the ratios between the detected fluorescence intensities over the four oxides are sufficient in order to fit the theoretical curve. In the case of interference of GFP-vinculin, a long stripe of the fusion protein lying over two oxides would enable estimation of such ratios (figure 6.2, right). However, due to destructive interference over both oxides 3 and 4, the stripes of GFP-vinculin clusters over these two oxides are not visible (figure 6.2). Thus the ratio between intensities over oxide 1 and 2 are only reasonably obtainable. Often, the edge between two

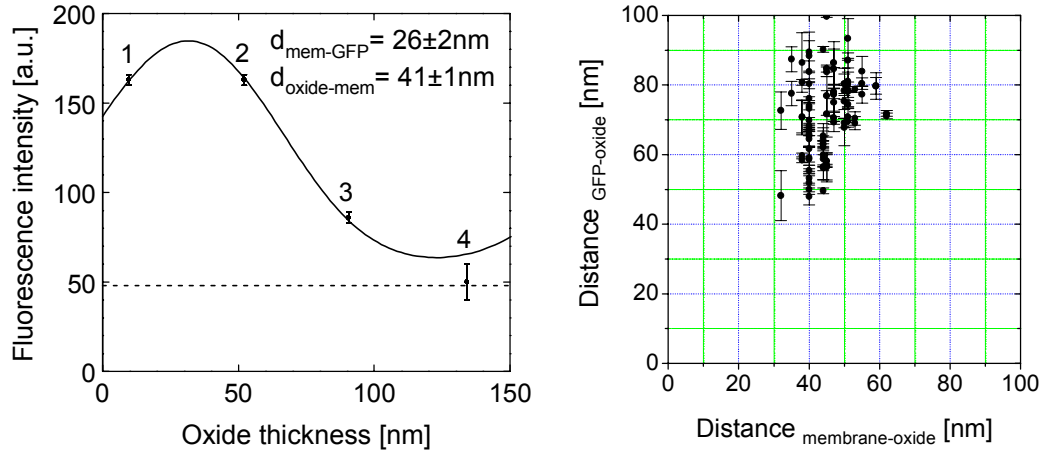


Figure 6.3: Estimation of GFP-oxide distance in the case of GFP-vinculin expressed in GD25-β1A cultured on fibronectin. Left: An example of fitted curve to the fluorescence intensity of GFP. The data points are the brightest pixels from each of the four oxides. The data are from the oxides neighboring the box b of figure 4.4. Right: A result of analysis from 86 distance calculations. Weighted average comes out to be $d_{\text{GFP}_i \text{ oxide}} = 76 \pm 20 \text{ nm}$.

oxides was difficult to be identified and the transition in fluorescence intensity around the edge was not clear. Thus although the ratio between fluorescence intensities over oxide 1 and 2 could be obtained from many data sets, no consistent values were collected. Roughly, the intensities on these oxides were similar to one another and were much brighter than on oxide 3 and 4.

Another possibility is to consider only the brightest detected intensities over each of the four oxides that are near one another to fit a theoretical curve. This process requires a statistical studies based on a large collection of data in order to produce a comfortable estimation. In most cases, theoretical curves were not able to be fitted optimally to the data points chosen in this manner, which can be seen by an example of the fitted curve in figure 6.3. For this analysis, random orientation of GFP molecules were assumed and the calculation was based on

$$d_{\text{GFP}_i \text{ oxide}} = d_{\text{GFP}_i \text{ membrane}} + d_{\text{membrane}} + d_{\text{membrane}_i \text{ oxide}}$$

where $d_{\text{GFP}_i \text{ membrane}}$ is the distance from GFP to the cytoplasmic side of the ventral membrane and d_{membrane} was set to 4 nm. The result varies within a large range; many calculated values are also with large stochastic errors (figure 6.3, right). The weighted average from the calculation of 86 data sets was $d_{\text{GFP}_i \text{ oxide}} = 76 \pm 20 \text{ nm}$. This corresponds to $d_{\text{GFP}_i \text{ membrane}} = 26 \pm 26 \text{ nm}$ based on the value of $d_{\text{membrane}_i \text{ oxide}}$ for the case of GD25-β1A cells cultured on fibronectin, as taken from the table 3.1.

6.0.3 GFP-β1 integrin to substrate

Due to the expression pattern of GFP-β1 integrin fusion protein that lack clusters in the form of stripes, only the second approach discussed for GFP-vinculin is applicable in this case. In the

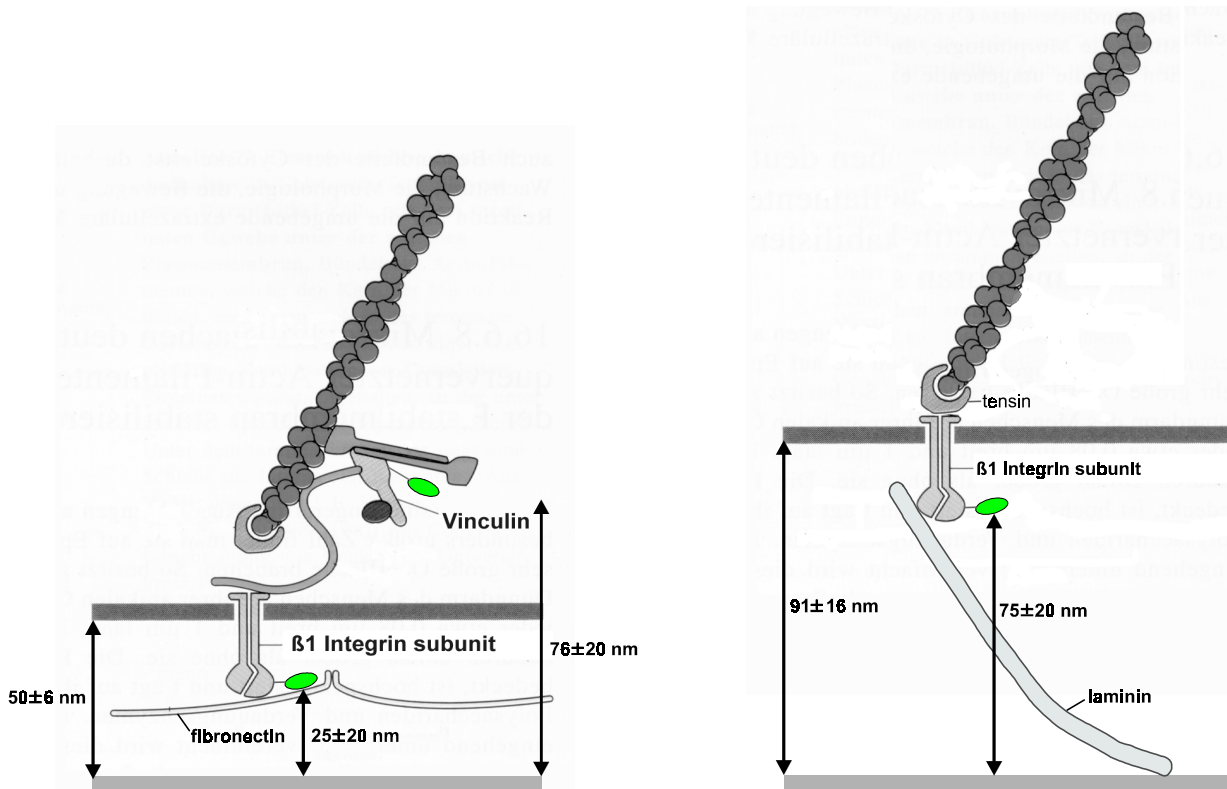


Figure 6.4: *DilC₁₈-oxide and GFP-oxide distance according to FLIC microscopy. Rough estimations are made based on the interference effect of detected GFP intensities from FLIC micrographs of GD25/GD25-β1A cells on fibronectin (left) and laminin (right).*

same manner, GFP intensities over the four oxides could be used to roughly estimate the GFP-substrate distance. When fibroblasts were cultured on fibronectin, GFP tagged to the extracellular side of β1 integrin was most visible on oxide 2 and 3 (figure 5.3), which corresponds to a rough estimation of 25 ± 20 nm. Similarly, on laminin, the interference effect of GFP (figure 5.6) has corresponded approximately to $d_{\text{GFP}_i \text{ oxide}} = 75 \pm 20$ nm. In figure 6.4, the estimated values are depicted into a modified version of the illustration adapted from [1].

Chapter 7

Comparison of distance measurements

According to the well-accepted model, we had expected that the membrane at focal contacts represented as vinculin would sharply approach the substrate. This notion is based for example, on the IRM images where focal contacts appear as dark contrast against gray background that has been interpreted to estimate the distance between the ventral cell surface and the substratum to be within 15 nm [48][55][71][79]. However, the correlation studies with FLIC microscopy and GFP-tagging of vinculin and $\beta 1$ integrin have shown that this is not the case. In order to find theoretically and experimentally the cause of the different observations with regard to cell-substrate distance at so-called focal contacts, we have performed similar correlation experiments with TIRAF microscopy and IRM.

First, a simple evaluation of both techniques with respect to optical parameters of the cell system is presented; many previous studies have ignored for instance, cell membrane [72], since they assumed the membrane thickness to be very thin, and further assumed similar optical properties for cytoplasm and cell-substrate gap as layers of water.

Secondly, results from experiments performed with the same system using GD25- $\beta 1$ A cells as for FLIC microscopy are presented to evaluate TIRAF microscopy and IRM. The culturing condition, biochemical labeling of focal contact by GFP-vinculin transfection, same substrate treatment and the same measuring condition for the cells were retained. Due to limitation in the instrumental setup at this point, we have separated the experiments into two parts;

i) for quantitative analysis of cell-substrate distance by TIRAF microscopy, GD25- $\beta 1$ A cells were cultivated without transfection by GFP-vinculin, since simultaneous observation of fluorescent protein was still not possible with this setup. The estimated distances were compared with the values obtained from FLIC microscopy.

ii) simultaneous observation of GD25- $\beta 1$ A cells were done with TIRAF, IRM and CFP-vinculin, where only qualitative analysis was possible. The images were compared also based on the TIRAF measurements from part i).

7.1 Dependence on cell parameters

For the three methods, IRM, TIRAF and FLIC microscopy, effect of refractive indices of mem-

brane and the cell-substrate gap and the membrane thickness on the estimation of distance are discussed in this section. For this evaluation, calculation is simplified to a case for monochromatic incident light disregarding aperture integration and correction at the same time retaining the actual experimental parameters.

Local increase in the refractive index of cytoplasm at focal contacts are discussed also in previous studies [7][13][72]. The molecules bound to the cytoplasmic side of the plasma membrane at focal contacts could become large, stacked to 50 nm, since membrane-bound integrin for example alone spans from the membrane by around 15 nm [26][65]. To evaluate its influence on calculation by each theory, we have represented this layer of molecules by a thickening of the plasma membrane with index of refraction at 1.45. In [8], refractive index of cell membrane is described at close contacts between 1.354-1.368, at focal contacts between 1.38-1.40 and otherwise between 1.353-1.368. Represented as an averaged layer of 0-350 nm dense cytoplasm, Bailey and Gingell have estimated the local refractive index to be 1.38 or 1.40 for cytoplasmic protein concentration of 25% or 35%, respectively [7]. Instead of using an averaged value, in our studies, calculations are performed to compare the site of focal adhesion, as represented as thickening of the plasma membrane, and the remaining region assuming absence of protein accumulation.

Also discussed in [7] is an local variation in the refractive index of the water gap between the cell and the substrate due to ECM protein coating. In their models, they have taken the same values as for the local refractive index for cytoplasm depending on the protein concentration. Additionally, they have incorporated the glycosylation of the ECM proteins at the cell surface by assuming a layer of 5-30 nm beside the membrane to have refractive index of either 1.348 or 1.364 for 10% or 20% sucrose solution, respectively. In the present study, this effect of denser medium underneath the cell is evaluated with a model by increasing the refractive index of the water gap layer from 1.33 to 1.37.

7.1.1 TIRAF microscopy

Since the evanescent field excites the fluorophore in the cell-substrate gap, relative fluorescence to background increases with increasing cell-substrate gap; the effect of parameters can be observed in the penetration depth given by the expression (12) in chapter 2. The graphs in figure 7.1 is based on a calculation incorporating the parameters from our actual experimental setup, where incident angle is 68.285^\pm and $\lambda_{inc} = 488\text{nm}$.

Refractive index of membrane and membrane thickness

For the case of fluorescence in the water gap, in agreement with analysis in [37], detected intensity increases with increasing refractive index of cytoplasm or membrane. This effect becomes large, when a stack of protein would be treated as thickening of the membrane, as shown by the graph in figure 7.1 (left). Thus consistent with the analysis in [54], increasing either the refractive index

or the thickness of membrane reduces the computed distance between substrate and cell.

Refractive index of cell-substrate gap

Variation in refractive index of the water/medium under the cell has larger effect as that of membrane/cytoplasm as shown in figure 7.1 (right). This effect is most prominent in the case of incident angle close to the critical angle. Increasing refractive index of the medium that contain fluorophore has opposite effect on the calculated distance as increasing that of the layer above. Denser medium reduces the depth of penetration of the evanescent field as one sees in the equation (12). Thus decrease in the field energy results in regions of high refractive index appearing darker with the same distance. This effect is discussed in [8] and [54]; there, refractive index of the water gap is characterized between 1.33-1.40 for focal contacts. This local variation in the optical property leads to local variation in the critical angle in the range between $61-67^\pm$ for attaining evanescent field in this layer. With refractive index of the water gap 1.33, critical angle is 67.808^\pm and with 1.40, 64.970^\pm . Thus incident angle in this range may result in locations in the cell image that are not being excited by evanescent radiation. This effect however becomes smaller with increasing incident angle. However at larger angle, a negative effect takes place; above 74^\pm , background noise is found to increase when observing ventral cell membrane [14]. Additionally, as apparent again from the expression for the depth of penetration, the magnitude of field strength decreases with increasing incident angle [37][44]. Taking these into account, for the present experiment, incident angle high enough was chosen to avoid the above case thus to ensure that critical angle is attained everywhere, but not too large to avoid decrease in its sensitivity.

The critical parameters in TIRAF microscopy are the refractive index that determine the strength of evanescent field in the cell-substrate gap. The thickness of the layer beyond the cell membrane has small effect. Thus adhesion structures with dense ECM protein clusters influence the distance calculation stronger than the presence of any aggregation of cytoskeletal proteins.

7.1.2 IRM

Here, an incident monochromatic light at $\lambda = 577\text{nm}$ normal to the interface is considered. The graphs in figure 7.2 are obtained by the equation (16), but omitting the integration over the aperture, thus also the aperture weight function for both excitation as well as for detection. Amplitude and phase of the sinusoidal relationship between the detected intensity and the cell-substrate distance are influenced by the parameters such as refractive indices of membrane and medium and the thickness of the membrane. Since the intensity of the detected reflection is strongly dependent on the phase difference between the ray from each interphase, the thickness of the layer is critical in the calculation. At this wavelength, changes in refractive index of the membrane or the cell-substrate gap appear to have minimal effect. More critical parameter is found to be therefore the thickness of a dense layer above the ventral cell membrane, modeled here as a thickening of the membrane itself.

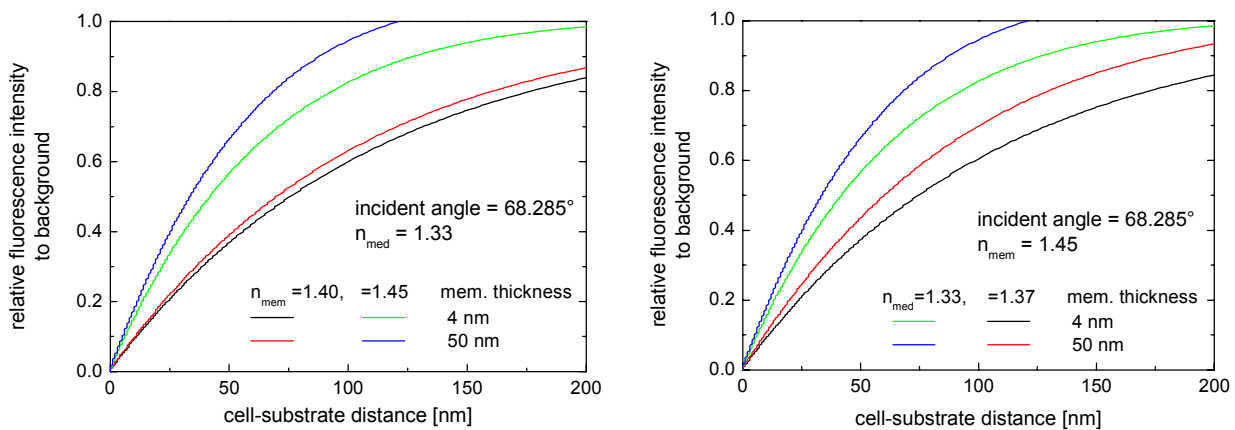


Figure 7.1: TIRAF microscopy: Theoretically calculated relative fluorescence intensities for the present experimental setup (i.e. incident angle is set to 68.285°) without aperture integration of the detected light. Calculation of cell-substrate distance by TIRAF microscopy depends on the optical parameters of the layer system used. Left: Dependency on refractive index and thickness of the membrane. The graph shows that if there is a thick layer (50 nm) of protein with similarly high index of refraction as for lipid membrane, then the calculated distance deviates only slightly from a model assuming a thin layer (4 nm) of membrane, specially if a lower index of refraction, $n_{\text{mem}} = 1.40$, is chosen. However, the relationship between the fluorescence intensity and cell-substrate distance is quite sensitive to refractive index of membrane. Right: Dependency on refractive index of the cell-substrate gap. The relative fluorescence decreases with increasing refractive index, which is an opposite dependency as on the refractive index of membrane.

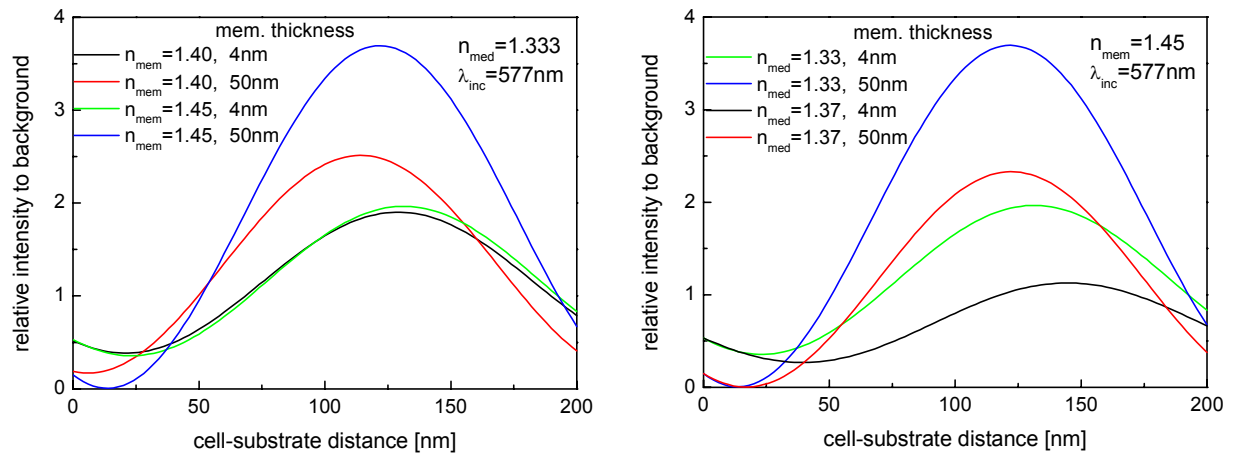


Figure 7.2: IRM: Theoretically calculated detected relative intensities for a simplified case of monochromatic incident light at $\lambda_{inc} = 577\text{nm}$ perpendicular to the interfaces. The refractive index of cytoplasm is set to 1.37 and thickness of $3 \mu\text{m}$. Calculation of cell-substrate distance by IRM depends also on the optical parameters of the layer system used. Left: Dependency on refractive index and thickness of the membrane. The graph shows that if there is a thick layer (50 nm) of protein with similarly high refractive index comparable to lipid membrane, then the calculated distance deviates substantially from a model assuming a thin layer (4 nm) of membrane. The effect is similar whether $n_{mem} = 1:40$ or $1:45$ is chosen; denser medium reduces the relative reflectivity if the cell-substrate distance is less than around 35 nm, however the effect switches at this value. Right: Dependency on refractive index of the cell-substrate gap and on the membrane thickness.

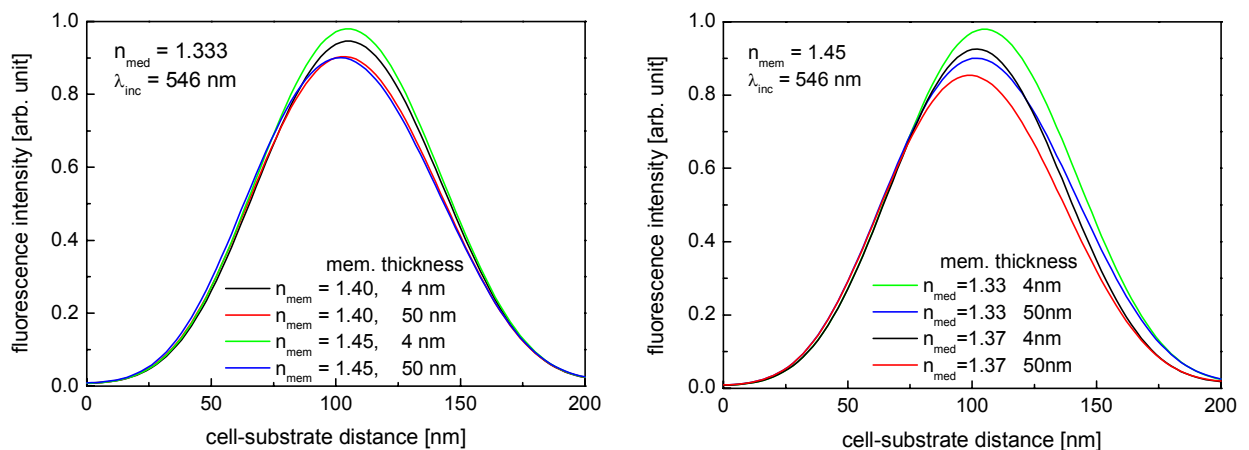


Figure 7.3: FLIC microscopy: Theoretical calculation of fluorescence intensity of DiI₁₈ embedded in a cell membrane illuminated at $\lambda_{em} = 546\text{nm}$ perpendicular to the surface and detected by an emission filter with $\lambda_{em} = 570 \text{ ; } 655\text{nm}$. The fluorescence intensity at each cell-substrate distance is almost identical regardless of the variation in optical parameters, specially up to around cell-substrate gap of about 75 nm.

Refractive index of membrane and membrane thickness

IRM images are strongly affected by the optical properties at the cytoplasmic side of the membrane. In agreement with the modelling presented in [7], local increase in refractive index at the cytoplasmic side represented here as thickening of membrane decreases the detected irradiation until the cell-substrate distance reaches around 35 nm (figure 7.2, left). If the lower membrane is further than about 35 nm from the substrate, thickening of the optically dense layer drastically increases the reflected intensity and also increases sensitivity to the refractive index of that layer.

Refractive index of cell-substrate gap

In the case of interference reflections, increase in the refractive index of the water gap to represent the presence of ECM proteins has the same effect as for the membrane; higher the refractive index, lower the reflectivity. The effect becomes more prominent with water gap larger than around 35 nm (figure 7.2, right). As also discussed in [7], the effect of protein coating maybe minimal, since protein is present in both cell and background areas. ECM protein is however present at higher concentration at focal contacts corresponding to increase in refractive index. The calculations still show smaller effect relative to changes in optical properties of the cytoplasmic side.

Looking at the switch of the effect of increasing membrane thickness, one could say that on laminin, focal contacts could appear darker only due to reduced cell-substrate distance. However the increase in detected light due to dense cytoplasmic protein clusters could counter balance this local variation. Thus it is difficult to simply assume that there is no close contact or that focal contacts are not formed from the IRM images.

In the case of cells attached to fibronectin, the lowest measured reflection at focal contacts in IRM images could arise from the following three causes; i) a local increase in density of protein in the cytoplasm, ii) a high density of ECM clusters under the membrane or iii) a reduced distance between the membrane and the glass substrate. At the cell periphery with thin cytoplasm, reflection from the upper membrane may also affect the detected interference intensity.

7.1.3 FLIC microscopy

The simplified case with DiIC₁₈ excited by a monochromatic incident light at $\lambda_{inc} = 546\text{nm}$ normal to a homogeneous layer of silicon dioxide and reflected at silicon is employed here to demonstrate the effect of optical parameters for the multilayer system. The graphs in figure 7.3 are obtained for a case of no oxide layer and also omitting again the aperture integration and correction for the excitation and the detection. The result exhibits both properties of the excitation of fluorophore similar to TIRAF microscopy and of the reflected light at silicon similar to IRM.

FLIC microscopy deals with interference between the incident and the reflection of both excitation and emission. The dependency on the density of each layer between the interfaces becomes negligibly small, a similar phenomenon seen in IRM. The interference is influenced by the phase

difference among the interfering fields, which makes it sensible to the thickness of each layer. Because of the dominating effect of the reflecting silicon surface, this sensitivity is also reduced to minimal effect. The four oxide steps calibrates the fluorescence intensity to cell-substrate separation relationship. The selective marking of the cell membrane with DiIC₁₈ reduces the effect of local variation in optical properties of other layers on the detected intensity. The graphs in figure 7.3 show only minimal deviations due to changes in refractive index of the membrane from 1.40 to 1.45, or that of the cell-substrate gap from 1.333 to 1.37. Specially for the case where the cell-substrate distance is smaller than around 75 nm, which is the range most relevant to cell cultures on fibronectin, the choice of the optical parameters have essentially no influence on the relationship between fluorescence intensity and its corresponding cell-substrate separation. Thus the detected fluorescence intensity in FLIC microscopy is essentially insensitive to possible local variation due to clusters of ECM proteins or cytoskeletal proteins, but only to the cell-substrate distance.

7.2 Analysis of experimental data

7.2.1 TIRAF microscopy

Under the same conditions as the experiments performed with FLIC microscopy as described in chapter 3, the cell-substrate distance was measured using TIRAF microscopy. As specified in chapter 2, fibroblast cells were cultivated on glass plates of thickness 1 mm, which were cleaned and silanized prior to coating with ECM protein. Here, the cell-substrate distance was estimated for the cases with fibronectin- and laminin-coated substrates. As shown in the following figures 7.4 and 7.5, the distances measured for fibronectin with TIRAF microscopy matched roughly the values obtained with FLIC microscopy, specially in the cases where the lower membrane was smooth on the substrate (figure 7.4, right). The calculation based on the theory for TIRAF microscopy has yielded larger distances for the cells attached to fibronectin with rough membrane, as depicted by the graph in figure 7.5. The large membrane region is approximately 75 nm away from the substrate, with recurring closer contacts at around 50-55 nm. Also upward bulging ranging between 100 nm and even 150 nm were found frequently. According to the line profile of the distance estimated with TIRAF microscopy, structures which could be identified as patches of focal contacts in these cells attached to fibronectin were in fact far away from the substrate. The smallest distances estimated were never under around 40 nm, as demonstrated by the example in figure 7.4. Since an accurate estimation of the distance based on FLIC theory could only be obtained for relatively homogeneous membrane region, it is not clear whether this is an actual discrepancy or is coming solely from the first impression.

The cell-substrate distance for the cells adhered to laminin-coated glass plates obtained from the TIRAF measurements on the other hand were in closer agreement with that from the FLIC

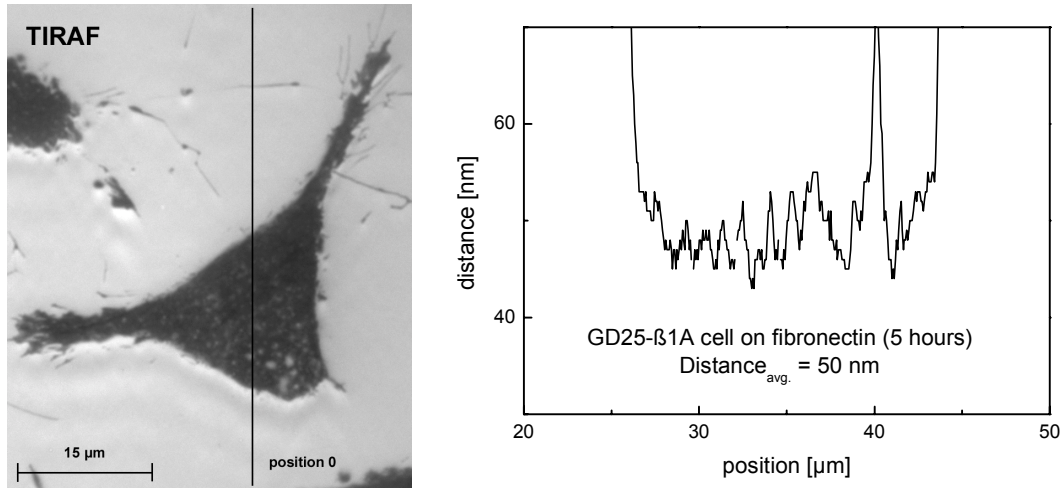


Figure 7.4: TIRAF image of a GD25-β1A cell cultivated on fibronectin-coated glass. An example of a cell adhered to the substrate with smooth membrane. The graph at the right shows the ventral membrane-substrate separation topography along the line labeled in the image over the cell. A fluctuation of the separation width ranges within around 10 nm. The estimated average separation agrees approximately with the distance calculated with FLIC theory.

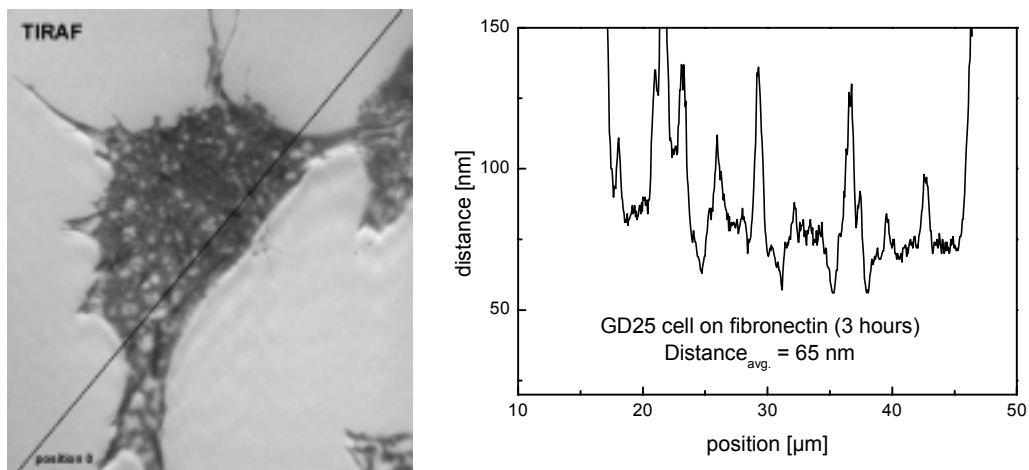


Figure 7.5: GD25-β1A cell cultivated on fibronectin exhibiting rough membrane attachment to the substrate. Right: Analysis of this TIRAF image indicates that the membrane is at the lowest point, around 50 nm away from the substrate. Upward bulging separates up to 100 nm or greater from the substratum surface. Focal contacts-like pattern of close apposition spans unexpectedly large cell-substrate gap.

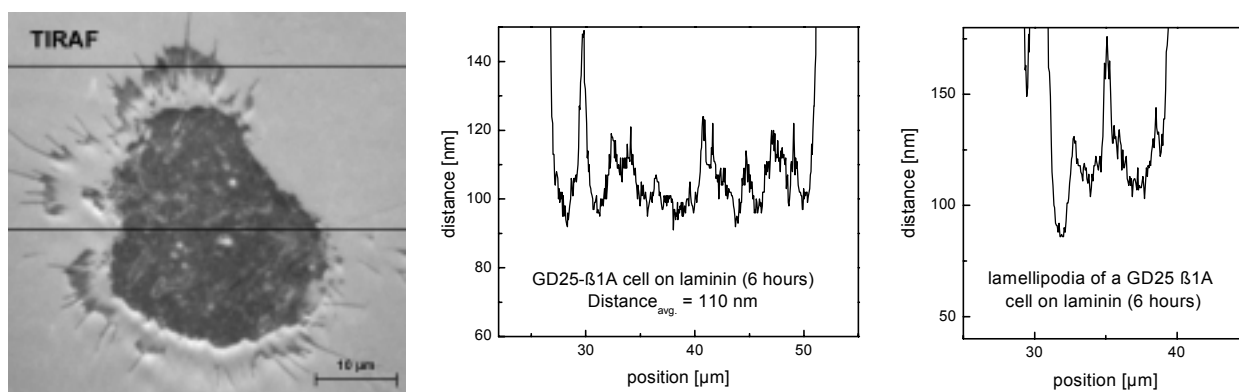


Figure 7.6: TIRAF image and distance analysis of GD25-β1A cell cultured on laminin. The graph in the middle shows the profile of membrane-substrate distance along the line across the cell body. In agreement with the values obtained from FLIC theory, the cell is on average around 100 nm away from the substrate. The graph on the right side shows the distance profile across a lamellipodia structure.

measurements. As shown in figure 7.6, the cells were on average 100-110 nm away from the substrate, only slightly larger than what is estimated from FLIC microscopy. As shown by the graph at the right side in figure 7.6, lamellipodia extended from the cell body often appeared as high fluorescence region at their roots around the cell body, and then became darker at the extensions. Since lamellipodia are found to be very thin structure, contribution of excited fluorescence molecules above the lamellipodia cannot be excluded. Thus these neighboring bright and dark regions of lamellipodia could be in one way explained, that at the thin root of lamellipodia, the upper membrane ends well within the penetration depth of exponentially decaying evanescent field, therefore the fluorescence molecules above this upper membrane is also excited by the evanescent field. The emitted fluorescence by these molecules above the structure addition to the fluorescence emitted below the cell could account for the unusual bright area between the cell body and the cell periphery. The effect of fluorescence stimulated beyond the lamella due to penetration of the thin cytoplasmic layer by the evanescent wave is discussed also in [37]. On the other hand, the outermost periphery of lamellipodia is thick enough, i.e. the upper membrane positions further than the penetration depth, thus the fluorescence molecules above the upper membrane do not experience the evanescent field. A more direct interpretation of the interrupting bright region surrounding the cell body is that the ventral cell membrane is in fact far away at this area and it becomes closer to the substrate again at the periphery.

As discussed in the previous section, the dependence of calculated distance on membrane thickness at refractive index of membrane between 1.40-1.45 becomes stronger with increasing cell-substrate gap. For instance, setting $n_{\text{mem}} = 1.45$, the case for the figure 7.4, the average distance at the labeled cross section varies from about 50 nm to 40 nm, whereas the distance of a cell attached on laminin in figure 7.6 varies from approximately 110 nm to 80 nm, in the range of

membrane thickness between 4 nm and 50 nm. Calculation with higher angle of incidence up to 85^\pm yields also similar modulation in the estimated cell-substrate distance due to varying membrane thickness and refractive index of membrane.

The dependency of the calculated distance on the refractive index of membrane, n_{mem} , and of the cell-substrate gap, n_{med} , are opposite to each other. For a multilayer system with membrane thickness of 4 nm and $n_{\text{med}} = 1.337$, the estimated distance reduces only by about 2% if n_{mem} is varied from 1.40 to 1.45. However, for a model setting $n_{\text{mem}} = 1.45$ and thickness to be 4 nm, the cell-substrate distance for the cell in figure 7.4 estimated to 50 nm increases to 80 nm if the n_{med} is varied from 1.33 to 1.37. The same variation increases the value for the cell in figure 7.6 from 110 nm to 140 nm. Thus the local variation of optical properties in the region of focal contacts results in superposition of over- and underestimation of the cell-substrate distance. The estimated values here indicate that rather the under-estimation dominates at focal contacts (i.e. in the regions with small distances) appeared as reduction in detected fluorescence intensity if the distance is determined with the optical parameters that ignore modulation in n_{mem} , n_{med} and membrane thickness.

An approximation of cell-substrate distance is presented in [72] for fluorescence in water gap based on the assumption that cell membrane can be neglected, thus by simplifying a glass/water/membrane/cytoplasm layer system to a glass/water/cytoplasm system. Further, they have combined the two-phase glass/water and the glass/cytoplasm interfaces to approximate the fluorescence intensity excited in the three-phase system. Here, the analysis relies on the assumption that membrane thickness is much smaller than the incident wavelength. Thus at membrane region where this assumption applies, the % error of ignoring the membrane layer is confined within 2.5%. It becomes more critical at sites such as focal contacts, which consist of stacking of cytoplasmic molecules and ECM proteins.

We have simplified our calculation in several ways; first we did not integrate the detection of fluorescence over the aperture and further ignored any changes in the fluorophore quantum efficiency as a function of distance from the substratum and orientation to the substratum surface. We have also neglected any presence of fluorescence excited by scattered light and inhomogeneous fluorophore distribution. Significant effect due to the excitation of fluorescence by light scattered from the solid/liquid interface for protein adsorption is mentioned in [72]. The variation in fluorescent dye concentration affects the detected intensity specially at the region of high protein concentration around focal contacts or of high fibronectin concentration, since it locally excludes fluorescent dyes [54]. However for small molecules such as rhodamine green (MW = 411), this effect is minimal.

7.2.2 TIRAF microscopy and IRM

Using the setup as described in chapter 2, images of IRM, TIRAF and CFP-vinculin were ob-

tained. The distribution of CFP-vinculin matched closely the dark patches in IRM images. TIRAF images showed similar membrane structure to FLIC images with upward ruffling that aligned parallel to the vinculin stripes.

The relative intensities obtained theoretically are used as reference to approximate the cell-substrate distance from the experimental values of relative intensities. Possible choices of optical parameters that describe the multilayer system is considered specifically for positions with vinculin clusters in CFP images correlated to dark patches in both TIRAF and IRM images that represent focal contacts. The graphs in figure 7.10 are calculated for the IRM setup including the aperture integration and correction with incident ray at $\theta_{inc} = 577\text{nm}$. A very rough approximations of the cell-substrate distances (figure 7.11) are made for several cell parameter combinations based on these graphs. The dark patches in IRM co-localized with vinculin, normally interpreted as focal contacts with membrane closely apposed to the substrate, did not correspond to small cell-substrate distances. Based on the dependency of relative intensities on the cell-substrate distance for several optical parameters (graphs in figure 7.10), the dark intensities could not possibly arise from reduced distances. The list of rough estimations in figure 7.11 shows that the optical properties chosen for the calculation influence strongly in determining the cell-substrate distance.

7.3 Discussion

As in the analysis of FLIC microscopy, TIRAF microscopy and IRM require a model for the multilayer system. In these techniques, the estimated distance depends strongly on the optical parameters chosen for the model used. The model appropriate for each experimental case is not trivial to be defined. Thus results from these methods are difficult to be interpreted accurately. Strong influence of cytoplasmic properties on IRM images has been known [7][13]. The exact architecture of the molecular arrangement around the membrane is required in order to define a model with accurate varying index of refraction.

The dark pattern seen with IRM could represent either sites of high index of refraction, which occurs with stacking of protein at the membrane, or sites of close contacts. With GFP/CFP-tagging, we have seen that the focal adhesion plaques consist of vinculin aggregates which would alone certainly lead to thickening of the layer with a higher index of refraction. Indeed at focal contacts, tight microfilament bundles and aggregation of cytoskeletal proteins are formed at the cytoplasmic side. The point contacts with only little microfilament bundling and aggregation of cytoskeletal proteins, in fact, appear brighter than the stripes of focal contacts in IRM images, which could indicate that there is either no close contacts or no major accumulation of proteins [3][71]. IRM is sensitive to changes in the thickness of a layer with increased refractive index above and including the cell membrane.

On the other hand, a variation in the thickness of the membrane or the cytoplasm beside the

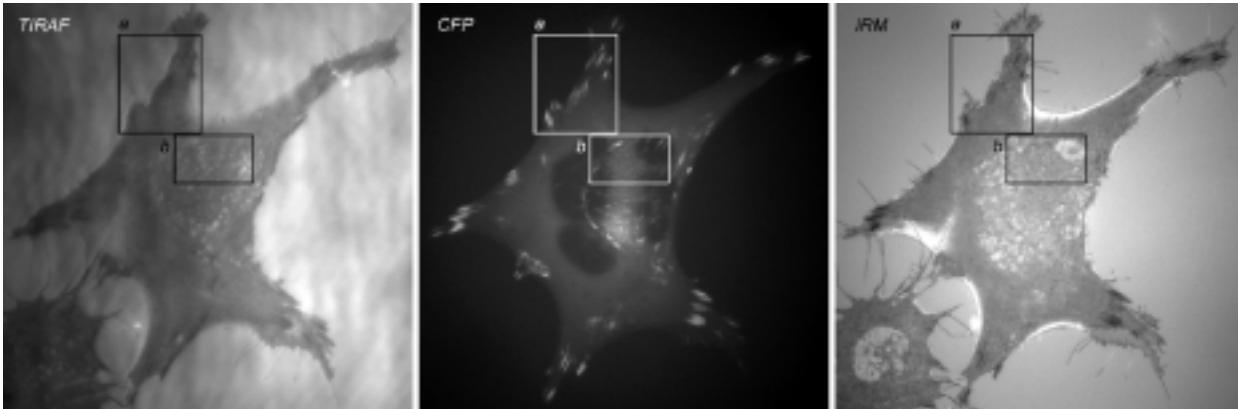


Figure 7.7: GD25- β 1A cell expressing CFP-vinculin construct. The cell was allowed to adhere 2 hours on fibronectin-coated glass coverslip. The images were obtained with a set-up as described in chapter 2, subsequently within a few minutes intervals in the order of TIRAF, IRM, then CFP-vinculin image.

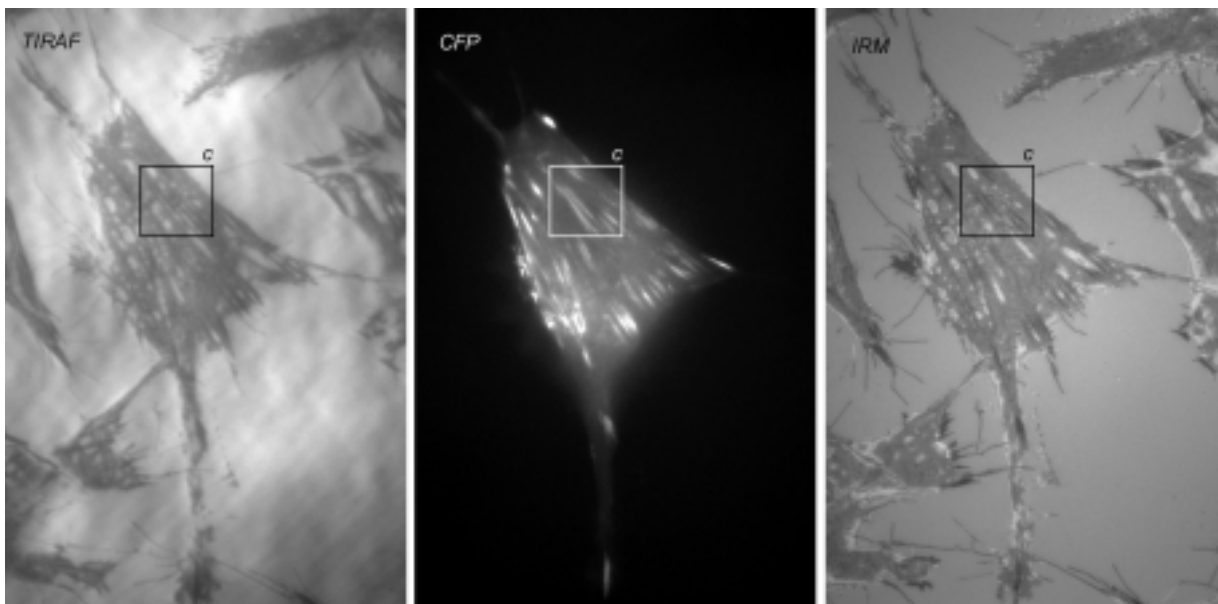


Figure 7.8: GD25- β 1A expressing CFP-vinculin plated on fibronectin for 4 hours. Vinculin has formed parallel stripes of clusters that correlate closely with dark patches in TIRAF and IRM images. These stripes in TIRAF image however are not dark, but rather are at the average fluorescence intensity. The presence of patterns with higher intensities between the stripes contribute to their darker appearances. Enlargement of the labeled area, box c is shown in the following figure.

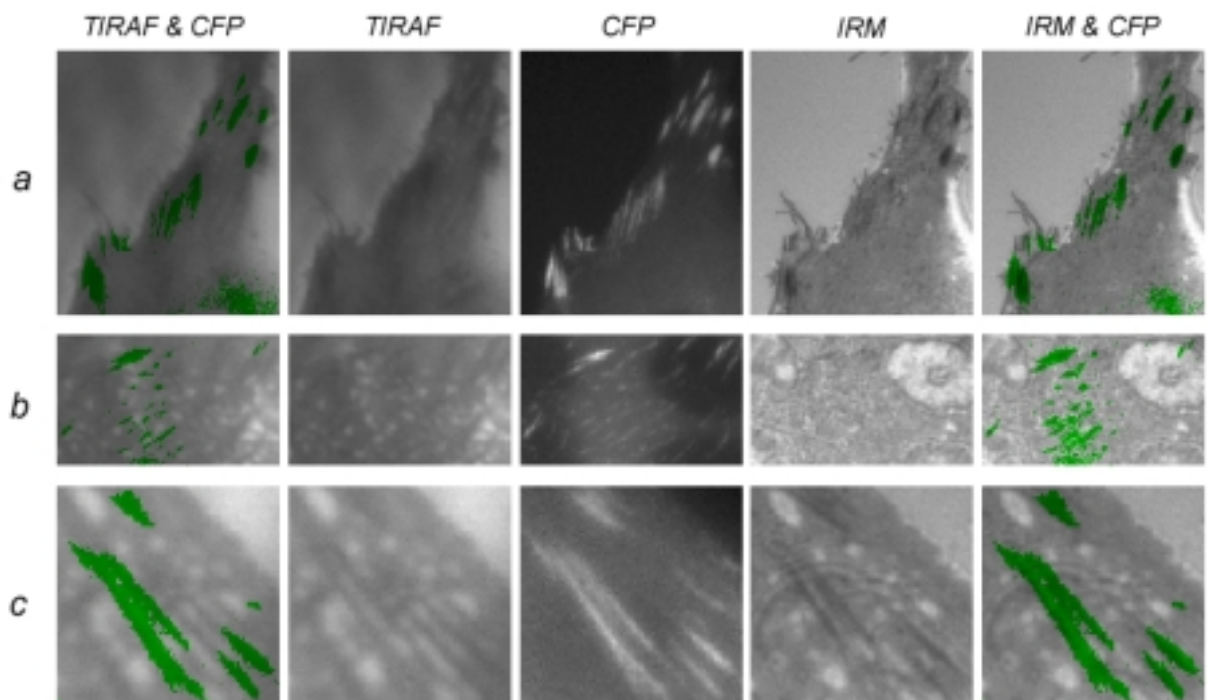


Figure 7.9: Close up of focal contacts labeled by CFP-vinculin. Conserving the detected intensity of the TIRAF/IRM images, distribution of CFP-vinculin clusters are depicted as green in the combined images. A rough comparison of relative intensities to the background (i) at focal contacts (vinculin) and (ii) at predominating area of the cell in TIRAF image and the same for IRM image, (iii) and (iv), respectively, are: in **box a:** (i) 0.7 (ii) 0.9 (iii) 0.4 (iv) 0.8, in **box b:** (i) 0.8 (ii) 0.8 (iii) 0.6 (iv) 0.9, in **box c:** (i) 0.5 (ii) 0.6 (iii) 0.6 (iv) 0.8. In TIRAF images, upward bulging similar to that in FLIC images are present between the parallel stripes of vinculin clusters.

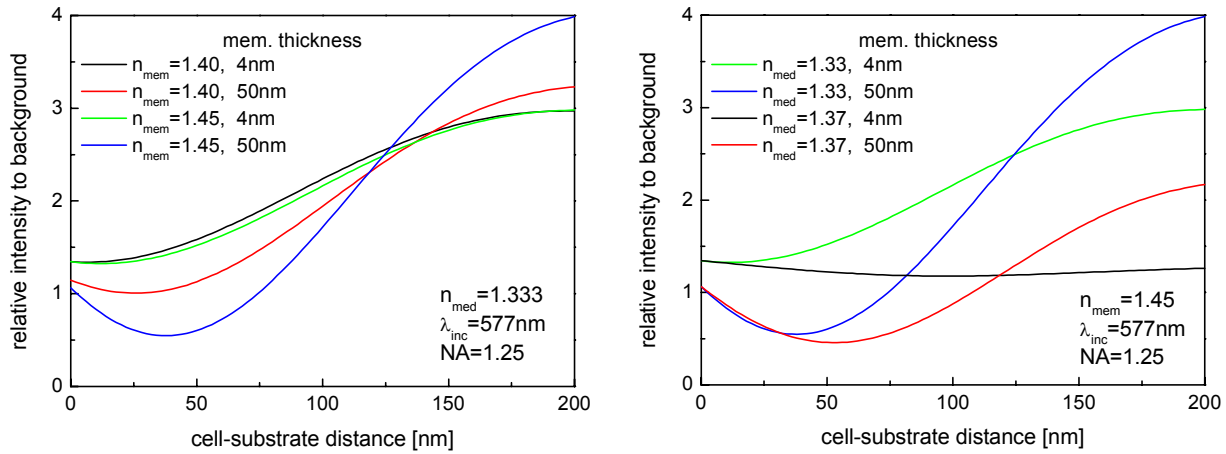


Figure 7.10: Dependence of IRM calculation on cell parameters with the experimental setup used for the combined microscopy; the selected incident ray is at $\lambda_{inc} = 577\text{nm}$. All the rays are integrated through the aperture with $NA = 1:25$ for both illumination and detection.

| | relative intensity | cell parameters: $n_{mem}/d_{mem}/n_{med}$ | corresponding cell-substrate distance at $\lambda_{inc} = 577\text{nm}$ | examples in box: |
|--------------------------------|--------------------|---|--|------------------|
| focal contacts or CFP-vinculin | 0.4 | 1.45/4nm/1.333 | not possible | a |
| | | 1.45/50nm/1.37 | 50nm | |
| | 0.6 | 1.45/4nm/1.333 | not possible | b and c |
| | | 1.45/50nm/1.333 | 25 or 50nm | |
| | | 1.45/4nm/1.37 | not possible | |
| average or predominating area | 0.8 | 1.45/50nm/1.333 | 10 or 60nm | a and c |
| | 1.0 | 1.45/50nm/1.333 | 65nm | b and c |
| | | 1.40/50nm/1.333 | 30nm | |
| | 1.2 | 1.45/4nm/1.333 | 50nm | b |
| | | 1.45/50nm/1.333 | 80nm | |
| | | 1.45/4nm/1.37 | 80nm | |
| | | 1.40/50nm/1.333 | 50nm | |

Figure 7.11: Very rough approximation of corresponding cell-substrate distance to the measured relative intensities in IRM images. Positions of interests are selected from the boxes of the previous figure and the corresponding rough distance estimations are made for several cell parameters based on the graphs in figure above.

membrane with increased refractive index has modest effect on the detected fluorescence intensity in TIRAF microscopy, compared to the effect on reflected light in IRM images. Instead, TIRAF depends strongly on the refractive index of the layer itself containing the fluorophore and its bordering layer. A local variation in refractive index of the cell-substrate gap modulates the detected fluorescence intensity substantially without varying the width of the gap. Since the presence of local accumulation of ECM protein and receptors result in denser medium at focal contacts, this reduces the local electric field strength; i.e. dark patches in TIRAF images imply either close contact or high refractive index between the cell and the substrate. The sensitivity to local variation in optical properties of the layer system is indicated by a study on close correlation between vinculin and focal contact defined by TIRF [14]; the area of focal contacts defined as dark patches in TIRF images is found to increase with increasing incident angle. Here, immunostaining was used to determine the area of vinculin staining, independently to be employed as a reference. At the cell periphery, the images from TIRAF microscopy are also difficult to be analyzed for distance calculation, since we cannot exclude the possibility of fluorescent dyes above the thin lamellipodia and filopodia contributing to the detected intensity. IRM images at the cell periphery are strongly affected by the reflection from the upper membrane. FLIC micrographs are influenced by fluorescence of dyes in upper membrane at thin cell periphery.

Chapter 8

Conclusions

8.1 Finally...

Cell adhesion studied by well established and by new microscopy techniques together with recent techniques in molecular biology have provided several new information as well as lead to new questions with regard to the behavior of cells.

GFP-tagging and FLIC microscopy

Rough membrane in the presence of vinculin in fibroblasts compared with smooth membrane in the absence of vinculin in cells in neuronal culture suggest that upon cell attachment to solid surface, membrane deformation is caused by cytoskeletal reorganization which involves recruitment of "focal adhesion" proteins.

Exclusion of $\beta 1$ integrin expression at such upward/downward bulges in membrane of fibroblasts indicate that $\beta 1$ integrins bound to fibronectin maintains the basic membrane-substrate distance, 50-60nm. Otherwise, membrane ruffling is induced due to cytoskeletal reorganization.

$\beta 1$ integrin-ECM protein (laminin/fibronectin) interaction is not necessarily the cause of membrane deformation described in the previous two statements, since the cells in neuronal culture exhibited smooth membrane inspite of the presence of $\beta 1$ integrins.

Correlation among roughness in membrane with $\beta 1$ integrin and vinculin expression pattern in fibroblasts on fibronectin shows that adhesion to fibronectin through $\beta 1$ integrin that further develop aggregation of vinculin do lead to membrane ruffling.

$\beta 1$ integrin-ECM protein interactions are responsible for cell attachment and motility, which further leads to recruitment of cytoskeletal proteins such as vinculin. This cytoskeletal reorganization seem to induce membrane ruffling that provide forces necessary for attachment or movement.

Vinculin in fibroblasts cultured on fibronectin were clustered into stripes that seem to cause membrane ruffling. Whereas the cells in neuronal cultures consisting predominantly of astrocytes clustered vinculin only at the cell periphery maintaining rather smooth membrane at cell body. Previous studies have shown that primary astrocytes from rat and mouse do not express integrin $\alpha v\beta 3$ [60], but bind to fibronectin via $\alpha v\beta 5$ and $\alpha v\beta 8$, which do not co-localize with focal con-

tact or end of actin filaments [87]. On the other hand, fibroblasts bind to fibronectin mainly via $\alpha_5\beta_1$, and $\alpha_5\beta_1$ integrin translocates from focal contacts. Our correlation studies show that the distribution of β_1 integrins closely match the membrane ruffling in these cells. It could be that the translocation of $\alpha_5\beta_1$ from the focal contacts containing $\alpha_v\beta_3$ integrin observed as vinculin cluster causes ruffling of the membrane. In another words, the ruffling could be the site of fibrillar adhesions, not focal adhesion, which is the reason that vinculin clusters do not exactly match the membrane roughness but are always in the vicinity, and astrocytes neither form vinculin clusters nor exhibit membrane ruffling due to lack of the organization of $\alpha_v\beta_3$ and $\alpha_5\beta_1$ integrins.

Distance measurement

Most optical methods require knowledge of membrane components at interface for accurate distance evaluation, due to sensitivity of the techniques to optical parameters of the layer system being studied.

”Focal contacts” are plaques of optically dense medium due to high protein concentration extracellularly and intracellularly, and not necessarily sites of close contacts. FLIC microscopy which is insensitive to optical parameters shows discrepancy in the estimation of the cell-substrate distance. This discrepancy becomes prominent with methods such as IRM that have stronger dependency on the optical parameters compared to rather insensitive method such as TIRAF.

At cell periphery, it is difficult to evaluate cell-substrate distance all the three methods due to the thin cytoplasmic layer and high concentration of cytoskeletal proteins such as vinculin.

In IRM images, regions with minimal upper membrane effect can be informative for analyzing the cytoplasmic structure of the ventral cell membrane. Dark reflections represent either close apposition of the lower membrane to the substrate or an increase in refractive index right above the membrane. In TIRAF images, regions of low fluorescence intensities represent either close contact or an increase in refractive index of the cell-substrate gap. FLIC microscopy provides the most unbiased estimation of the optical cell-substrate separation regardless of the optical properties of the multilayer system. If these three techniques can be combined, the knowledge of the absolute cell-substrate distance would allow analysis of IRM images to determine the structure of the cytoplasmic side of the lower membrane and TIRAF images to characterize the optical property of cell-substrate gap at site of cell adhesion visualized by GFP-tagging.

8.2 Perspectives

Construction of the GFP-labeled proteins has been a useful tool in a wide range of studies. Alone GFP-vinculin and GFP- β_1 integrin could be applied further to visualize cellular processes *in vitro* or *in vivo*.

Through evaluation of microscopy techniques used in experiments with cell cultures, more accu-

rate interpretation of data become possible and to take advantage of nature of each method.

In this section, improvements and further studies which could be performed with the techniques and work as presented here are discussed; first to pursue biological interests and secondly with regard to further development of the instrumental setup.

Biological studies

Of all, establishment of cell lines stably expressing the fusion construct would improve the condition of the experiments and would widen the possibility for other applications, such as to create a transgenic mouse that expresses GFP-tagged vinculin or integrin $\beta 1$. With the two fluorescence proteins used, GFP and CFP (refer to materials and method section), simultaneous observation of labeled vinculin and integrin $\beta 1$ would be possible. If an appropriate, long-term membrane marker could be developed, a time-lapse study of vinculin and integrin $\beta 1$ distribution, and membrane architecture could also be simultaneously performed. This would be useful in investigating growth cone movements and axon guidance.

Development of such an experimental setup can be used to study the roles played by the extracellular environment on cell adhesion by varying the substrate coating. For example, other ECM proteins could be used to observe influence of ECM-integrin $\beta 1$ interaction on distribution of integrin $\beta 1$ and vinculin. GFP-labeling of fibronectin [66] and laminin would visualize ECM assembly induced by binding to integrins. Or as described in [90], dynamics of fibronectin uniformly adsorbed on the culture substrate being cleared from under the focal contact to be re-organized into fibrils could be studied. If GFP hangs at one end of the ECM molecule, FLIC microscopy could be applied to estimate the distance between the GFP and the substrate, thus the orientation of adsorbed protein relative to the solid surface could be determined. This can be done for both the molecules under the cell and free of the cell. Since cytoplasmic tail of α -subunits is known to be the most varying region that give integrin heterodimers ligand specificity [81], labeling of α -subunit with GFP could be useful in clarifying the relationship between vinculin and integrin distributions.

Additionally, functional studies could be performed through pharmacological techniques; agonists to interfere with or growth factors to stimulate cell adhesions and motilities could be applied to observe their influences on the dynamics of the adhesion molecules and the cell membrane. Also changes in vinculin and integrin distribution and cell-substrate distance with respect to the stages in cell cycle would be an interesting aspect. Previous studies have shown for example, that adhesion to fibronectin of mitotic cells as compared to that of interphase cells is reduced. Also, mitotic cells have been shown to express higher levels of $\alpha v\beta 3$ and low levels of $\alpha 5\beta 1$ integrins at the cell surface as compared to interphase cells [2]. In primary culture prepared from rat hippocampus, recognition of cell types would be important in accurate analysis of the experimental data. Effect of various components comprising the culture medium on cell adhesion should be

investigated in order to attain a defined condition of the experiments.

Methodical

A feasible following step in improving the experimental setup of the combined measurement among TIRAF microscopy, IRM and GFP/CFP-tagging is to enable quantitative analysis of the TIRAF images. The emerging laser light from the optical fibre should be polarized and the prism to glass coverslip coupling should be optimized in order to avoid disturbance due to interference. Then it would be possible to obtain images in this combined setup comparable to that from quantitative TIRAF microscopy performed in the present study. Since the sensitivity of TIRAF microscopy changes with varying incident angles, distance dependence of fluorophore concentration can be directly determined by digitally collecting images over a range of incident angle [14]. Effect of scattered light from the solid/liquid interface for protein absorption that possibly excite fluorescence can be eliminated also by variable angle TIRAF microscopy [14][36].

Analysis of TIRAF images to evaluate cell-substrate distance should be done with more accuracy by considering the parameters with regard to the optical setups, such as the fluorophore and the objective used for detection. The analysis of TIRAF measurements would also acquire more accuracy by incorporating more precise refractive indices of the cell systems. Index of refraction of biological systems could be measured by TIRF refractometry as presented in [54]. If the thickness of the thin films are known, they could also be obtained by quantitative reflection contrast microscopy, where all the reflected light is gathered by the objective lens [8].

A time-lapse study as mentioned in the previous section could be performed also with the TIRAF-IRM-GFP/CFP. TIRAF images at various incident angles, IRM image and image of CFP fusion protein distribution could be collected periodically over certain period of time from a single cell to investigate dynamics of cell adhesion and motility. Such time-lapse observation with TIRAF microscopy is presented in [86][32].

Similar to the TIRAF-IRM-CFP setup, TIRAF-FLIC-CFP microscopy may be possible using silicon chip as a substrate. The thin layer of silicon dioxide would replace the thin glass coverslip. Here, total internal reflection could be attained at the oxide/medium interface with a critical angle of 65.6° ($n_{\text{ox}} = 1.46$) and evanescent wave in the membrane layer could be ensured only if the incident angle is greater than 83.3° . This setup would allow simultaneous comparison between membrane and volume marking.

Additionally, comparative studies with surface plasmon resonance (SPR) microscopy, transmission electron microscopy (TEM) and frozen thin-section electron microscopy should be performed. Preliminary experiments with SPR with similar setup as presented in [35] show that the cell-substrate distance could be measured with this method by digitally varying the incident angle. In order to perform correlation study with the distribution of protein expression, its lateral resolution must still be improved.

Chapter 9

Appendix

A. Abbreviations

- | BSA - bovine serum albumin
- | Da, kDa - Dalton, kilo Dalton
- | DMEM - Dubecco's Modified Eagle's Medium
- | ECFP, CFP - (enhanced) cyan fluorescent protein
- | ECM - extracellular matrix
- | EDTA - ethylene diamine tetraacetic acid
- | EGFP, GFP - (enhanced) green fluorescent protein
- | FBS - fetal bovine serum
- | FCS - fetal calf serum
- | FLIC - fluorescence interference contrast
- | HEPES - N-(2-hydroxyethyl)piperazine-N'-(2-ethanesulfonic acid)
- | IRM - interference reflection microscopy
- | PBS - phosphate-buffered saline
- | RICM - reflection interference contrast microscopy
- | SPR - surface plasmon resonance
- | TEM - transmission electron microscopy
- | TIRAF - total internal reflection aqueous fluorescence
- | TIRFM - total internal reflection fluorescence microscopy
- | Tris - tris(hydroxymethyl)aminomethane

Literature

- [1] B. Alberts, D. Bray, J. Lewis, M. Raff, K. Roberts, and J. D. Watson, *Molecular biology of the cell*, second ed., Garland Publishing, Inc., New York, NY 10016 U.S.A., 1989.
- [2] N. Anilkumar, A. K. Bhattacharya, P. S. Manogaran, and G. Pande, *Modulation of $\alpha 5\beta 1$ and $\alpha v\beta 3$ integrins on the cell surface during mitosis*, *J. Cell. Biochem.* **61** (1996), 338–349.
- [3] C. O. Arregui, S. Carbonetto, and L. McKerracher, *Characterization of neural cell adhesion sites: Point contacts are the sites of interaction between integrins and the cytoskeleton in PC12 cells*, *J. Neurosci.* **14** (1994), 6967–6977.
- [4] Z. Avnur and B. Geiger, *Substrate-attached membranes of cultured cells: Isolation and characterization of ventral cell membranes and the associated cytoskeleton*, *J. Mol. Biol.* **153** (1981), 361–379.
- [5] D. Axelrod, *Carbocyanine dye orientation in red cell membrane studies by microscopic fluorescence polarization*, *Biophys. J.* **26** (1979), 557–573.
- [6] ———, *Cell-substrate contacts illuminated by total internal reflection fluorescence*, *J. Cell Biol.* **89** (1981), 141–145.
- [7] J. Bailey and D. Gingell, *Contacts of chick fibroblasts on glass: Results and limitations of quantitative interferometry*, *J. Cell Sci.* **90** (1988), 215–224.
- [8] J. Bereiter-Hahn, C. H. Fox, and B. Thorell, *Quantitative reflection contrast microscopy of living cells*, *J. Cell Biol.* **82** (1979), 767–779.
- [9] M. Born and E. Wolf, *Principles of optics*, 6th ed., Pergamon Press Ltd, Oxford, England, 1980.
- [10] D. Braun, *Capacitive stimulation of mammalian cells on silicon chips imaged at optical resolution with voltage-sensitive dyes*, Ph.D. thesis, Technischen Universität München, 2000.
- [11] D. Braun and P. Fromherz, *Fluorescence interference-contrast microscopy of cell adhesion on oxidized silicon*, *Appl. Phys. A* **65** (1997), 341–348.
- [12] ———, *Fluorescence interferometry of neuronal cell adhesion on microstructured silicon*, *Phys. Rev. Lett.* **81** (1998), 5241–5244.
- [13] J. S. Burmeister, L. A. Olivier, W. M. Reichert, and G. A. Truskey, *Application of total internal reflection fluorescence microscopy to study cell adhesion to biomaterials*, *Biomaterials* **19** (1998), 307–325.

- [14] J. S. Burmeister, G. A. Truskey, and W. M. Reichert, *Quantitative analysis of variable-angle total internal reflection fluorescence microscopy (VA-TIREM) of Cell/Substrate contacts*, *J. Microsc.* **173** (1994), 39–51.
- [15] K. Burridge, K. Fath, T. Kelly, G. Nuckolls, and C. Turner, *FOCAL ADHESIONS: Transmembrane junctions between the extracellular matrix and the cytoskeleton*, *Ann. Rev. Cell Biol.* **4** (1988), 487–525.
- [16] K. Burridge and J. R. Feramisco, *Microinjection and localization of a 130k protein in living fibroblasts: A relationship to actin and fibronectin*, *Cell* **19** (1980), 587–595.
- [17] K. Burridge, G. Nuckolls, C. Otey, F. Pavalko, K. Simon, and C. Turner, *Actin-membrane interaction in focal adhesions*, *Cell Diff. Develop.* **32** (1990), 337–342.
- [18] M. L. Condic and P. C. Letourneau, *Ligand-induced changes in integrin expression regulate neuronal adhesion and neurite outgrowth*, *Nature* **389** (1997), 852–856.
- [19] M. D. Coutu and S. W. Craig, *cDNA-derived sequence of chicken embryo vinculin*, *Proc. Natl. Acad. Sci. USA* **85** (1988), 8535–8539.
- [20] S. W. Craig and R. P. Johnson, *Assembly of focal adhesions: Progress, paradigms, and portents*, *Curr. Opin. Cell Biol.* **8** (1996), 74–85.
- [21] A. S. G. Curtis, *The mechanism of adhesion of cells to glass: A study by interference reflection microscopy*, *J. Cell Biol.* **20** (1964), 199–215.
- [22] J. A. DePasquale and C. S. Izzard, *Evidence for an actin-containing cytoplasmic precursor of the focal contact and the timing of incorporation of vinculin at the focal contact*, *J. Cell Biol.* **105** (1987), 2803–2809.
- [23] R. Deutzmann, M. Aumailley, H. Wiedemann, W. Pysny, R. Timpl, and D. Edgar, *Cell adhesion, spreading and neurite stimulation by laminin fragment E8 depends on maintenance of secondary and tertiary structure in its rod and globular domain*, *Eur. J. Biochem.* **191** (1990), 513–522.
- [24] J. A. Eble, A. Ries, A. Lichy, K. Mann, H. Stanton, J. Gavrilovic, G. Murphy, and K. Kuhn, *The recognition sites of the integrins $\alpha 1\beta 1$ and $\alpha 2\beta 1$ within collagen IV are protected against gelatinase A attack in the native protein*, *J. Biol. Chem.* **271** (1996), 30964–30970.
- [25] E. Engvall and U. M. Wewer, *Domains of laminin*, *J. Cell Biochem.* **61** (1996), 493–501.

-
- [26] E. M. Erb, K. Tangemann, B. Bohrmann, B. Müller, and J. Engel, *Integrin alphaIIb beta3 reconstituted into lipid bilayers is nonclustered in its activated state but clusters after fibrinogen binding*, *Biochem.* **36** (1997), 7395–7402.
- [27] H. P. Erickson, N. Carrell, and J. McDonagh, *Fibronectin molecule visualized in electron microscopy: A long, thin, flexible strand*, *J. Cell Biol.* **91** (1981), 673–678.
- [28] R. Fässler, M. Pfaff, J. Murphy, A. A. Noegel, S. Johansson, R. Timpl, and R. Albrecht, *Lack of $\beta 1$ integrin gene in embryonic stem cells affects morphology, adhesion, and migration but not integration into the inner cell mass of blastocysts*, *J. Cell Biol.* **128** (1995), 979–988.
- [29] J. L. R. Fernandez, B. Geiger, D. Salomon, and A. Ben-Ze'ev, *Suppression of vinculin expression by antisense transfection confers changes in cell morphology, motility, and anchorage-dependent growth of 3T3 cells*, *J. Cell Biol.* **122** (1993), 1285–1294.
- [30] R. Fleischmajer, J. S. Perlish, E.D. MacDonald, A. Schechter, A. D. Murdoch, R. V. Iozzo, and Y. Yamada, *There is binding of collagen IV to $\beta 1$ integrin during early skin basement membrane assembly*, *Annals. NY Acad. Sci.* **857** (1998), 212–227.
- [31] A. J. Garcia and D. Boettiger, *Integrin-fibronectin interactions at the cell-material interface: Initial integrin binding and signaling*, *Biomaterials* **20** (1999), 2427–2433.
- [32] P. Geggier and G. Fuhr, *A time-resolved total internal reflection aqueous fluorescence (TIRAF) microscope for the investigation of cell adhesion dynamics*, *Appl. Phys. A* **68** (1999), 505–513.
- [33] G. Geiger, *A 130k protein from chicken gizzard: Its localization at the termini of microfilament bundles in cultured chicken cells*, *Cell* **18** (1979), 193–205.
- [34] F. G. Giancotti, *Complexity and specificity of integrin signalling*, *Nat. Cell Biol.* **2** (2000), E13–E14.
- [35] K. F. Giebel, C. Bechinger, S. Herminghaus, M. Riegel, P. Leiderer, U. Weiland, and M. Bastmeyer, *Imaging of Cell/Substrate contacts of living cells with surface plasmon resonance microscopy*, *Biophys. J.* **76** (1999), 509–516.
- [36] D. Gingell and O. Heavens, *Elimination of the effects of stray light in measurements by total internal reflection aqueous fluorescence (TIRAF)*, *J. Microsc.* **182** (1996), 141–148.

- [37] D. Gingell, O. S. Heavens, and J. S. Mellor, *General electromagnetic theory of total internal reflection fluorescence: The quantitative basis for mapping cell-substratum topography*, *J. Cell Sci.* **87** (1987), 677–693.
- [38] D. Gingell and I. Todd, *Interference reflection microscopy*, *Biophys. J.* **26** (1979), 507–526.
- [39] B. M. Gumbiner, *Cell adhesion: The molecular basis of tissue architecture and morphogenesis*, *Cell* **84** (1996), 345–357.
- [40] R. W. Gundersen, *Interference reflection microscopic study of dorsal root growth cones on different substrates: Assessment of growth cone-substrate contacts*, *J. Neurosci. Res.* **21** (1988), 298–306.
- [41] W. N. Hansen, *Electric fields produced by the propagation of plane coherent electromagnetic radiation in a stratified medium*, *J. Opt. Soc. Am.* **58** (1968), 380–390.
- [42] E. G. Hayman, M. D. Pierschbacher, Y. Ohgren, and E. Ruoslahti, *Serum spreading factor (vitronectin) is present at the cell surface and in tissues*, *Proc. Natl. Acad. Sci. U.S.A.* **80** (1983), 4003–4007.
- [43] O. S. Heavens, *Use of the approximations in cell studies by total internal reflection fluorescence microscopy (TIRF)*, *J. Microsc.* **180** (1995), 106–108.
- [44] O. S. Heavens and D. Gingell, *Film thickness measurement by frustrated total reflection fluorescence*, *Opt. Laser Tech.* **23** (1991), 175–179.
- [45] D. C. Hocking, J. Sottile, and P. J. McKeown-Longo, *Activation of distinct $\alpha 5\beta 1$ -mediated signaling pathways by fibronectin's cell adhesion and matrix assembly domains*, *J. Cell Biol.* **141** (1998), 241–253.
- [46] R. Holmes, *Preparation from human serum of an alpha-one protein which induces the immediate growth of unadapted cells in vitro*, *J. Cell Biol.* **32** (1967), 297–308.
- [47] A. F. Horwitz, *Integrins and health*, *Scientific American* (1997), 46–53.
- [48] R. O. Hynes, *Integrins: Versatility, modulation, and signaling in cell adhesion*, *Cell* **69** (1992), 11–25.
- [49] B. M. Jockusch, P. Bubeck, K. Giehl, M. Kroemker, J. Moschner, M. Rothkegel, M. Rüdiger, K. Schlüter, G. Stanke, and J. Winkler, *The molecular architecture of focal adhesions*, *Annu. Rev. Cell Dev. Biol.* **11** (1995), 379–416.

-
- [50] B.-Z. Katz, E. Zamir, A. Bershadsky, Z. Kam, K. M. Yamada, and B. Geiger, *Physical state of the extracellular matrix regulates the structure and molecular composition of cell-matrix adhesions*, *Mol. Biol. Cell* **11** (2000), 1047–1060.
- [51] C. Kibler, F. Schermutzki, H. D. Waller, R. Timpl, C. A. Müller, and G. Klein, *Adhesive interactions of human multiple myeloma cell lines with different extracellular matrix molecules*, *Cell Adh. Comm.* **5** (1998), 307–323.
- [52] A. Lambacher, *Fluoreszenz-interferenz-kontrast-mikroskopie von membranen auf silizium*, Ph.D. thesis, Universität Ulm, 1994.
- [53] A. Lambacher and P. Fromherz, *Fluorescence interference-contrast microscopy on oxidized silicon using a monomolecular dye layer*, *Appl. Phys. A* **63** (1996), 207–216.
- [54] F. Lanni, A. S. Waggoner, and D. L. Taylor, *Structural organization of interphase 3T3 fibroblasts studied by total internal reflection fluorescence microscopy*, *J. Cell Biol.* **100** (1985), 1091–1102.
- [55] D. A. Lauffenburger and A. F. Horwitz, *Cell migration: A physically integrated molecular process*, *Cell* **84** (1996), 359–369.
- [56] B. Ludin and A. Matus, *GFP illuminates the cytoskeleton*, *Trends Cell Biol.* **8** (1998), 72–77.
- [57] E. E. Marcantonio, J. L. Guan, J. E. Trevithick, and R. O. Hynes, *Mapping of the functional determinants of the integrin $\beta 1$ cytoplasmic domain by site-directed mutagenesis*, *Cell Reg.* **1** (1990), 597–604.
- [58] G. R. Martin and R. Timpl, *Laminin and other basement membrane components*, *Ann. Rev. Cell Biol.* **3** (1987), 57–85.
- [59] L. McKerracher, M. Chamoux, and C. O. Arregui, *Role of laminin and integrin interactions in growth cone guidance*, *Mol. Neurobiol.* **12** (1996), 95–116.
- [60] R. Milner, X. Huang, J. Wu, S. Nishimura, R. Pytela, D. Sheppard, and C. Ffrench-Constant, *Distinct roles for astrocyte $\alpha v \beta 5$ and $\alpha v \beta 8$ integrins in adhesion and migration*, *J. Cell Sci.* **112** (1999), 4271–4279.
- [61] T. J. Mitchison and L. P. Cramer, *Actin-based cell motility and cell locomotion*, *Cell* **84** (1996), 371–379.
- [62] D. F. Mosher, *Fibronectin*, Academic Press, Inc., San Diego, U.S.A., 1989.
- [63] M. Mrksich, *Tailored substrates for studies of attached cell culture*, *CMLS, Cell. Mol. Life Sci.* **54** (1998), 653–662.

- [64] M. V. Nermut, P. Eason, E. M. Hirst, and S. Kellie, *Cell/substratum adhesion in RSV-transformed rat fibroblasts*, *Exp. Cell Res.* **193** (1991), 382–397.
- [65] M. V. Nermut, N. M. Green, P. Eason, S. S. Yamada, and K. M. Yamada, *Electron microscopy and structural model of human fibronectin receptor*, *EMBO J.* **7** (1988), 4093–4099.
- [66] T. Ohashi, D. P. Kiehart, and H. P. Erickson, *Dynamics and elasticity of the fibronectin matrix in living cell culture visualized by fibronectin-green fluorescent protein*, *Proc. Natl. Acad. Sci. USA* **96** (1999), 2153–2158.
- [67] R. Pankov, E. Cukierman, B.-Z. Katz, K. Matsumoto, D. C. Lin, S. Lin, C. Hahn, and K. M. Yamada, *Integrin dynamics and matrix assembly: Tensin-dependent translocation of $\alpha 5 \beta 1$ integrins promotes early fibronectin fibrillogenesis*, *J. Cell Biol.* **148** (2000), 1075–1090.
- [68] J. S. Ploem, *Reflection-contrast microscopy as a tool for investigation of the attachment of living cells to a glass surface*, r. v. furth ed., Blackwell Scientific Publications, Oxford, 1975.
- [69] G. J. Price, P. Jones, M. D. Davison, B. Patel, R. Bendori, B. Geiger, and D. R. Critchley, *Primary sequence and domain structure of chicken vinculin*, *Biochem. J.* **259** (1989), 453–461.
- [70] J. Rädler and E. Sackmann, *Imaging optical thicknesses and separation distances of phospholipid vesicles at solid surfaces*, *J. Phys. II France* **3** (1993), 727–748.
- [71] C. M. Regen and A. F. Horwitz, *Dynamics of $\beta 1$ integrin-mediated adhesive contacts in motile fibroblasts*, *J. Cell Biol.* **119** (1992), 1347–1359.
- [72] W. M. Reichert and G. A. Truskey, *Total internal reflection fluorescence (TIRF) microscopy*, *J. Cell Sci.* **96** (1990), 219–230.
- [73] A. Renaudin, M. Lehmann, J.-A. Girault, and L. McKerracher, *Organization of point contacts in neuronal growth cones*, *J. Neurosci. Res.* **55** (1999), 458–471.
- [74] P. D. Richardson and M. Steiner, *Principles of cell adhesion*, CRC Press, Inc., Boca Raton, Florida, U.S.A., 1995.
- [75] K. Rubin, M. Hook, B. Obrink, and R. Timpl, *Substrate adhesion of rat hepatocytes: Mechanism of attachment to collagen*, *Cell* **24** (1981), 463–470.
- [76] M. Schindl, E. Wallraff, B. Deubzer, W. Witke, G. Gerisch, and E. Sackmann, *Cell-substrate interactions and locomotion of dictyostelium wild-type and mutants defective in three cytoskeletal proteins: A study using quantitative reflection interference contrast microscopy*, *Biophys. J.* **68** (1995), 1177–1190.

-
- [77] I. Schwartz, D. Seger, and S. Shaltiel, *Vitronectin*, *Int. J. Biochem. Cell Biol.* **31** (1999), 539–544.
- [78] D. Seger, Z. Gechtman, and S. Shaltiel, *Phosphorylation of vitronectin by casein kinase II*, *J. Biol. Chem.* **273** (1998), 24805–24813.
- [79] L. B. Smilenov, A. Mikhailov, R. J. Pelham Jr., E. E. Marcantonio, and G. G. Gundersen, *Focal adhesion motility revealed in stationary fibroblasts*, *Science* **286** (1999), 1172–1174.
- [80] H. B. Streeter and D. A. Rees, *Fibroblast adhesion to RGDS shows novel features compared with fibronectin*, *J. Cell Biol.* **105** (1987), 507–515.
- [81] N. Tawil, P. Wilson, and S. Carbonetto, *Integrins in point contacts mediate cell spreading: Factors that regulate integrin accumulation in point contacts vs. focal contacts*, *J. Cell Biol.* **120** (1993), 261–271.
- [82] R. Timpl and J. C. Brown, *The laminins*, *Matrix Biol.* **14** (1994), 275–281.
- [83] S. Tominaga, *Murine mRNA for the β -subunit of integrin is increased in BALB/c-3T3 cells entering the G1 phase of the G0 state*, *FEBS Lett.* **238** (1988), 315–319.
- [84] G. A. Truskey, J. S. Burmeister, E. Grapa, and W. M. Reichert, *Total internal reflection fluorescence microscopy (TIRFM) II. topographical mapping of relative cell/substratum separation distances*, *J. Cell Sci.* **103** (1992), 491–499.
- [85] S. Vassanelli and P. Fromherz, *Transistor probes local potassium conductances in the adhesion region of cultured rat hippocampal neurons*, *J. Neurosci.* **19** (1999), 6767–6773.
- [86] M. Dong Wang and D. Axelrod, *Time-lapse total internal reflection fluorescence video of acetylcholine receptor cluster formation on myotubes*, *Dev. Dyn.* **201** (1994), 29–40.
- [87] E. A. Wayner, R. A. Orlando, and D. A. Cheresh, *Integrins $\alpha\beta3$ and $\alpha\beta5$ contribute to cell attachment to vitronectin but differentially distribute on the cell surface*, *J. Cell Biol.* **113** (1991), 919–929.
- [88] K. Webb, V. Hlady, and P. A. Tresco, *Relative importance of surface wettability and charged functional groups on NIH 3T3 fibroblast attachment, spreading, and cytoskeletal organization*, *J. Biomed. Mater. Res.* **41** (1998), 422–430.
- [89] K. Wennerberg, L. Lohikangas, D. Gullberg, M. Pfaff, S. Johansson, and R. Fässler, *$\beta1$ integrin-dependent and -independent polymerization of fibronectin*, *J. Cell Biol.* **132** (1996), 227–238.

-
- [90] E. Zamir, M. Katz, Y. Posen, N. Erez, K. M. Yamada, B.-Z. Katz, S. Lin, D. C. Lin, A. Bershadsky, Z. Kam, and B. Geiger, *Dynamics and segregation of cell-matrix adhesions in cultured fibroblasts*, *Nat. Cell Biol.* **2** (2000), 191–196.
- [91] Q. Zhang, T. Sakai, J. Nowlen, I. Hayashi, R. Fässler, and D. F. Mosher, *Functional $\beta 1$ -integrins release the suppression of fibronectin matrix assembly by vitronectin*, *J. Biol. Chem.* **274** (1999), 368–375.
- [92] J. Zheng, R. E. Buxbaum, and S. R. Heidemann, *Measurements of growth cone adhesion to culture surfaces by micromanipulation*, *J. Cell Biol.* **127** (1994), 2049–2060.
- [93] A. Zilker, H. Engelhardt, and E. Sackmann, *Dynamic reflection interference contrast (RIC-) microscopy: A new method to study surface excitations of cells and to measure membrane bending elastic moduli*, *J. Phys. France* **48** (1987), 2139–2151.